NASA Technical Memorandum 104566, Vol. 37

SeaWiFS Technical Report Series

Stanford B. Hooker and Elaine R. Firestone, Editors

Volume 37, The Fourth SeaWiFS Intercalibration Round-Robin Experiment (SIRREX-4), May 1995

B. Carol Johnson, Sally S. Bruce, Edward A. Early, Jeanne M. Houston,
Thomas R. O'Brian, Ambler Thompson, Stanford B. Hooker, and James L. Mueller

May 1996

NASA Technical Memorandum 104566, Vol. 37

SeaWiFS Technical Report Series

Stanford B. Hooker, Editor
NASA Goddard Space Flight Center
Greenbelt, Maryland

Elaine R. Firestone, Technical Editor
General Sciences Corporation
Laurel, Maryland

Volume 37, The Fourth SeaWiFS Intercalibration Round-Robin Experiment (SIRREX-4), May 1995

B. Carol Johnson
Sally S. Bruce
Edward A. Early
Jeanne M. Houston
Thomas R. O'Brian
Ambler Thompson
National Institute of Standards and Technology
Gaithersburg, Maryland

James L. Mueller
Center for Hydro-Optics and Remote Sensing
San Diego State University
San Diego, California

Stanford B. Hooker
NASA Goddard Space Flight Center
Greenbelt, Maryland

National Aeronautics and
Space Administration

Goddard Space Flight Center
Greenbelt, Maryland 20771

1996

This publication is available from the NASA Center for AeroSpace Information,
800 Elkridge Landing Road, Linthicum Heights, MD 21090-2934, (301) 621-0390.

ABSTRACT

This report documents the fourth Sea-viewing Wide Field-of-view Sensor (SeaWiFS) Intercalibration Round-Robin Experiment (SIRREX-4), which was held at the National Institute of Standards and Technology (NIST) on 3–10 May 1995. The agenda for SIRREX-4 was established by a consensus reached at the conclusion of SIRREX-3: there should be an emphasis on training and work to foster and encourage uniform use of accepted protocols for calibrating radiometric instruments in the laboratory. The goal was to host the activity in a setting where proper techniques could be discussed and demonstrated. It seemed appealing to split the day between morning lectures and afternoon laboratory exercises or *practicals*. The former gave the user community a chance to present what was important to them and discuss it with acknowledged experts in radiometry, while the latter presented a unique opportunity for training and evaluation in the presence of these same experts. The five laboratory sessions were concerned with 1) determining the responsivity of a spectroradiometer and the spectral radiance of an unknown integrating sphere source, 2) demonstrating spectral field calibration procedures for an integrating sphere using three different instruments, 3) measuring spectral radiance using the plaque method, 4) setting up and aligning lamp calibration transfer standards using the NIST specifications for irradiance measurements, and 5) characterizing radiometric instruments. In addition to documenting some supplemental studies performed outside the laboratory sessions, this report includes an evaluation of the hardware that has been used during the SIRREX activities plus a critical evaluation of SIRREX objectives.

1. INTRODUCTION

Experience with satellite sensors such as the Coastal Zone Color Scanner (CZCS) has underscored the importance of sustained and coordinated programs to verify sensor calibration and derived products, especially as more rigorous specifications on measurement uncertainties are required to address the geophysical and biological problems that have been identified by the science community. As a second-generation ocean color radiometer, the Sea-viewing Wide Field-of-view Sensor (SeaWiFS) instrument offers a variety of design improvements over the CZCS, which should provide the capability to meet the mission objectives (Hooker et al. 1993).

Two important goals of the SeaWiFS Project are to determine, from the SeaWiFS radiance measurements, 1) normalized water-leaving radiance with an uncertainty of 5%, and 2) chlorophyll *a* concentration with an uncertainty of 30%. (All uncertainties are expressed as relative standard uncertainties, $k = 1$, unless otherwise noted.†) These goals are very ambitious, and can only be achieved by augmenting the SeaWiFS measurements with a program of ongoing validation measurements to verify the radiometric uncertainty and long-term stability of the SeaWiFS instrument's radiance responsivities, and to validate the atmospheric correction models and algorithms used to convert SeaWiFS radiances to normalized water-leaving radiances. One of the principal approaches to this critical aspect of validation will be frequent direct comparisons between SeaWiFS estimates and *in situ* measurements of water-leaving radiances. Because the primary goal is to demonstrate that normalized water-leaving radiances derived from SeaWiFS data have uncertainties of less than 5%, the comparative *in situ* radiometric measurements must be calibrated to an uncertainty less than 5%.

The only economically feasible approach to acquiring a large and globally distributed database of *in situ* radiometric measurements for SeaWiFS validation, is to solicit contributions of data from the oceanographic community at large, and to provide assurance that the aggregate data set will be of uniform quality and have an uncertainty less than 5%. The SeaWiFS Project at the National Aeronautics and Space Administration (NASA) Goddard Space Flight Center (GSFC) is addressing this problem through the SeaWiFS Calibration and Validation Program (McClain et al. 1992). At the outset, the Project sponsored a workshop to draft protocols for ocean optics measurements to support SeaWiFS validation (Mueller and Austin 1992), which include instrument performance specifications, and requirements for instrument characterization and calibration. The importance of the protocols to the community was established by the considerable expansion of the original document to accommodate a broader range of measurements, techniques, and sampling considerations (Mueller and Austin 1995).

Of the oceanographers and institutions expected to contribute ocean radiometric measurements to the SeaWiFS validation database (Hooker et al. 1994), only a few are equipped to calibrate and characterize radiometric instruments. Domestic laboratories which currently engage in at least some aspects of the characterization and calibration of oceanographic radiometers include GSFC; the Center for Hydro-Optics and Remote Sensing (CHORS) at San Diego

† The guidelines for evaluating and expressing the uncertainty of measurement results, as followed in this document are given in Taylor and Kuyatt (1994).

State University (SDSU); the University of Miami (UM); the University of California at Santa Barbara (UCSB); the University of Arizona (UA); and the Moss Landing Marine Laboratory (MLML) in collaboration with Dennis Clark of the National Oceanic and Atmospheric Administration (NOAA).

Several manufacturers of in-water radiometers participate in these activities and these include Biospherical Instruments, Inc. (BSI) in San Diego, California, and Satlantic, Inc. in Halifax, Nova Scotia, Canada. The SeaWiFS instrument is being characterized and calibrated by its manufacturer, the Hughes Santa Barbara Research Corporation (SBRC) in cooperation with Orbital Sciences Corporation (OSC). Internationally, several institutions are actively engaged in instrument calibration and characterization, but the two with explicit involvement with the SeaWiFS Project are the Plymouth Marine Laboratory (PML) in Plymouth, England, and the Joint Research Centre (JRC) in Ispra, Italy.

The strategy adopted for SeaWiFS validation is to calibrate all involved instruments within a network consisting of these, and possibly a few additional laboratories. In recognition of the need to maintain internal consistency between calibrations of *in situ* instruments and that of the SeaWiFS instrument itself, the SeaWiFS Project, under the Calibration and Validation Program, has implemented an ongoing series of SeaWiFS Intercalibration Round-Robin Experiments (SIRREXs). The purpose of this program is to transfer the National Institute of Standards and Technology (NIST) scale of spectral irradiance through GSFC to all participating laboratories in the SeaWiFS ocean community, and to the calibration standards used to calibrate the SeaWiFS instrument for radiance responsivity.

The specific objectives of the SIRREX activities include the following:

1. Intercalibrate FEL-type lamp working standards of spectral irradiance used at the participating laboratories, and to reference each to the NIST scale of spectral irradiance by way of a secondary standard to be maintained at GSFC;
2. Intercalibrate integrating sphere sources of spectral radiance used at the various laboratories;
3. Intercompare plaques used to transfer the scale of spectral irradiance from an FEL lamp to a scale of spectral radiance; and
4. Intercompare transfer radiometers and other support electronics, most critically shunts and voltmeters, used to support radiometric calibrations at each laboratory.

The first SIRREX was held at CHORS on 27–31 July 1992 (Mueller 1993) and demonstrated the NIST scale of spectral irradiance was *not* transferred from the GSFC secondary standard (FEL lamp F269) to the 17 other lamps with an uncertainty of (approximately) 1%. An uncertainty of 1% is expected, based on the uncertainty in the NIST scale of spectral irradiance, and general experience with the process of transferring spectral irradiance using monochromators. (Refer to Walker et al. 1987a, however, note that Walker's expanded uncertainties correspond to $k = 3$ values.) Experience was gained at SIRREX-1 in the methods of comparing the spectral radiance scales of sphere and plaque sources, as well as the performance of voltmeters and resistors that are used to determine lamp operating currents.

The second SIRREX was held at CHORS on 14–25 June 1993 (Mueller et al. 1994) and showed that spectral irradiance lamps measured using the GSFC standard irradiance lamp (F269) are consistent with the program goals, because the uncertainty of these measurements was assessed to be about 1%. This was not true for the spectral radiance measurements, however, where once again the internal consistency of the results was used to assess the uncertainty. The failure was attributed to inadequate performance and characterization of the instrumentation. For example, spatial non-uniformities, spectral features, and sensitivity to illumination configuration were observed in some of the integrating sphere sources. The results of SIRREX-2 clearly indicated the direction for future work, with the main emphasis on instrument characterization and the assessment of the measurement uncertainties so that the results may be stated in a more definitive manner.

The third SIRREX was held at CHORS during 19–30 September 1994 (Mueller et al. 1995). The spectral irradiances of the FEL lamps were intercompared with a Type A uncertainty of approximately 1% which was also obtained during SIRREX-2. The data for lamps common to both SIRREX-2 and SIRREX-3, however, differed by an average of 1.5%. The 1.1–1.5% uncertainties associated with sphere radiance transfers, and sphere characterizations in SIRREX-3 were a significant improvement over the 5–7% results obtained during both SIRREX-1 and SIRREX-2. The inability to positively identify and quantify specific sources of uncertainty in these earlier experiments was rectified by better characterization of the transfer radiometers (vignetted fields of view, relative spectral response functions, and stability of absolute responsivities) and spheres (spatial uniformity, Lambertian quality, and temporal stability).

The spatial nonuniformity of the spectral radiance of the GSFC sphere, which was identified as a major source of uncertainty in measurements of this sphere during SIRREX-2 was corrected by recoating the sphere. Immediately before and during SIRREX-3, the radiances of the GSFC and CHORS spheres were both verified to be spatially uniform within less than 0.5% and to be uniform angularly up to 15° from normal within less than 1.2% and 0.7%, respectively. One of the most troubling developments during SIRREX-3 was a shift in the spectral irradiance of F269,

the secondary working standard for all SIRREX activities, which occurred on 21 September 1994.

1.2 SIRREX-4

In the progress from the first to the third SIRREX, uncertainties in the traceability to NIST of intercomparisons between the spectral irradiance of lamps improved from 8% to 2% to 1%. Intercomparisons of sphere radiance showed little improvement between SIRREX-1 and SIRREX-2, with uncertainties as large as 7% in both experiments. In SIRREX-3, however, more rigorous characterization of both spheres and transfer radiometers reduced the uncertainties to approximately 1.5% in absolute spectral radiance and 0.3% in radiance stability for most spheres, and clearly identified inadequate lamp current regulation as the source of the larger (2%) uncertainty in the stability of radiance in the CHORS sphere.

Plaque reflectance measurements in SIRREX-3 represent a qualitative improvement over results obtained during the earlier SIRREXs, primarily due to the improved performance of the SeaWiFS Transfer Radiometer (SXR). However, significant improvements are needed in this technique if several poorly quantified uncertainties are to be resolved, including the development of proper methods for stray light baffling, goniometric corrections for FEL off-axis irradiances, and quantitative characterization of the bidirectional reflectance distribution function (BRDF) of Spectralon™† plaques. Intercomparisons between shunts and voltmeters have been done in all three SIRREXs, and in general, the equipment used by all participants met the specified levels of uncertainty for radiometric calibration measurements. In the first and second SIRREXs, minor problems were identified with particular voltmeters which were either corrected or the instruments were taken out of service for this particular application.

In addition to the concerns about plaques, SIRREX-3 clearly demonstrated the need for rigorous laboratory practices. The shift in the spectral irradiance of lamp F269 emphasized the need to closely adhere to several extremely important protocols for usage and record keeping associated with FEL lamps in general, and with NIST secondary standards in particular. Lamp operating hours should always be recorded. The voltage across the lamp terminals, as well as the lamp operating current, should be measured and recorded during each use of a lamp. As a matter of routine practice, the irradiance of a NIST secondary standard of spectral irradiance should be transferred locally to several additional working standard FEL lamps, and the transfer periodically verified for each of the local working standards at intervals of 20–30 lamp hours.

The local working standards should be used as the reference in most laboratory experiments, including lamp transfer intercomparisons, with the NIST secondary standard usage limited to occasional verification of the working standard reference lamp. This procedure will minimize the operating time accumulated on the NIST secondary standard, which should be returned to NIST for recalibration at intervals of 20–30 operating hours. Lamp hours were not regularly logged for lamp F269, and lamp operating voltages were not recorded. Had the lamp's voltage history been maintained, the time at which the values changed on 21 September would have been more easily detected. Moreover, there was no firm determination of the number of operating hours accumulated on F269, although GSFC's estimate was something in excess of 200 hours. That number of hours following the lamp's calibration by NIST in October 1992 is an order of magnitude too large for this lamp to have been regarded as a reliable secondary working standard for SIRREX intercomparison experiments.

Given the repeated failures in laboratory technique during the first three SIRREXs, the primary recommendation from SIRREX-3 was ... *there should be an emphasis on training and work to foster and encourage uniform use of accepted protocols for laboratory calibration of radiometric instruments.* This was the starting point for the planning and execution of SIRREX-4. The idea was to host the activity in a setting where proper technique could be discussed and demonstrated. It seemed appealing to split the day between morning lectures and afternoon laboratory exercises or *practicals.* The former would give the user community a chance to present what was important to them and discuss it with acknowledged experts in radiometry, while the latter would present a unique opportunity for training and evaluation in the presence of these same experts.

1.3 SIRREX-4 Agenda

Wednesday, 3 May (Gaithersburg Hilton)

0800	*Registration*	J. Hardware
0830	Introductions	S. Hooker
0845	Welcome to NIST	S. Krammer
0900	Introduction to SIRREX-4	S. Hooker
0930	SIRREX-1, -2, and -3 Summary	J. Mueller
1000	EOS Calibration Requirements	J. Butler
1015	*Break*	
1030	Logistics and Goals of SIRREX-4	C. Johnson
1100	SXR Description and Calibration	C. Johnson
1130	*Lunch*	
1330	Uncertainties in Experiments According to NIST and the ISO	M. Levenson
1430	CoASTS and PICASSO	G. Zibordi
1500	SEI and PRIME	G. Moore

† "Spectralon" is a registered trademark of Labsphere, Inc., North Sutton, New Hampshire. Identification of commercial equipment to adequately specify the experimental problem, does not imply recommendation or endorsement by the National Institute of Standards and Technology, nor does it imply that the equipment identified is necessarily the best available for the purpose.

1530	*Break*	
1600	*Carpool to NIST*	
1630	NIST Tours	
	• High Accuracy Cryogenic Radiometer (HACR)	T. Gentile
	• Aperture Area Facility	J. Fowler
	• UV Network Site	A. Thompson
1800	*Evening Adjournment*	

Thursday, 4 May (NIST Building 245)

0730	*Registration*	J. Hardware
0800	NIST Spectral Radiance and Irradiance Measurements and Uncertainties	C. Gibson
0830	NIST Detector Spectral Response Scales and Uncertainties	T. Larason
0900	MOS-Priroda and MOS-IRS	K. Sümnich
0930	Ocean Color Imager (OCI)	L. Lee
1000	*Break*	
1020	Radiometric Questionnaire	C. Cromer
1030	Groups Respond to Questionnaire	
1030	Discuss Questionnaire	
1200	*Lunch*	
1330	Laboratory Exercises	*NIST Labs*
1530	*Break*	
1550	Continue Laboratory Exercises	
1730	Rapid Results Meeting	C. Johnson
1800	*Dinner*	
2000	Videos and Discussion	*Hilton*
2100	*Evening Adjournment*	

Friday, 5 May (NIST Building 245)

0730	*Registration*	J. Hardware
0800	Spectral Irradiance/Radiance Scale Realization	J. McLean
0845	OCTS/ASTER Intercomparison	J. Butler
0930	Recommended Data Practices	T. Early
1000	*Break*	
1020	Recommended Lamp Practices	A. Thompson
1050	BRDF and Radiance Realizations Using Diffuse Plaques	C. Asmail
1200	*Lunch*	
1330	Laboratory Exercises	*NIST Labs*
1530	*Break*	
1550	Continue Laboratory Exercises	
1730	Rapid Results Meeting	C. Johnson
1800	*Dinner*	
2000	Videos and Discussion	*Hilton*
2100	*Evening Adjournment*	

Monday, 8 May (Gaithersburg Hilton)

0730	*Registration*	J. Hardware
0800	MER Calibrations at BSI	J. Ehramjian
0830	OCR Calibrations at Satlantic	S. McLean
0900	Calibrations at CHORS	J. Mueller
1000	*Break*	
1020	Airborne Oceanographic Lidar (AOL)	D. Berry
1030	Plymouth Atmospheric Correction Experiment (PACE)	S. Hudson
1050	Radiometric Scales for Field Work	A. Thompson
1200	*Lunch*	
1330	Laboratory Exercises	*NIST Labs*
1530	*Break*	
1550	Continue Laboratory Exercises	
1730	Rapid Results Meeting	C. Johnson
1800	*Dinner*	
2000	Videos and Discussion	*Hilton*
2100	*Evening Adjournment*	

Tuesday, 9 May (Gaithersburg Hilton)

0730	*Registration*	J. Hardware
0800	SeaWiFS Radiometric Characterization	B. Barnes
0830	Solar Calibration of SeaWiFS	B. Barnes
0900	MODIS Characterization	W. Barnes
1000	*Break*	
1020	MERIS and ScaRaB	H. Rinck
1040	Plaque Discussion	J. Mueller
1200	*Lunch*	
1330	Laboratory Exercises	*NIST Labs*
1530	*Break*	
1550	Continue Laboratory Exercises	
1730	Rapid Results Meeting	C. Johnson
1800	*Dinner*	
2000	Videos and Discussion	*Hilton*
2100	*Evening Adjournment*	

Wednesday, 10 May (Gaithersburg Hilton)

0730	*Registration*	J. Hardware
0800	Poor and Good Radiometric Practice: Examples and Lessons Learned	B. Saunders
0900	Wavelength Interpolation	C. Cromer
1000	*Break*	
1020	Plenary Discussion (SIRREX-5, Wavelength Interpolation, etc.)	S. Hooker
1200	*Lunch*	
1330	Laboratory Exercises	*NIST Labs*
1530	*Break*	
1550	Continue Laboratory Exercises	
1730	Rapid Results Meeting	C. Johnson
1800	*Dinner*	
2000	Videos and Discussion	*Hilton*
2100	*Evening Adjournment*	

The laboratory space was not sufficient to allow everyone to participate in the practicals, so a smaller group of

Table 1. Laboratory schedule for participant groups A–E during SIRREX-4. Lab II measurements always included the SXR.

Lab	*Thursday*	*Friday*	*Monday*	*Tuesday*	*Wednesday*
I	A	B	C	D	E
II	B $L(\theta)$	C $L(\theta)$	D $L(\lambda)$ w/photom.	E $L(\lambda)$ w/746	A $L(\lambda)$ w/746
III	C	D	E	A	B
IV	D	E	A	B	C
V	E Slit-Scattering	A λ Calib.	B Lamp Irradiance	C Point Spread	D Spectral Resp.

the particpants was selected to do hands-on work in the laboratories, and another small group was selected to observe the work. In general, everyone got a chance to see some aspect of the laboratory exercises. The group designations and the laboratory exercises involved in SIRREX-4 are shown in Table 1.

In addition to splitting the day into morning lectures and afternoon laboratory exercises, time was allotted at the end of the day for the presentation of daily rapid results, so everyone could quantify how well the exercises were progressing and then discuss any aspect of the day's activities. Videos of laboratory setups and the morning lectures were shown after dinner, and these served as another discussion opportunity for the particpants. Every effort was made to provide a variety of settings for discussion and an exchange of ideas. The individuals involved with SIRREX-4, and their differing modes of participation, are listed in Appendix D.

2. LAB I: MONOCHROMATORS

The principal objective of Lab I was to determine the responsivity of a spectroradiometer and the spectral radiance of an unknown integrating sphere source. A highly automated low level radiance (LLR) mapping spectroradiometer (Walker and Thompson 1995a) at NIST was used to illustrate the techniques for determining a spectroradiometer's responsivity with a source of known spectral radiance and by utilizing this responsivity, determine the spectral radiance of an unknown sphere source. The mapping spectroradiometer's source table is equipped with x, y, and z linear translation stages which can programmably position either source at the focal plane of the monochromator and its foreoptics. The monochromator itself was equipped with a silicon photodiode detector.

The known sphere source, an Optronic Laboratories, Inc. (OL) model 420 (hereafter designated as Opt420), is a highly uniform internal NIST secondary standard whose spectral radiance was determined at the Facility for Automated Spectral radiometric Calibrations (FASCAL), described by Walker et al. (1987b). The Opt420 has also been used to calibrate the SXR. The sphere source with an unknown spectral radiance was a Photo Research Model LS6E, designated as Spec4020. The two sphere sources were operated in constant current (Walker and Thompson 1995b) mode at 5.8000 A for the Spec4020 and at 6.5000 A for the Opt420.

The procedure was to scan the monochromator (5 nm bandpass) once from 380–900 nm at 20 nm intervals and measure the signal from both sphere sources at each wavelength. The number of readings at each wavelength was five, both for signal and the shutter readings. This complement of measurements was carried out on May 4, 5, 8, 9, and 10.

The general measurement equation governing the response of the instrument to incident radiation is given by

$$S(\lambda) = L(\lambda)R(\lambda) \tag{1}$$

where λ is the wavelength, $S(\lambda)$ is the output signal, $L(\lambda)$† is the spectral radiance of the source, and $R(\lambda)$ is the responsivity of the instrument. The responsivity of the instrument, as determined by the measurements of the Opt420, is given by

$$R(\lambda) = \frac{\hat{S}(\lambda)}{\check{L}(\lambda)} \tag{2}$$

where $\hat{S}(\lambda)$ is the output signal of the known source and $\check{L}(\lambda)$ is the spectral radiance predicted from the known source. The two sphere sources that are being measured in this experiment are very similar in spectral shape and intensity, so any linearity or stray light effects will also be similar. The radiance of the unknown source Spec4020 is given by

$$\tilde{L}(\lambda) = \frac{\tilde{S}(\lambda)}{R(\lambda)} \tag{3}$$

where $\tilde{S}(\lambda)$ and $\tilde{L}(\lambda)$ are the output signal and the spectral radiance, respectively, of the unknown source.

The spectral responsivity of the LLR spectroradiometer, as calculated by (2), is shown in Fig. 1. There are two distinct regions in this curve. The first, a broad peak centered about 575 nm is largely controlled by the grating blazed at 500 nm with some shift in the maximum imparted by the responsivity curve of the silicon detector. The second region, at wavelengths longer that 820 nm is largely

† The usual notation for spectral radiance is $L_\lambda(\lambda)$, but for consistency with previous documents, $L(\lambda)$ is used throughout this report.

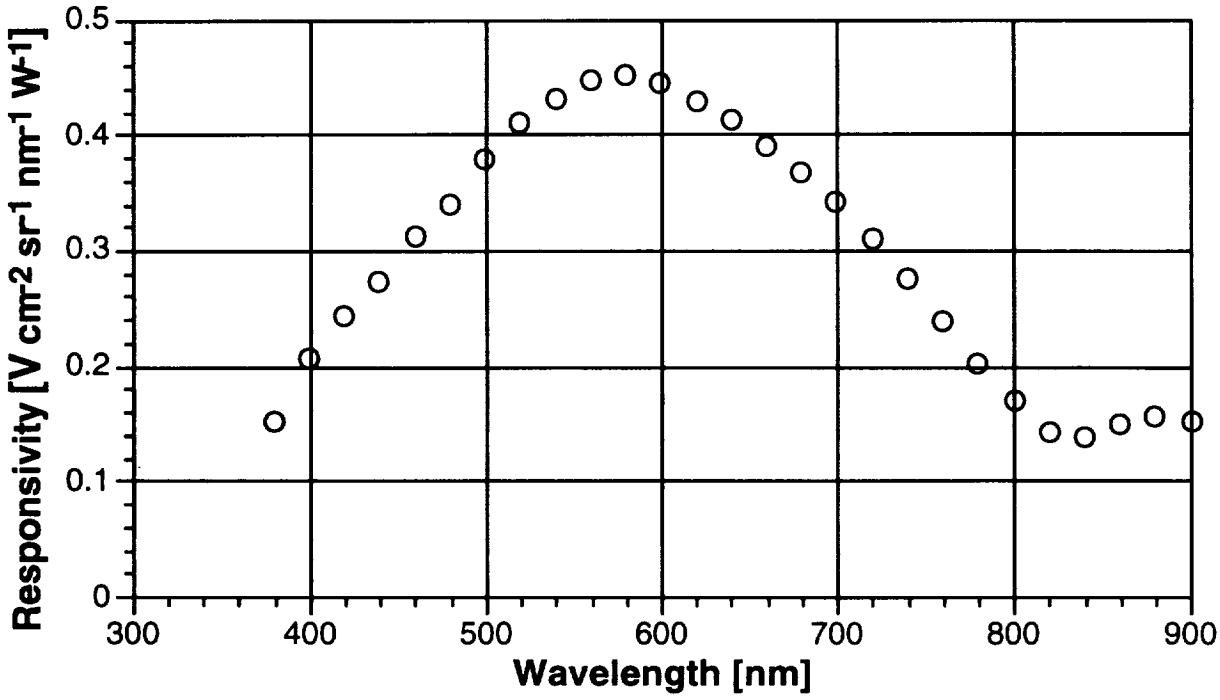

Fig. 1. Spectral responsivity of the LLR spectroradiometer.

controlled by the high responsivity of the silicon detector in this wavelength region. Using (3), the radiance of the unknown source can be calculated from the responsivities in Fig. 1 and this is shown in Fig. 2. As can be seen in Fig. 2, the Spec4020 has a much higher output and a higher color temperature than the Opt420. Since these same operations were carried out over five days, the stability of the spectroradiometer system can be assessed. The result of this assessment can be seen in Fig. 3.

The responsivity of the instrument varied in a wavelength dependent fashion by 0.12% at short wavelengths to about 0.02% at wavelengths greater than 800 nm. The variablity of the determinations of the unknown's spectral radiance was significantly less at wavelengths longer than 440 nm. The difference in the variability between the responsivity and the source radiance can be explained by the method of determination of the values of responsivity and radiance. The instrument and detector are not temperature controlled and therefore some variation in responsivity is to be expected due to fluctuations in the room temperatures. The determination of the radiance of the unknown is essentially a determination of the ratio of the two sphere source signals which are measured sequentially. This compensates for variations in the instrument responsivity. If the determination of the unknown's radiance was dependent on a single determination of the instrument responsivity, then the variability of that radiance would be much larger.

3. LAB II: SPHERES

The principal objective of the Lab II exercise was to demonstrate spectral radiance field calibration procedures for the GSFC integrating sphere using three different instruments: the SXR in the spectral range 411–775 nm, a calibrated photometer, and the GSFC OL 746 spectroradiometer measuring in the spectral range 380–900 nm. The latter was fitted with an integrating sphere irradiance collector (ISIC). The GSFC sphere had been calibrated for spectral radiance at NIST shortly before the SIRREX-4 laboratory exercises by comparison to a spectral radiance standard gas-filled strip lamp (Early and Johnson 1996). The four results, the three SIRREX-4 field calibration simulations, and the NIST calibration were intercompared to demonstrate the uncertainties inherent in field calibrations.

3.1 Sphere Source

The GSFC source is a 107 cm (42 inch) diameter barium sulfate coated sphere with a 39.5 cm (15.5 inch) diameter circular exit aperture. The sphere is internally illuminated by up to 16 baffled 45 W quartz halogen lamps positioned uniformly along the vertical circumference of the sphere. Each bank of four lamps is controlled by a precision current source. To provide the necessary dynamic range for SeaWiFS radiance calibrations, which are scheduled to occur approximately 4–8 weeks before the launch of the SeaWiFS

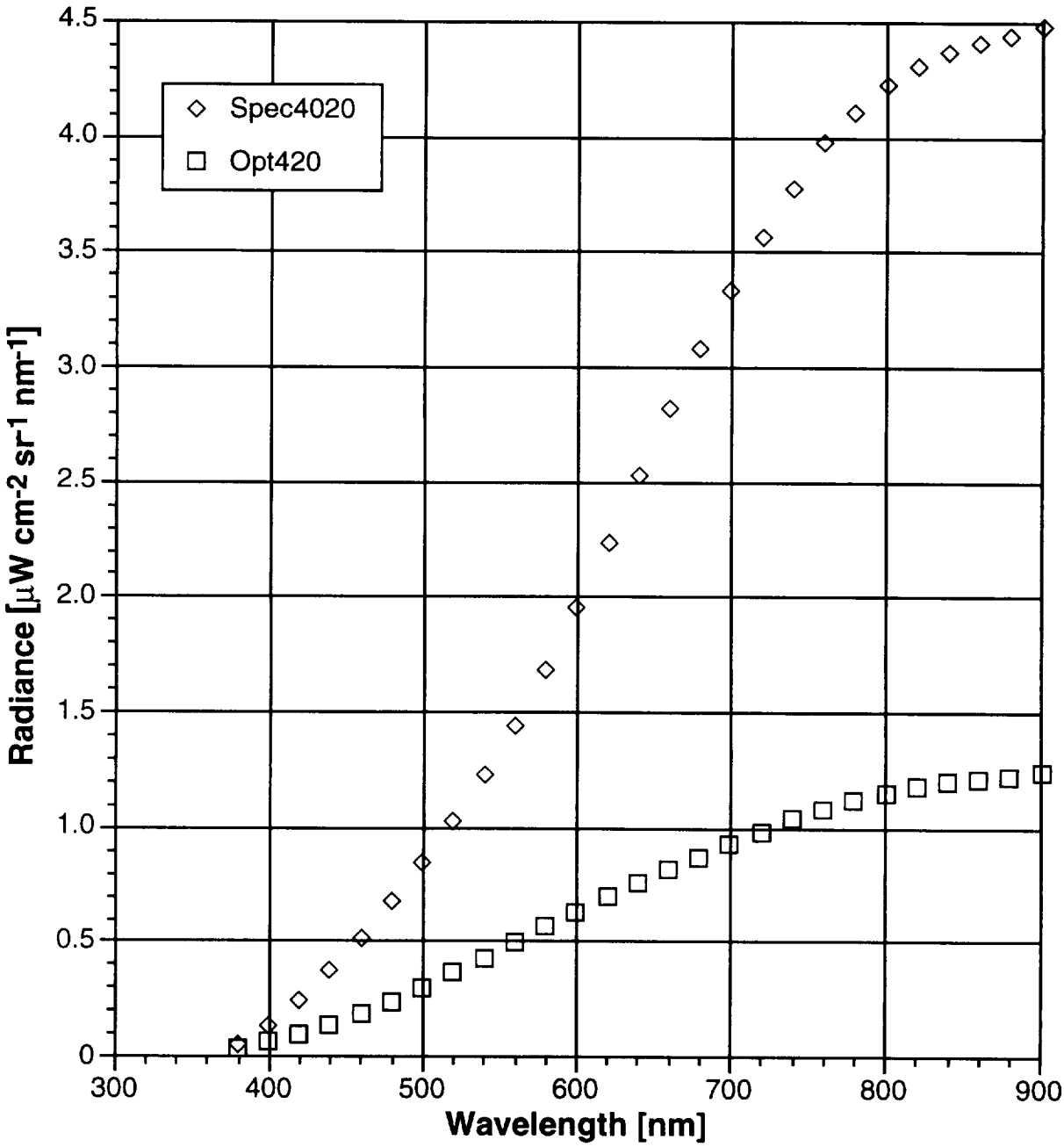

Fig. 2. Spectral radiance of the two integrating spheres (in units of $\mu\mathrm{W\,cm^{-2}\,sr^{-1}\,nm^{-1}}$).

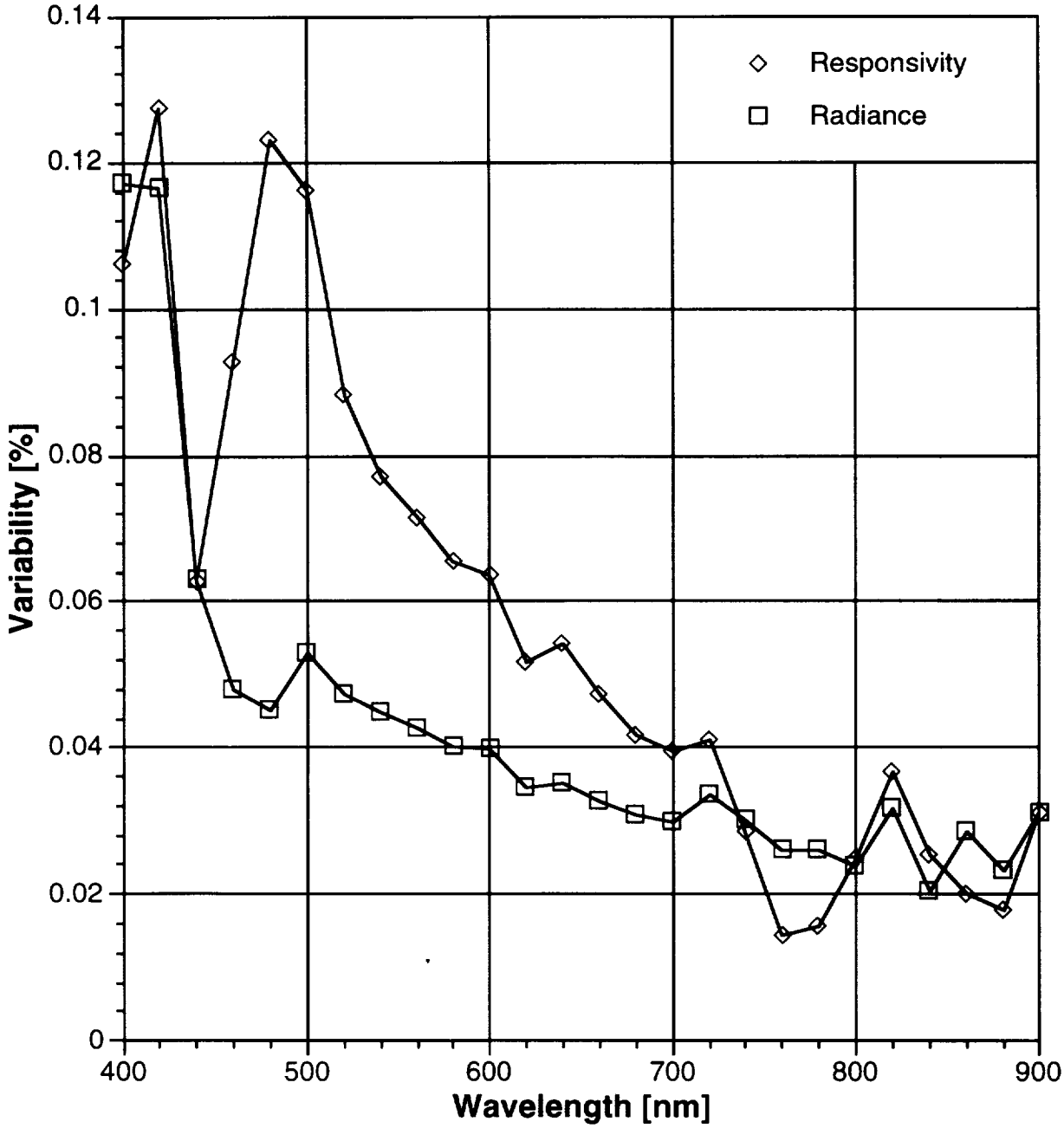

Fig. 3. Average variation in responsivity and radiance determinations. The quantity plotted is the standard deviation of the five days, normalized to the mean, calculated at each wavelength, and expressed in percent.

instrument, the sphere is calibrated and operated with 1, 4, 8, and 16 lamps on. At each dynamic range setting, the same lamps are always used to eliminate error due to variation between different lamps. The GSFC sphere is similar to the sphere described by Hovis and Knoll (1983).

In April 1995, the GSFC sphere was calibrated at NIST for spectral radiance in the range 380–1,100 nm at each of the four radiance settings by comparing the GSFC sphere radiance to the radiance of a gas-filled strip lamp transferring the spectral radiance scale maintained by FASCAL (Walker et al. 1987b). Details of the calibration procedure and results are reported elsewhere (Early and Johnson 1996).

Normally, sphere source stability is achieved by a two hour warm up at the chosen radiance setting (Cooper pers. comm.). This warm up time was shortened during laboratory exercises—typically to about 30 minutes—to minimize lamp utilization and thus preserve the NIST spectral radiance calibration, which may not be reliable after 50 hours of lamp operation. In stepping down (from more lamps to fewer) the sphere source equilibrates within a few minutes. Thus the sphere is most efficiently and accurately used by always stepping down in radiance level (number of lamps on) following warm up. The standard procedure used in the laboratory exercises was to warm up the sphere with all 16 lamps on, make the required measurements, and then step down to fewer lamps on. This procedure had to be modified for some exercises as noted below.

The sphere was mounted on a frame permitting height and leveling adjustments. After positioning the sphere at an appropriate height, the sphere aperture plane was made vertical by leveling the frame against a bubble level held at various positions across the aperture cover. A plumb bob was used to mark the position on the laboratory floor directly below the aperture cover center indicator as a reference point for distance measurements required in various calibrations. The projection of the sphere aperture plane onto the laboratory floor was estimated by connecting marks on the floor made by plumb lines from the edges of the sphere aperture. A drafting triangle was used to mark the normal to the sphere aperture plane (through the marked center of the cover plate) on the laboratory floor. This line constituted the *optic axis* for the SXR measurements.

3.2 SXR Calibrations

The SXR was used to measure the sphere radiance on each of the five laboratory exercise days. In addition, on 4 and 5 May, the SXR was used to investigate the angular distribution of the sphere radiance.

The SXR is a six channel radiometer calibrated for spectral radiance over the approximate wavelength range of 400–800 nm (Johnson et al. 1996). Each measurement channel consists of a temperature stabilized silicon detector, a narrow bandpass interference filter, and a precision current-to-voltage amplifier. The instrument uses both refractive and reflective optics to image the approximately 2.4° full-angle field of view (FOV) onto the six detectors. The SXR can be bore-sight focused from approximately 0.85 m to infinity. The SXR has been used at SIRREX-2, SIRREX-3, the Marine Optical Buoy (MOBY) field site in Honolulu, and at Nippon Electric Corporation (NEC) in Yokohama, Japan.

All measurements with the SXR were made with the same digital voltmeter (DVM): a Hewlett Packard (HP) 34401A, serial number (S/N) 3146A28915. The SXR was controlled and the data logged using a Macintosh computer running custom software which sequentially recorded signals from each channel as selected by the operator. All of the relevant measurement parameters—including SXR detector and ambient temperature, number of samples averaged, SXR amplifier gain (unity in all measurements reported here), focus setting of the SXR lens, distance from the SXR to the sphere aperture, SXR orientation about the optical axis, number of sphere lamps burning, and any other relevant information—were recorded in each data file and in the laboratory notebooks. The SXR electronics and temperature control system, as well as the DVM, were warmed up for at least 24 hours before any measurements were made.

3.2.1 SXR Radiance Measurements

The SXR was mounted on a standard camera tripod providing height and rotation (or pitch and yaw) adjustments. Before each measurement, the SXR was carefully aligned to the sphere aperture plane center (as indicated by the cover plate center marking) by using the bore-sight. The height was adjusted by leveling the SXR case against a carpenter's level and adjusting the tripod height until the cover plate mark was centered in the SXR FOV. Focusing was achieved by first focusing the bore-sight for optimal sharpness of the field stop edges, as viewed through the eyepiece, and then visually focusing the objective lens on the aperture cover target. The first step is best achieved using a flashlight to illuminate the objective lens. This procedure is both subjective and dependent on the operator's visual acuity.

Different laboratory participants chose focus settings varying by 20% or more as indicated by the objective lens scale with the SXR in the same position. There was no appreciable difference in the SXR radiance measurements as a function of focus setting in these exercises. If the SXR is properly aligned and focused, the target radiance should underfill each highly uniform detector (neglecting small corrections due to the nonzero point-spread function of the instrument), so small variations in instrument focus should negligibly affect radiance measurements. To confirm the alignment procedures, it is imperative that all SXR data include the focus setting and distance from the source to the SXR.

The distance measurement was made from the face plate of the SXR (not the objective lens) to the target. In the laboratory exercises, this distance was measured by finding the point on the laboratory floor directly beneath the face plate of the properly aligned SXR using a plumb bob, and measuring the distance from this point to the corresponding sphere aperture reference mark on the floor. Most sphere radiance measurements were made with the SXR face plate approximately 1 m from the aperture plane (utilizing a focus setting of about 0.85–1.1 m depending on the operator). Some measurements were made with the SXR approximately 2.5 m from the aperture plane. As expected for radiance measurements on a nearly lambertian source (Section 3.1.2) there was no appreciable difference between closer and further view measurements. All measurements were made with the bore-sight lens cap blocking ambient light from entering the SXR through the alignment optics.

The SXR radiance measurements can be slightly dependent on the SXR orientation around the optical axis, since different channels have different point-spread functions, thus it is important to record the SXR orientation. The system used in these exercises was to indicate the *compass* position of the thermoelectric cooler (TEC) label on the SXR rear plate. TEC at the top of the rear plate is *north*, TEC at the bottom of the plate is *south*, etc. All measurements were made with the TEC label pointing north.

The typical measurement sequence consisted of 10 samples averaged for each of the 6 channels, requiring about 2 minutes. Usually this sequence was immediately repeated once or twice to collect more data. Rather than recording data for a longer time in each channel, this procedure permitted examination of possible short-term fluctuations in measured radiance in each channel. As expected, no such fluctuations were observed.

A complete measurement cycle included measurement of the dark current or *background* in each channel, which was acquired by executing the following steps:

1) Placing the lens cap over the objective (and with the bore-sight cap in place as always);
2) Removing the lens cap and measuring the ambient light scattered out of the sphere into the SXR, obtained at the end of the exercise with all the lamps turned off; and
3) Measuring the sphere radiance with the desired number of lamps on.

To reduce the ambient light field, the laboratory room lights were turned off during the measurements. Ambient light remained from the control computer monitor screen scattering off the white (rather shiny) walls of the laboratory.

Typical background (dark current) raw signals were approximately −3 mV in each channel and remained very stable throughout all the measurements. Typical ambient signals varied from about −3 to 6 mV depending on the channel. Sphere signal levels were approximately 170–570 mV (depending on the channel) per lamp, giving signal to ambient ratios of about 100 to 1. All signals were quite stable during measurement cycles. Typical standard deviations of about 10–100 μV were recorded, generally independent of the signal levels.

Over the five days of the exercise, the variation in the measured radiance values in each channel and at each lamp setting was about ±0.5%. The SXR radiance measurements were compared to the NIST spectral radiance calibration by interpolating the radiance calibration data (recorded at 10 nm intervals) to the effective SXR wavelengths using a cubic spline fit. Figure 4 summarizes the SXR radiance measurement results. Note there is a reproducible systematic difference between the sphere radiance measured by the SXR and the NIST radiance calibration, although, this difference is well within the mutual uncertainties of the calibration of the SXR itself and the NIST radiance calibration of the sphere (perhaps on the order of 0.5%). The reproducible wavelength-dependent differences, however, suggest systematic uncertainties in the SXR calibration, the NIST spectral radiance calibration of the sphere, the cubic spline calibration interpolation, or a combination of these factors.

3.2.2 SXR Lambertian Measurements

On 4 and 5 May, the SXR was used to investigate the dependence on observation angle of radiance from the GSFC sphere. The SXR measured the sphere radiance at angles of 0°, ±5°, ±10°, and ±15° from the sphere optic axis (as defined in Section 3.2).

Angles were measured in the horizontal plane, with the sphere optic axis defined as 0°. The FOV for the radiance measurement always passed through the sphere aperture center (as marked on the cover plate) and measurements at different angles thus sampled different portions of the back wall of the sphere. An alternative approach, not used in these exercises, would be to view the same portion of the sphere back wall at different angles with the SXR FOV passing through different portions of the sphere aperture plane.

The measurements in this exercise (viewing through the aperture center) investigate the uniformity of spectral radiance from different portions of the sphere back wall, treating the aperture plane as the apparent source. The alternative approach treats the sphere back wall as the apparent source and investigates the distribution of radiance from one portion of the back wall. Each technique provides different information that may be useful or critical for different uses of the integrating sphere. There was insufficient time during these exercises to make both types of measurements.

Using the sphere optic axis as previously defined, positions were marked on an arc on the laboratory floor corresponding to the desired viewing angles at constant distance from the sphere aperture center. Using a plumb bob

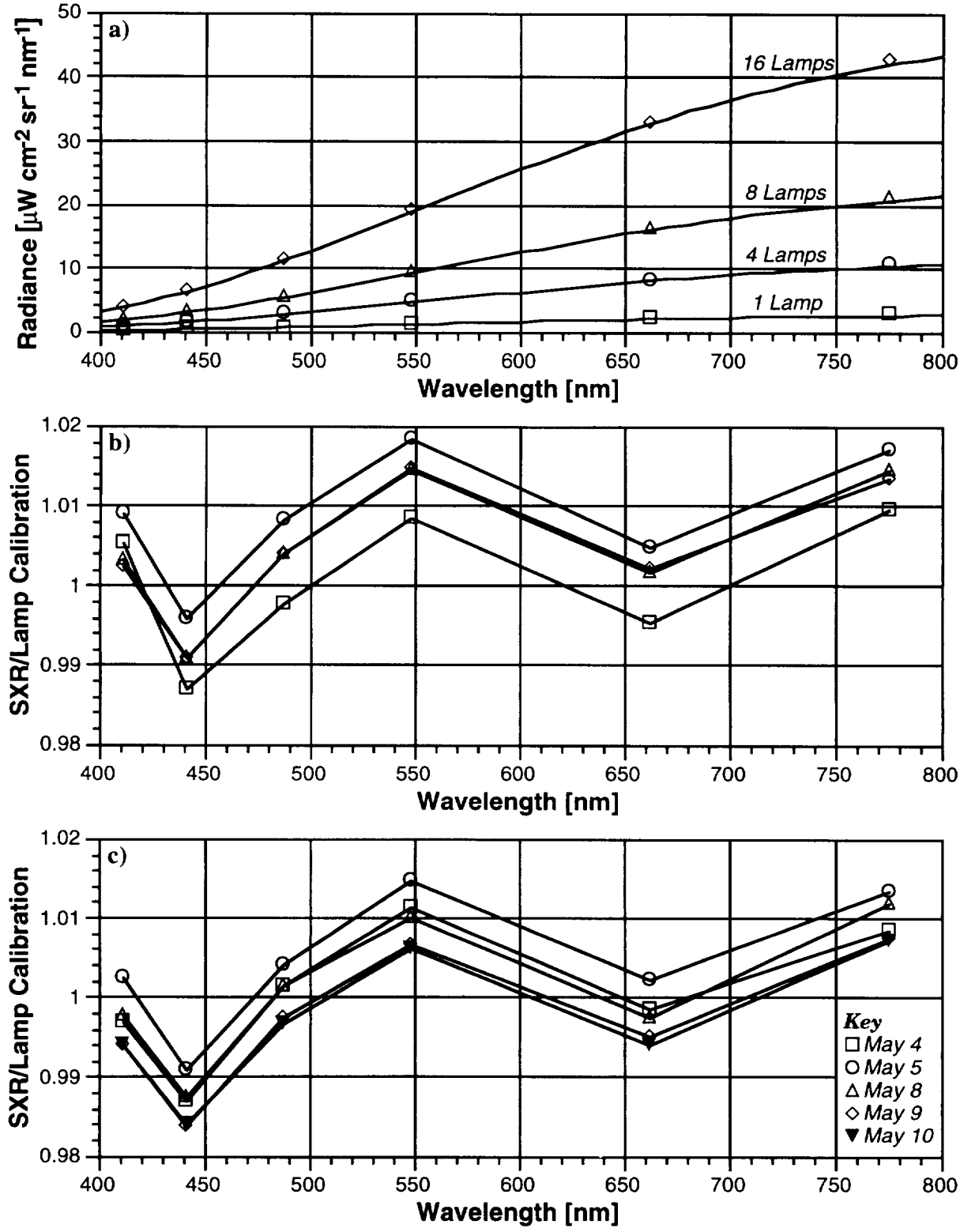

Fig. 4. Sample radiance calibrations using the SXR: **a)** the GSFC sphere measured on 5 May with the SXR at different lamp levels compared to the NIST calibration based on the standard gas-filled strip lamp, **b)** the ratio of the GSFC radiance calibration based on the SXR and the NIST calibration radiance on 5 May (same lamp codes as in panel **a)**, and **c)** the ratio of the GSFC radiance calibration (16 lamps) based on the SXR and the NIST standard radiance lamp over the five days of the laboratory exercises.

suspended from the SXR face plate, the SXR was positioned at the desired location, bore-sight aligned to the sphere cover center mark, and focused as previously discussed. This alignment procedure required several iterations of positioning the instrument using the plumb bob and then making small repositioning adjustments after visually aligning the SXR. Two arcs were used, one corresponding to a distance of approximately 1 m from the SXR face plate to the sphere aperture center, the other at a distance of about 2.5 m. Along each arc, positions were selected randomly to avoid possible systematic error due to the significant times between measurements at different positions.

The results are summarized in Fig. 5 showing the GSFC relative spectral radiance (16 lamps on) as a function of SXR azimuthal viewing angle at a viewing distance of 99.5 cm from the sphere aperture center, measured on two different days. Several measurement cycles (as described above) were made at each position and the average values are shown in Fig. 5. Dark current readings were recorded for each measurement cycle, but only a single ambient measurement was recorded with all sphere lamps off. The results are normalized to the 0° measurements (along the sphere optic axis), and are quite consistent across the six spectral channels. Studies at different lamp settings could not be made due to the limited laboratory time, the lengthy SXR alignment procedure, and the need to make several other types of measurements.

The approximately 1% peak-to-peak apparent relative radiance variation across the 30° of viewing angle depends on both the nonuniformity of the illumination of the sphere back wall and the FOV (approximately 2.4°) of the SXR. Smaller FOV measurements would be necessary to better spatially resolve the sphere wall radiance variations. These results are in excellent agreement with the findings at SIRREX-3 (Mueller et al. 1995).

3.3 Photometer Calibration

On 8 May, a calibrated NIST photometer was used to measure the GSFC sphere radiance using the *two-aperture* method (Appendix A) of converting irradiance measurements to radiance. The purpose of this exercise was to corroborate the radiance measurements using an independent detector-based technique and to instruct the participants in the use of photometers and photometric units. The SXR was also used to measure the sphere spectral radiance on 8 May.

The NIST photometer is a filter radiometer closely approximating the relative spectral transmittance of the photopic $V(\lambda)$ curve with a filter, a silicon photodetector, a precision transimpedance amplifier, and a precision field stop aperture (Cromer et al. 1993). The photometer was calibrated at NIST for illuminance ($\mathrm{lm\,m^{-2}}$) against the NIST standard photometric scale, with the spectral responsivity of the photometer was measured at the NIST Spectral Comparator Facility (Fig. 6).

3.3.1 Photometric Units

The photometer was used to measure the GSFC sphere illuminance, which indirectly corroborates the NIST spectral radiance calibration of the sphere. Using the measured sphere spectral radiance (Early and Johnson 1996), the spectral irradiance at the photometer aperture was calculated from knowing the areas of the two apertures and the distance between them (Appendix A). Since the spectral responsivity of the photometer was also known, the sphere illuminance incident on the photometer could also be predicted, by multiplying the spectral irradiance by the spectral response of the photometer and integrating over wavelength, and compared to the directly measured illuminance. The good agreement (0.4–0.6%) between the predicted and measured illuminances corroborated the spectral radiance calibration as well as the NIST photometric scales. Walker et al. (1991) have demonstrated the efficacy of this technique which was used at SIRREX-1 and the agreement was approximately 1% (Mueller 1993). A similar procedure has been used to corroborate filter radiometers for radiance temperature scale realizations (Tsai et al. 1995).

In the sphere measurement, the sphere source radius r_1 was 0.1975 m, the photometer aperture radius r_2 was approximately 0.0015 m, and the separation distance d was 1.828 m, giving $\delta \approx 10^{-8}$ (Appendix A), which was neglected in the calculations. The expected illuminance was calculated by fitting a 1 nm interval cubic spline to the measured spectral radiance at each lamp setting, and was compared to the measured illuminance with the sphere operating at 16, 4, and 1 lamp on (the 8 lamps on setting was omitted due to time constraints). The results are summarized in Table 2.

Table 2. Illuminance measurement of the GSFC sphere.

Lamps On	Illuminance [$\mathrm{lm\,m^{-2}}$]		*Percent Difference*
	Measured	*Predicted*	
1	33.773	33.564	0.623
4	132.930	132.400	0.401
16	546.820	544.040	0.511

To measure the sphere illuminance, the photometer was placed in a custom mount on a tripod and aligned along the sphere optic axis marked on the laboratory floor. A careful attempt was made to align the photometer aperture parallel to, and coaxial with, the sphere aperture based on length measurements and visual inspection of the arrangement. An attempt was made to align the photometer using retroreflections of a helium-neon (HeNe) laser (633 nm) off the photometer filter front face, but the low red reflectance of the filter package and small size of the aperture defeated this attempt.

The photometer was used with the amplifier set to the same gain (10^7) used in the illuminance calibration. The

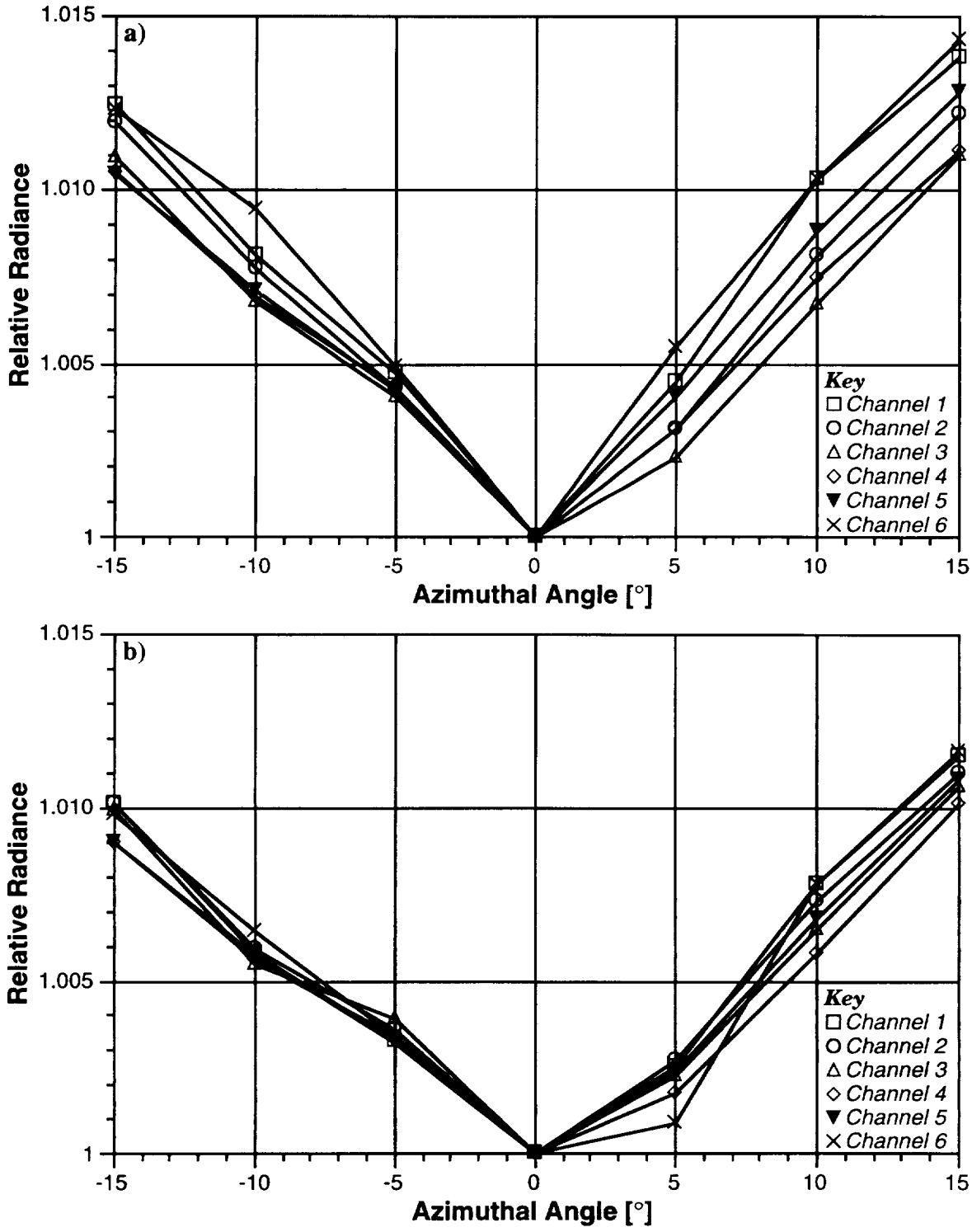

Fig. 5. The spatial distribution of the GSFC sphere radiance (16 lamps) as a function of the SXR azimuthal viewing angle through the sphere aperture center relative to that at 0°, recorded on two different days: **a)** 4 May, and **b)** 5 May.

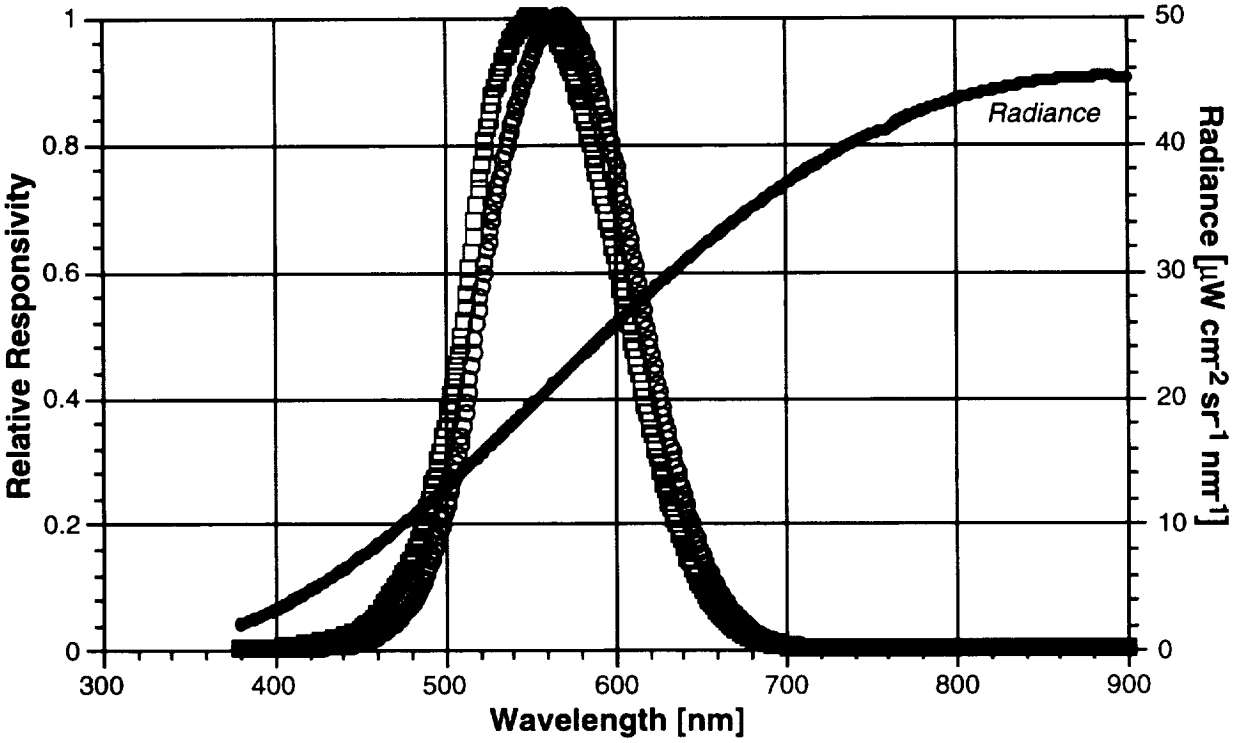

Fig. 6. Photometer spectral responsivity (squares) and the product of the spectral responsivity and the radiance (circles) plotted with GSFC sphere radiance (16 lamps from the NIST spectral radiance calibration). Both responsivity curves are normalized to the maximum values.

photometer voltage signal was read using the same DVM and data collection software as was used for the SXR. As with the SXR, a measurement cycle included measurement of the signal while the photometer was illuminated by the sphere, while the photometer was covered with a light-tight cap (dark current or background), and while the photometer observed the sphere with all lamps off (ambient light reflected by the sphere). The photometer has a rather large FOV (at least 18°) so extra attention was given to baffling the area around the sphere aperture with black cloth and eliminating as much ambient light as possible.

The measurement distance (approximately 1.8 m) was chosen to give a strong but unsaturated signal with all 16 lamps on, and also to ensure that the entire sphere aperture was contained within the photometer's FOV, which had not been measured before the exercise. The aforementioned 18° estimate for the photometer FOV comes from knowing the separation between the detector and the aperture in the photometer. The FOV was indirectly investigated by varying the measurement distance d until the measured and predicted illuminance showed significant variation. At a separation of approximately 0.9 m, the measured illuminance was approximately 2% smaller than predicted, implying that the photometer FOV was insufficient to observe the entire sphere aperture (subtending about 25° at this distance). At separation distances between about 1.2–4 m, the measured and predicted illuminances agreed to within a few tenths of one percent, implying that the photometer FOV is between about 20–25°, sufficient to include the entire source aperture for separations greater than approximately 1.2 m.

3.4 Calibrations Using the OL 746

On 9 and 10 May, the OL 746 was used to make spectral radiance calibrations of the GSFC sphere in the 380–900 nm range using the two-aperture method. The SXR radiance calibrations were also continued. This exercise was intended to demonstrate the calibration and use of the OL 746 in field spectral radiance calibrations, and to compare the laboratory spectral radiance calibration results with the NIST spectral radiance calibration based on a standard gas-filled strip lamp.

3.4.1 Spectroradiometer

The OL 746 is a single grating monochromator with selectable entrance and exit slits, a choice of different detectors and order sorting filters, a precision transimpedance amplifier, integrated chopper, and phase-sensitive detection electronics. For spectral irradiance measurements, a 10.2 cm (4 inch) diameter halon-coated integrating sphere with a 2.5 cm (1 inch) diameter input aperture is affixed to the entrance slit. When equipped with an integrating sphere (irradiance collector) mounted on the entrance slit,

it is designated the OL 746/ISIC. A grating carousel permits selection of one of three different gratings to cover a broad spectral range. The spectroradiometer operation is automated using a personal computer running software developed at GSFC. Further details and results about the configuration and operation of the OL 746/ISIC can be found in Section 6.

The spectral range 380–900 nm was used in this exercise, representing mutual overlap between the NIST spectral radiance calibration of the GSFC sphere, the spectral irradiance calibration of the FEL lamp used to calibrate the OL 746, and the effective wavelength range of the SXR. This spectral range was covered using the 1,200 lines/mm (500 nm blaze) grating, 1.25 mm wide entrance and exit slits, and the silicon detector in the OL 746, with order-sorting filters automatically switched in during wavelength scans.

In all measurements made with the OL 746, the phase angle in the phase-sensitive detection system was properly set (as described in Section 6), wavelength scans were made from 380–900 nm in 10 nm increments, and up to 20 readings were averaged at each wavelength to obtain sufficient signal-to-noise ratios (SNRs). The instrument was warmed up for at least 18 hours before all measurements. In addition to measurements of the source signal (either the FEL lamp for calibration or the GSFC sphere), measurements were made of the background signal (or dark current, with the cover obscuring the integrating sphere entrance aperture) and the ambient signal (viewing the unilluminated GSFC sphere or FEL lamp), and the net signal was calculated as source signal minus.

The OL 746 was used to transfer a spectral irradiance calibration from an FEL irradiance standard lamp to the GSFC sphere, and the spectral irradiance measurements converted to spectral radiance using the two-aperture method.

3.4.2 Alignment and Calibration

The 746/ISIC is mounted on a platform that can rotate 90° to sequentially observe the FEL calibration source and the target source (GSFC sphere). The spectroradiometer on its platform was mounted on a small, portable optical table placed near the GSFC aperture. Using the provided alignment laser (which temporarily replaces the input sphere) and FEL lamp mounting jig with the mount placed on an optical rail, the FEL jig center was aligned to the laser defining the nominal optical axis of the input sphere. Retroreflection of the laser from the alignment jig assured that the jig was normal to the optical axis. The input sphere was replaced and the laser relocated and directed through the alignment jig center to the marked center of the sphere aperture cover. Retroreflection of the laser from a plane mirror placed on the input sphere aperture cover was used to ensure that the sphere aperture plane was normal to the previously defined optical axis. Finally, the provided spacing bar (nominally 50 cm long) was used to position the FEL alignment jig at the calibration distance from the input sphere aperture.

FEL lamp F316, calibrated for spectral irradiance by OL, was placed in the aligned mount and slowly ramped up to the calibration current of 8.00 A, as measured by a DVM (model HP 34401A) sampling the signal across a precision 0.01 W resistor. A system of baffles, 40 cm square, with a rectangular aperture (3×8 cm^2) was placed midway between the sphere aperture and lamp to limit the scattered light reaching the input sphere. Additional black cloth baffling was also used to reduce scatter from nearby and background surfaces. After the lamp had stabilized at 8.00 A for approximately 15 minutes, the 746/ISIC was calibrated from 380–900 nm. In addition to dark current and ambient signal measurements, a system shutter measurement was recorded with the FEL lamp on but the baffle aperture obscured with several layers of opaque black cloth.

Originally, FEL lamp F268 was to be used for the spectral irradiance calibration of the 746/ISIC, but this lamp failed during the calibration procedure on 9 May, and FEL lamp F316 was substituted.

3.4.3 Radiance Calibration of GSFC Sphere

Immediately following the spectral irradiance calibration of the 746/ISIC, the mounting platform was rotated to direct the spectroradiometer input sphere aperture toward the GSFC aperture. The optical table height and position were adjusted until the spectroradiometer input sphere aperture and GSFC sphere aperture were parallel and coaxial, indicated by use of a double-pointed alignment bar provided for this purpose, making the separation between the aperture centers 0.718 m.

The spectral irradiance of the GSFC sphere was measured with the spectroradiometer input sphere properly aligned. Dark current (spectroradiometer sphere aperture obscured) and source signal (16 lamps on) measurements were made, and the measurement cycle repeated as the GSFC sphere was stepped down through 8, 4, and 1 lamp on. An ambient signal was measured after all GSFC lamps were extinguished.

Previous users of the 746/ISIC have expressed concern over the temporal stability of the irradiance calibration of the instrument (Mueller et al. 1995). The complete measurement cycle (alignment and measurement with 16 lamps through no lamps on) was completed in approximately 90 minutes following the end of the spectroradiometer calibration. The optimal procedure would be to calibrate the spectroradiometer against the FEL lamp before each measurement cycle (each GSFC lamp setting), but there was insufficient time in this exercise.

A cubic spline fit to the FEL spectral irradiance calibration data was used to calibrate the 746/ISIC for absolute irradiance responsivity at the measurement wavelengths (380–900 nm in 10 nm intervals). The two-aperture

method (Appendix A) was used to determine the GSFC sphere spectral radiance $L(\lambda)$ from the measured spectral irradiance $E(\lambda)$. The wavelength offset of the 746/ISIC was measured in a separate laboratory exercise during SIREX-4 (Section 6). With the 1.25 mm wide entrance and exit slits, the actual monochromator wavelength λ_a as a function of the indicated wavelength λ_i is given (in nanometers) by

$$\lambda_a = \lambda_i - 0.61761 + 3.7110 \times 10^{-3}\lambda_i - 2.3770 \times 10^{-6}\lambda_i^2 \quad (4)$$

corresponding to an offset of about 0.4–0.8 nm over the 380–900 nm spectral range. Cubic spline fits were made of the FEL spectral irradiance calibration and the NIST spectral radiance calibration to include the actual measurement wavelengths of the OL 746.

The results for 10 May are summarized in Figs. 7 and 8, comparing the 746/ISIC spectral radiance calibration of the GSFC sphere with the NIST spectral radiance calibration based on a radiance standard lamp. (The results from 9 May were essentially the same.) The results below 400 nm have very large uncertainties because of the very low SNRs (on the order of one). The spectral radiance measurements of the GSFC sphere based on the 746/ISIC data, however, are consistently higher at longer wavelengths than the NIST spectral radiance calibration values. The source of this discrepancy is currently not known.

One possibility for the discrepancy is that the 746/ISIC measurements were not sufficiently baffled. The spectroradiometer input sphere has an essentially hemispherical FOV. Ideally, good baffling should be used to limit the input sphere FOV, suppress the background scatter, or to permit a system shutter measurement (see Fig. 25). None of these options were practical during this exercise, but they should be seriously considered when the 746/ISIC is used for mission-crucial measurements. It may be speculated that in this exercise, the poorly baffled laboratory environment (gloss enamel paint, linoleum floors, etc.) more efficiently scattered longer wavelength light into the spectroradiometer input sphere, resulting in anomalously large GSFC sphere radiance values at longer wavelengths. Additional investigation is needed to determine the actual source of these discrepancies. Good agreement between the 746/ISIC and the SXR was achieved at SIRREX-3 under similar conditions, but the room walls at CHORS are painted black (Mueller et al. 1995).

3.4.4 SXR Measurements

The SXR was used as on the previous days to measure the GSFC spectral radiance. The 9 and 10 May SXR measurements differed from the previous measurements in that the warm-up time for the GSFC sphere was reduced. Because the alignment procedure for the 746/ISIC was so lengthy, and because the 746/ISIC set-up blocked the SXR measurements, it was impractical to make both 746/ISIC and SXR measurements sequentially at each GSFC sphere lamp setting. Instead, the 746/ISIC was used for a complete measurement cycle (step-down from 16 through no lamps on) after a lengthy warm-up of the GSFC sphere. Then the GSFC sphere was reset to 16 lamps on for about 15 minutes before the first SXR measurement was made. Limited laboratory time and the need to limit lamp utilization prevented the optimal longer warm-up time. Nonetheless, over the five days of the exercise, the measurements agreed with the original SXR calibration to within 2% (Fig. 4c).

3.5 Uncertainties

A careful analysis of all measurement uncertainties has not been done. Such an analysis must include alignment and distance measurement uncertainties, statistical treatment of different signal levels for different measurements, and propagation of uncertainties through all calculations. However, the measurement results themselves can be used to grossly estimate the uncertainties.

The statistical uncertainties in the NIST calibration are less than 0.2% over 400–1,000 nm for 16 lamps on and less than 0.4% over 450–1,000 nm for 1 lamp on. The preliminary uncertainties in the radiance calibration of the SXR are on the order of 1–2% depending on the measurement channel.

Another source of uncertainty is the need to interpolate calibration data to the actual measurement wavelengths of the SXR and 746/ISIC. The interpolated value at a particular wavelength can vary depending on the type of nonlinear interpolation used and the presence of features at specific wavelengths. Cubic splines were used in this exercise primarily for convenience, and are not necessarily the optimal choice of interpolating function. Preliminary modeling of simulated spectral radiance calibration data sets suggests that in these exercises, the cubic spline interpolation uncertainties were not substantially larger than interpolation uncertainties based on single functional forms, such as the planckian times fifth order polynomial typically used to model spectral irradiance standards (Saunders and Shumaker 1977).

3.6 Conclusions

A principal conclusion is that the SXR radiance calibration of the GSFC sphere is corroborated by the NIST spectral radiance calibration based on a standard gas-filled strip lamp, within the mutual uncertainties of the two calibration methods. This result suggests that even under suboptimal conditions, such as what may be experienced under field conditions (laboratory with inadequate baffling, shorter than recommended GSFC lamp warm-up, alignment and operation of SXR by inexperienced personnel),

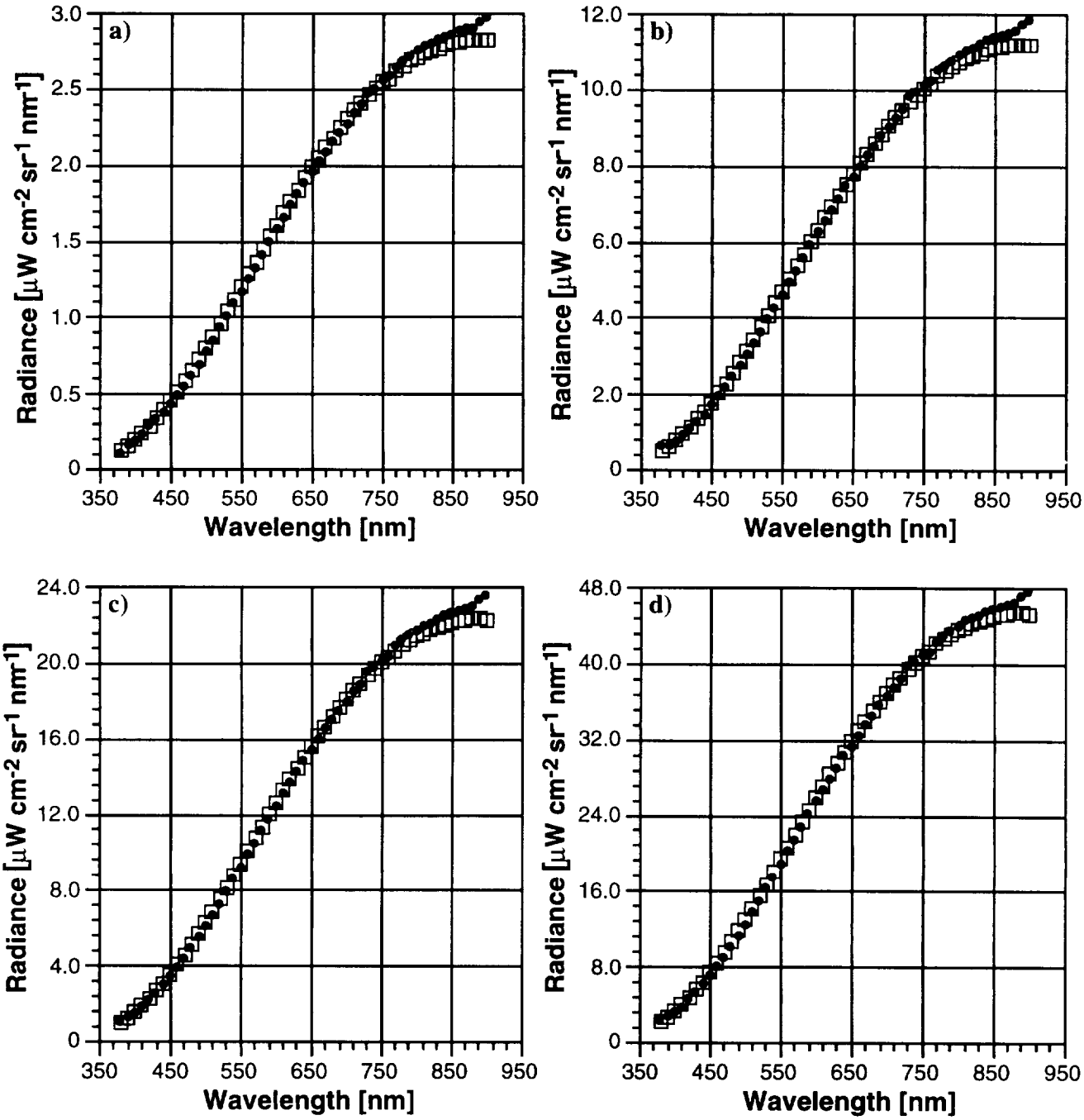

Fig. 7. A comparison of GSFC spectral radiance calibration based on 746/ISIC measurements (solid symbols) and the NIST spectral radiance calibration using a standard gas-filled strip lamp (open symbols). The radiance values from the two calibrations are shown for **a)** 1 lamp, **b)** 4 lamps, **c)** 8 lamps, and **d)** 16 lamps.

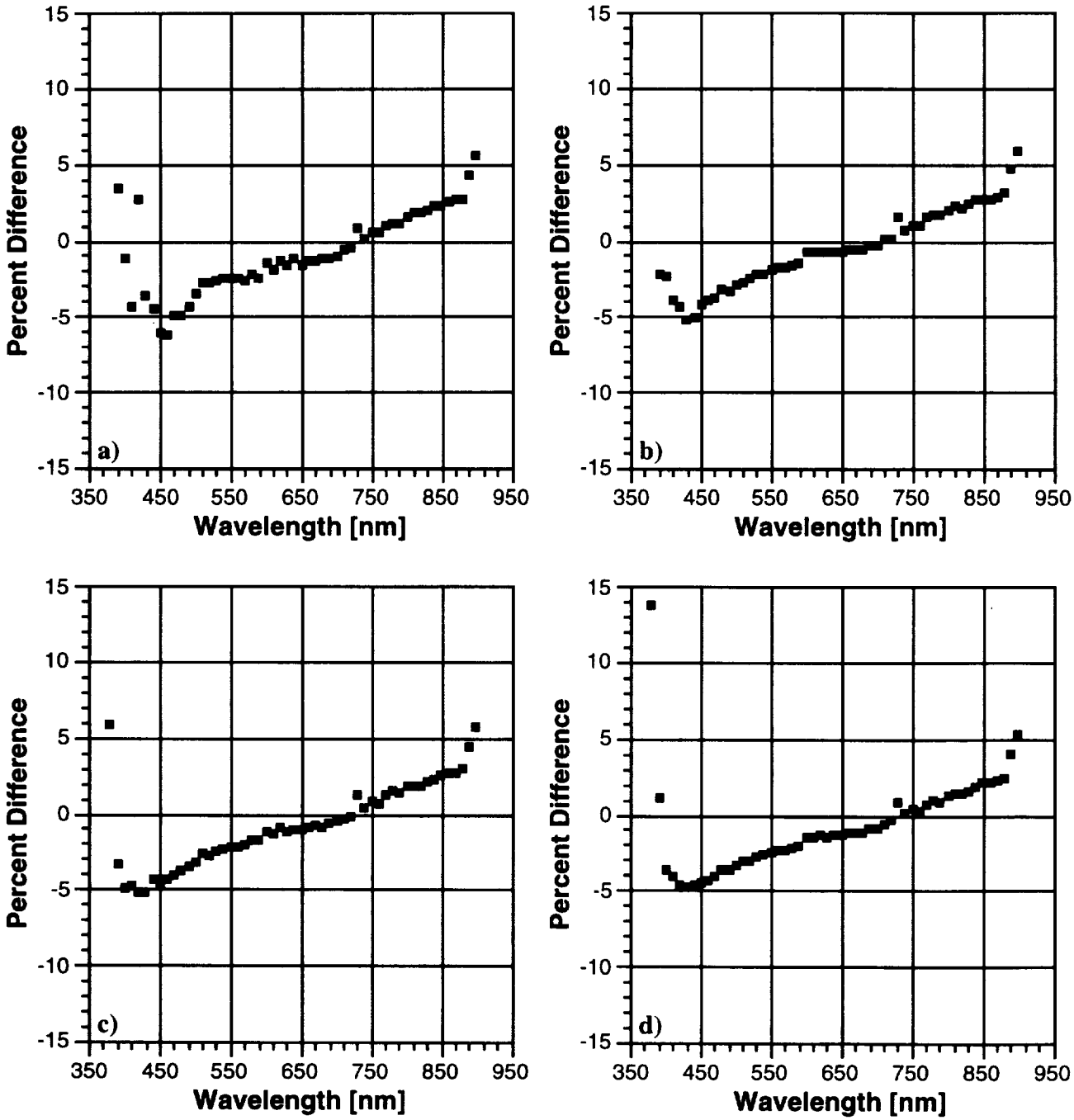

Fig. 8. Percent difference between the radiance calibrations shown in Fig. 7. The values shown are for a) 1 lamp, b) 4 lamps, c) 8 lamps, and d) 16 lamps. The quantities plotted are the 746/ISIC measurements minus the NIST calibration values, normalized to the NIST calibration values and expressed in percent.

the SXR can be used for meaningful radiance measurements. The measurements also suggest that the SXR and GSFC sphere remained stable within a few tenths of one percent over the five days of the exercise, including many alignments, measurement cycles, and gross movements of the SXR (such as to different laboratories for other measurements).

The photometer measurements indirectly corroborate the NIST spectral radiance calibration of the GSFC sphere as well as the NIST photodector scales. The photometer cannot, of course, provide information about the spectral distribution of radiance from the GSFC sphere. The photometer is rugged and simple to use, however, and may be useful as both a quick check and independent corroboration of sphere spectral radiance. For example, it can be used to indicate the possibility of radiance drifts due to lamp aging or other problems. The corroboration of the spectral radiance calibration also indirectly corroborates the SXR measurements which are commensurate with the radiance calibration.

The results of the calibration based on the 746/ISIC spectroradiometer were less satisfying. Under the conditions of the Lab II exercise, the spectral radiance calibration realized by the 746/ISIC appears to have an uncertainty on the order of ±5% compared to the other calibrations. There appear to be significant systematic, wavelength dependent discrepancies between the 746/ISIC measurements and the other techniques, however. As previously discussed, these results may indicate inadequate baffling during the measurement, but further study is needed to better understand the behavior of the spectroradiometer. In the meantime, calibrations conducted with the 746/ISIC should be corroborated by at least one other independent technique before the results are accepted for mission-critical measurements.

4. LAB III: PLAQUES

The objective of the Lab III exercise was to demonstrate the spectral radiance scale realization technique using plaques, to assess the types of systematic errors that contribute in this method, and to instruct the participants in this technique. The laboratory was also a test of the calibration of the SeaWiFS Aircraft Simulator (SAS-II) instrument, since the spectral irradiance scale on the lamp was known and the spectral radiance at the viewing angle could be calculated; for this laboratory a simplified measurement equation was used to relate lamp irradiance to plaque radiance. Finally, the objective of the laboratory was to examine the methods of radiometric calibration of a filter radiometer if the relative spectral responsivity is known from ancillary methods.

The SAS-II seven-channel radiometer (MVD/OCR-200) and a 45.72 cm (18 inch) square Spectralon plaque (Labsphere SRT–99–180 S/N 13172) were provided by Satlantic. Satlantic also sent the calibration report for the plaque, as measured by Labsphere, for 8°/hemispherical spectral reflectance (measured at the time of purchase); PC software; manuals for the aircraft simulator; and the SAS-II data acquisition software. The software from Satlantic included a calibration file for the radiometer, a program for running the measurement (`SASVIEW`), and an ASCII conversion program (`ASCIICON`), since the raw data is saved as a binary file.

The radiometer has a 5° full-angle FOV (at the 50% value) in air. It is immersible, and when immersed, its full-angle FOV is 6.3°. A summary of the instrument's specifications, including the center wavelength (CWL) and bandwidth for each channel, are given in Table 3.

Table 3. Instrument specifications for the SAS-II upwelling radiance sensor. The in-air saturation values are in units of $\mu W\,cm^{-2}\,nm^{-1}\,sr^{-1}$.

Channel Number	*CWL* [nm]	*Width* [nm]	*Saturation Value*
1	412.83	20	20
2	442.89	20	20
3	490.44	20	20
4	510.58	20	20
5	554.42	20	20
6	668.66	20	10
7	682.58	10	10

An alignment laser, the standard source, and the target were mounted on an optical rail. The distance from the source to the target was 150 cm. The SAS-II was mounted on a tripod and set to 45° off axis from the target. See Fig. 9.

A microscope slide was mounted onto the vinyl covering the target to allow for retroreflections for ease of alignment. Using the slide, the laser was aligned perpendicular to the plaque. Then an alignment jig was mounted in the lamp holder. The output of the laser passed through the alignment jig and reflected off of the microscope slide, and came back to the laser orifice for alignment. Two people were needed for the alignment adjustments: one to hold the slide and vinyl against the target, and another to make adjustments in the lamp fixture or the laser. The mounts for the laser and lamp had adjustments for x, y, z, and rotation about x and y.

An innovative method for determining the 45° angle was implemented. A mount was made that had a meter stick affixed to it with a hole drilled through the meter stick at the 10 cm indicator. A microscope slide was mounted over the hole. The laser beam passed through the hole when the mount was positioned on the rail between the target and the laser. When the target was turned 45°, the distance between the 10 cm indicator and the reflection from the target onto the meter stick was the same as the distance between the target and the meter stick along the laser-lamp-plaque axis.

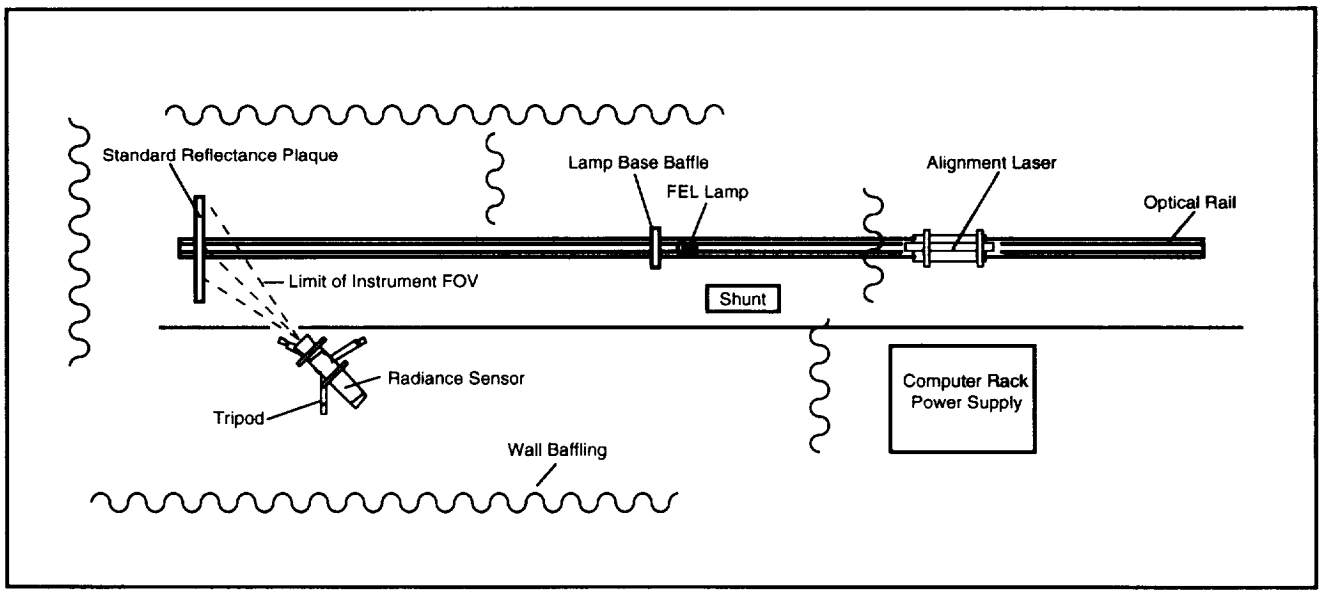

Fig. 9. Laboratory setup for plaque measurements.

The set-up, alignment, lamp warm up, data taking, and data analysis usually took 1.5 hours. The first set-up for each laboratory was typically where none of the parameters (distance, angle, etc.) were varied. The second set-up for the daily laboratory usually involved varying the distance, and sometimes varying the viewing angle of the radiometer for the target. Applying the r^{-2} correction for the distance tests would yield a similar answer from the first to second set up. Without the correction, a one or more percent change from one set-up to the next could be seen.

During set up, good laboratory procedures, such as, alignment, lamp handling, noncontact with the spectral reflectance standard's front surface, and lab book notation were all emphasized. The target came with a clear vinyl sheet covering the front surface that caused static build-up on the surface. Consequently, the surface was specked with dust, lint, and other foreign particles. The use of an aspirator was demonstrated as a good way to gently blow off the particles.

The time when the lamp was stabilizing was used for demonstrations and discussions about the care of the target, the construction of the plaque (the plaque was manufactured from two sections of Spectralon with a center seam along the vertical which did not join to produce a flush surface), and alternatives to the vinyl cover (such as a stand-off rigid frame with a tempered glass with a cross hair marked on it for alignment).

4.2 SAS-II Calibration

The spectral transmittances of the SAS-II filters were measured at Satlantic using a modified Cary-14 prism-grating monochromator. The illumination geometry was similar to that achieved using the apertures in the SAS-II radiometer. After the measurements, the radiometer was assembled and a source of known spectral radiance was used to assign a calibration coefficient to each channel. This calibration source was realized using a 1,000 W standard irradiance lamp, F360, (obtained from, and calibrated by, OL) and a diffuse Spectralon plaque (S/N 01873) from Labsphere. The plaque was illuminated at normal incidence from a distance of 1.5 m and the SAS-II instrument viewed the plaque at 45°. Baffling was used to eliminate stray light, and an on-axis baffle that blocked the direct flux from the lamp was used to estimate background signal. This calibration was performed at Satlantic on 12 April 1995.

After this measurement, the plaque 01873 was sent to Labsphere for revised reflectance measurements. At SIRREX-4, preliminary calibration coefficients (see below) for the SAS-II were used to determine the measured spectral radiance at the CWLs of the SAS-II using lamp F332 and Satlantic plaque 13172. Final calculations, which are reported here, were performed after the revised plaque (08173) data were available.

The measurement equation for a single channel of the filter radiometer measuring a source of spectral radiance $L(\lambda)$ is

$$S = \int L(\lambda) D(\lambda) d\lambda, \tag{5}$$

where S is the net counts or signal, $L(\lambda)$ is the spectral radiance of the source, and $D(\lambda)$ is the spectral radiance responsivity of the radiometer for the particular channel of interest.

Continuing the convention where calibration or known quantities are denoted by ($\hat{}$) and predicted values by ($\check{}$),

the calibration of the SAS-II, the average responsivity (calibration coefficient) was determined using

$$\overline{D} = \frac{\hat{S}}{\breve{L}(\lambda_c)}, \quad (6)$$

where λ_c is the CWL, $\hat{S}$ is known from a calibration measurement, and $\breve{L}(\lambda_c)$ is predicted from measurements of a source of known spectral radiance (the F360 lamp and 01873 plaque configuration). Satlantic calculated λ_c as the average of the wavelengths for which the filter response was 50% of the maximum value. These CWLs for the SAS-II are given in Table 3. This procedure is a variation of the method suggested in the SeaWiFS optical protocols (Mueller and Austin 1995), which defines the CWL in terms of the relative spectral responsivity of the radiometer.

The spectral radiance of a diffuse plaque illuminated by a standard lamp is (under several simplifying assumptions discussed further in Section 8),

$$\breve{L}(\lambda_c) = \frac{R(0°/45°, \lambda_c)}{\pi} \left(\frac{50}{\tilde{r}}\right)^2 \breve{E}(\lambda_c, 50 \text{ cm}), \quad (7)$$

where $R(0°/45°, \lambda_c)$ is the directional/directional reflectance factor (see Appendix B), $\tilde{r}$ is the (measured) distance from the lamp to the plaque in cm, and $\breve{E}(\lambda_c, 50 \text{ cm})$ is the spectral irradiance of the standard lamp at 50 cm interpolated onto λ_c. For the interpolation, Satlantic used Lagrange's formula for four consecutive data pairs as recommended by OL.

For the preliminary values for the reflectance factor (and hence the SAS-II preliminary calibration coefficients), Satlantic used 8°/hemispherical reflectances, $R(8°/h, \lambda)$, to estimate $R(0°/45°, \lambda_c)$. These values had been provided by Labsphere for plaque 01873 at the time of purchase. The final calibration coefficients were determined according to

$$F_{SL}^{-1} = \overline{D} = \frac{\hat{S}}{\frac{R(0°/45°, \lambda_c)}{\pi} \left(\frac{50}{\tilde{r}}\right)^2 \left|\breve{E}(\lambda_c, 50 \text{ cm})\right|_{F360}} \quad (8)$$

where F_{SL} is the inverse calibration coefficient given in Satlantic's product literature, $\left|\breve{E}(\lambda_c, 50 \text{ cm})\right|_{F360}$ is the spectral irradiance of standard lamp F360 at 50 cm interpolated onto λ_c, and the reflectance (R) factors for plaque 01873 were provided by the May 1995 Labsphere calibration before the plaque was cleaned.

For the SAS-II wavelengths, the average reflectance ratio $R(0°/45°, \lambda_c)/R(8°/h, \lambda)$ determined by Labsphere for plaque 01873 before they cleaned it was 0.990; after cleaning, this quantity increased to 1.004, which is equivalent within Labsphere's measurement uncertainties. The absolute value of $R(8°/h, \lambda)$ increased by about 0.8% and the absolute value of $R(0°/45°, \lambda_c)$ increased by about 2.2% with cleaning.

4.3 Satlantic Plaque Radiance Scale

Lamp F332, which is a 1,000 W standard irradiance lamp, was measured using the NIST FASCAL laboratory before SIRREX-4 and the spectral irradiance at 50 cm from the lamp on a coarse wavelength grid was assigned. The lamp was operated at 7.9 A and 110.8 V during this calibration. Next, the spectral irradiance data were fit to the model equation described by Walker et al. (1987a) or Saunders and Shumaker (1977)—a planckian times a polynomial (here a single linear term was sufficient):

$$E(\lambda, 50 \text{ cm}) = \left(\frac{a}{\lambda}\right)^5 \frac{1 + c\lambda}{e^{b/\lambda} - 1}. \quad (9)$$

This equation was used to predict the spectral irradiance at the SAS-II CWLs, $\breve{E}(\lambda_c)$. With $E(\lambda, 50 \text{ cm})$ known, then $L(\lambda_c)$ was calculated using

$$\breve{L}(\lambda_c) = \frac{1.02\, R(8°/h, \lambda_c)}{\pi} \left(\frac{50}{\tilde{r}}\right)^2 \left|\breve{E}(\lambda_c, 50 \text{ cm})\right|_{F332} \quad (10)$$

where $\tilde{r}$ is the measurement distance in Lab III, typically about 1.5 m, and $\left|\breve{E}(\lambda_c, 50 \text{ cm})\right|_{F332}$ is the irradiance measured with FEL F332.

The directional reflectance factors had to be estimated from the 8°/hemispherical data, since bidirectional measurements on plaque 13172 were not available at the time of SIRREX-4. Instead of assuming $R(0°/45°, \lambda)$ was 1.00 times $R(8°/h, \lambda)$, as had been done by Satlantic for plaque 01873 and the original (preliminary) calibration of the SAS-II, it was assumed that Spectralon is a nonlambertian diffuser with the general feature for the wavelengths used in this study $R(0°/45°, \lambda)$ is 1.02 times $R(8°/h, \lambda)$. This value was chosen because $R(0°/45°, \lambda)$ was found to be 1.015 times $R(8°/h, \lambda)$ at 550 nm for pressed polytetrafluoroethylene (PTFE) samples (Hsia and Weidner 1981) and it is not likely that Spectralon is more of a lambertian diffuser than pressed PTFE. This point is discussed further in Appendix B. These predicted spectral radiances, (10), are compared to the spectral radiances calculated from the measured signals and (6), $\breve{L} = \hat{S}/\overline{D}$ (using the final value for $\overline{D}$), and the results are shown in Table 4 and Fig. 10. The typical standard deviation for the SAS-II data was between 0.1–0.2% for all measurements.

In addition to a direct comparison of these results, Lab III considered (5) in more detail, since the relative spectral response data, $D(\lambda)$, had been provided along with the F_{SL} calibration factors. The general problem is that the measured signal for any radiometer depends on the relative spectral shape of the source that is being measured,

Table 4. Measured and predicted radiances for the SAS-II instrument, $\tilde{L}$ and $\check{L}$, respectively, as a function of CWL, laboratory experiment (day), and measurement distance ($\tilde{r}$). All radiance values are in units of $\mu W\,cm^{-2}\,sr^{-1}\,nm^{-1}$. The ratio of the measured to predicted values, $\tilde{L}/\check{L}$, is given for each measurement.

CWL [nm]	*Day*	$\tilde{L}$	$\check{L}$	$\tilde{L}/\check{L}$	$R(0°/45°)$	$\tilde{r}$ [cm]
412.83	4 May	0.08913	0.09162	0.97275	1.00557	148.5
	5 May	0.08971	0.09138	0.98176		148.7
	8 May	0.08789	0.09004	0.97613		149.8
	9 May	0.08751	0.08980	0.97448		150.0
	10 May	0.08771	0.08980	0.97670		150.0
442.89	4 May	0.13629	0.13850	0.98406	1.00695	148.5
	5 May	0.13685	0.13812	0.99077		148.7
	8 May	0.13450	0.13610	0.98825		149.8
	9 May	0.13402	0.13574	0.98730		150.0
	10 May	0.13416	0.13574	0.98834		150.0
490.44	4 May	0.22739	0.22989	0.98914	1.00876	148.5
	5 May	0.22911	0.22927	0.99931		148.7
	8 May	0.22452	0.22592	0.99384		149.8
	9 May	0.22387	0.22531	0.99359		150.0
	10 May	0.22388	0.22531	0.99365		150.0
510.58	4 May	0.26837	0.27298	0.98312	1.00939	148.5
	5 May	0.27067	0.27224	0.99422		148.7
	8 May	0.26550	0.26826	0.98970		149.8
	9 May	0.26442	0.26754	0.98833		150.0
	10 May	0.26414	0.26754	0.98728		150.0
554.42	4 May	0.36364	0.37046	0.98159	1.01049	148.5
	5 May	0.36710	0.36946	0.99361		148.7
	8 May	0.35991	0.36406	0.98861		149.8
	9 May	0.35910	0.36309	0.98903		150.0
	10 May	0.35826	0.36309	0.98670		150.0
668.66	4 May	0.59555	0.60143	0.99023	1.01156	148.5
	5 May	0.60132	0.59981	1.00252		148.7
	8 May	0.58935	0.59103	0.99716		149.8
	9 May	0.58776	0.58946	0.99712		150.0
	10 May	0.58678	0.58946	0.99547		150.0
682.58	4 May	0.62205	0.62413	0.99667	1.01151	148.5
	5 May	0.62771	0.62246	1.00844		148.7
	8 May	0.61479	0.61335	1.00236		149.8
	9 May	0.61211	0.61171	1.00065		150.0
	10 May	0.61129	0.61171	0.99931		150.0

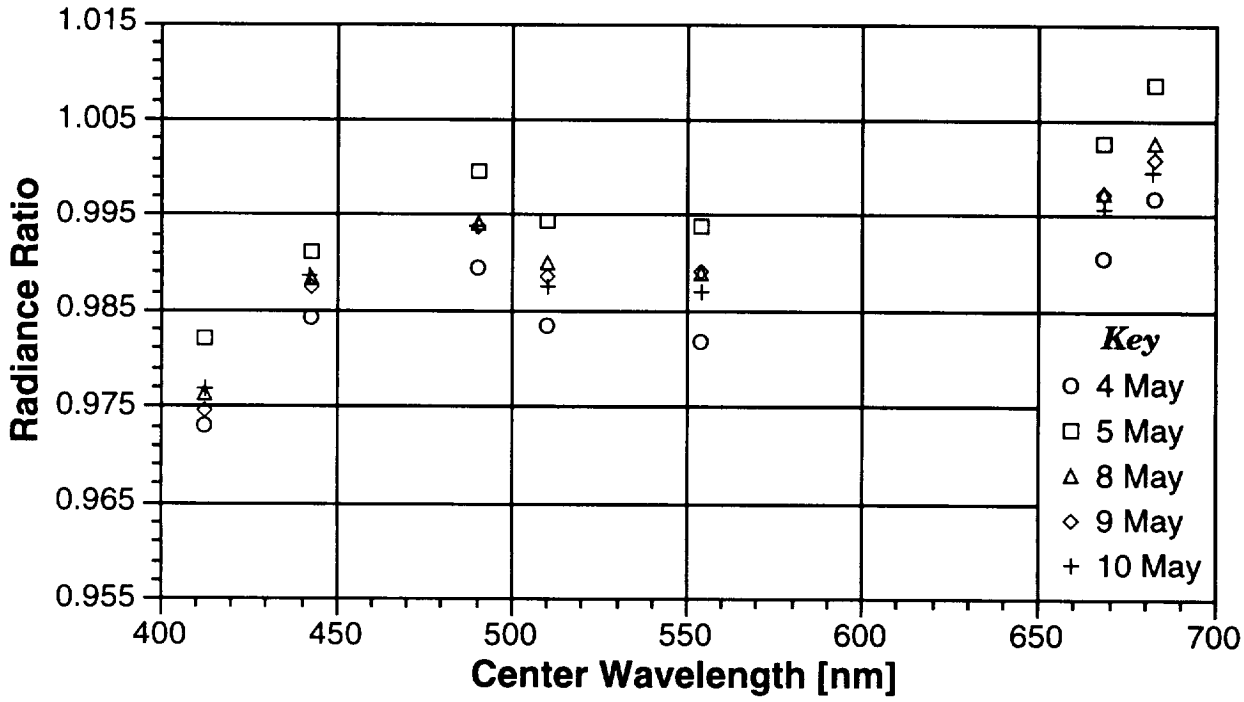

Fig. 10. SAS-II measured to predicted radiance ratio ($\tilde{L}/\check{L}$) for Lab III during days 4–10 May.

see (5). Appendix C discusses the consequences of the nonsimilarity of the spectral shape of the calibration and unknown sources, see (5). The error caused by neglecting the correction factor is negligible for the measurements at SIRREX-4 because the source used to calibrate the SAS-II and the source used in Lab III had a similar spectral distribution. This is not true, however, when filter radiometers such as the SAS-II are used to measure atmospheric or in-water spectral radiance (irradiance).

4.4 Discussion

The results in Fig. 10 indicate that the measured and predicted radiances agree to within −2.7% and +0.8% on all five days, with the largest discrepancy at the bluer wavelengths. The repeatability at any one wavelength is within about ±0.4%, with the results during the second week even more consistent (±0.2%). The SAS-II values and the predicted spectral radiances agree within the uncertainties estimated for the radiometer (at the 95% confidence level), although, the mean of the SAS-II values is lower than the predicted values by about 1%. The values are between 1.8% at 413 nm to 0.8% at 683 nm, and include uncertainty components associated with the NIST standard, the transfer by OL for lamp F360, the calibration of the Spectralon plaque 01873 by Labsphere, the accuracy of the current setting of the lamp, the distance to the plaque, the alignment of the plaque, and the aging of the lamp as well as the plaque. Not included are errors that could be caused by the viewing geometry, baffling, incorrect lamp mounting, or the method of applying the lamp calibration data. During SIRREX-4, the effect of the uncertainty in the measurement of the distance between the plaque and the lamp was made evident by varying $\tilde{r}$ from 148–150 cm, and measurements were also made at 200 cm.

The reproducibility of the SAS-II for this type of measurement is estimated by Satlantic to be about 0.2%, and at SIRREX-4 the measurement precision corresponded to about 0.2%, so the total reproducibility is estimated to be about 0.3%. It is possible, therefore, that there are unaccounted systematic effects in Lab III because the results of 4 and 5 May disagree in most cases by more than 0.3% from the average of the results on 8–10 May. This could be in the distance measurement, the lamp operation, the type of baffling used to eliminate stray radiant flux, or in the alignment of the SAS-II.

The average discrepancy of about 1% and the increased discrepancy at the bluer wavelengths could arise from several sources. For the average discrepancy, which indicates that the SAS-II is underestimating the spectral radiance, one possibility is the values used for the plaque reflectance (Fig. 10). This attempt to estimate $R(0°/45°, \lambda)$ from the $R(8°/h, \lambda)$ values for plaque 13172 in order to predict the spectral radiance is a source of error. The discussion in Appendix B indicates that assigning the ratio of these quantities to be 1.02 is not unreasonable (based on limited measurements of a specific plaque at NIST), but the measurements by Labsphere on the actual plaques relating to SIRREX-4 indicate that a value closer to unity should be used. If the value 1.01 had been used in (10), rather

than 1.02, the SAS-II measurements would agree on average with the predicted spectral radiances.

A second possibility that could explain the discrepancies is the accuracy of the irradiance scale assigned to the standard lamp F360 when it was used to calibrate the SAS-II in April 1995. An examination of the calibration history of this lamp after SIRREX-4 revealed it had been used an additional 85 hours since the last calibration by OL. This exceeds the recommendation by NIST and the normal practice at Satlantic, which is that the lamps should be recalibrated after every 50 hours of use. Remeasurement of F360 by OL in September 1995, however, resulted in irradiance values within ±0.5% of the original calibration, except for the values at 450 nm, which disagreed by about 1%.

Another possibility is the uniformity of the irradiance distribution at the plaques, over the FOV of the SAS-II, for lamps F360 at Satlantic and F332 at SIRREX-4. This is significant because F360 and F332 do not behave as ideal point sources; in fact, no two FEL lamps are alike with respect to the actual irradiance distribution. Finally, improper, incorrect, or inadequate baffling at SIRREX-4 must be considered as a likely source of error (see Section 7). In summary, Lab III illustrated the major problems with this technique of calibrating radiance-measuring instruments, stimulated a discussion on the procedures that will continue at SIRREX-5, illustrated a novel alignment procedure, and supplied information on the care of Spectralon plaques to the participants.

5. LAB IV: LAMPS

The goals of the irradiance laboratory were to learn how to set up and align FEL calibration transfer standards using the NIST specifications for irradiance measurements (Walker et al. 1987a), to learn the effects of baffling on the measurement, and to transfer a calibration from a standard (known) lamp to an *unknown lamp*. The experiment involved a straightforward irradiance calibration transfer wherein a standard lamp was measured and then exchanged for an *unknown* lamp. The geometry of the setup remains the same for both lamps and is not a factor in the transfer. Also, as in Section 4, because the lamps were similar in their spectral output, the product of the detector response function and the lamp irradiance remained nearly the same and did not factor into the calculations. Participants concentrated on how to align the lamps, how to set the 50 cm distance, what to look for when testing out the baffling in the measurement, and what effects a 1 mm error in the 50 cm distance has on the measurement.

Two calibrated NIST FEL irradiance lamps were used and a BSI model PRR-600 six-channel underwater radiometer was the detector. A summary of the instrument's specifications is given in Table 5. The cosine collector of this radiometer is designed to match that of a diffuse receiver for angles up to ±90° from normal incidence. UCSB provided the radiometer and BSI provided its operational software. In addition, a HeNe alignment laser was used to define the optical path.

Table 5. Instrument specifications for the PRR-600. The irradiance saturation values are in units of $\mu W\,cm^{-2}\,nm^{-1}$.

Channel Number	*CWL* [nm]	*Width* [nm]	*Saturation Value*
1	412	10	400
2	443	10	300
3	490	10	300
4	510	10	300
5	555	10	300
6	665	10	300

5.1 Procedures

The majority of the laboratory exercise concentrated on the alignment and setup of the lamp and the detector to locations on the same optical path separated by 50 cm. In this experiment, the laser and lamp were aligned to the radiometer. The laser that located the optical path had five degrees of freedom, and the lamp mount had six. The laser was positioned by placing a glass slide against the radiometer's cosine collector and aligning the laser retroreflection onto the beam port in the laser head. The lamp jig was centered and aligned perpendicular to the optical path using the laser beam retroreflection off its front plane. An accurately measured 50 cm long rod was placed between the radiometer and the lamp jig along their optical centers and the jig was translated so that the rod was barely touching both the front plane and the cosine collector. FEL lamp F423, the lamp of known calibration for this experiment, was then placed in the lamp mount.

Lamp operations followed the protocols given in Walker et al. 1987a. The lamps were slowly brought to full current, 7.8 A, via computer control so the filament would not be stressed, which could invalidate the calibration. Once on, a computer maintained and controlled the lamp current to ±0.0002 A, since fluctuations in the current affect the irradiance output. The lamp was operated for about 20 minutes before measurements started. At the end of the experiment, the computer reduced the lamp current to zero, and the lamp was allowed to cool for 15 minutes before removing it from the mount to a storage rack. The lamp continued cooling in an upright position, so the hot filaments would not permanently bow or alter its position, which could also invalidate the calibration.

During the lab, each lamp was turned on only once. Since the alignment of the baffles, lamp, and radiometer is critical to the measurements, the last alignment used to measure the irradiance output from the known lamp was taken to be the optimal and final configuration and remained unchanged for the unknown lamp.

Once the known lamp had stabilized, the setup was tested for baffling by adding black cloth around the detector to limit its FOV. The radiometer voltages were measured for each configuration and compared to the previous values (Fig. 11). When additional baffling did not change the measured voltages, the setup was considered complete. The optimal baffling configuration was found to be a black box with a circular front opening that surrounded the radiometer. Light, scattered from the room walls and from part of the baffling, was detectable at the red wavelength channels. Some of the room baffling was constructed using burgundy-colored panels and light reflected off these panels was seen by the 665 nm channel which compromised the measurement repeatability. After the second day, black felt cloth was used to cover some of the more critical areas of the burgundy baffles in order to eliminate this problem.

Measurements made in the final baffling conditions included one measurement with the lamp at 50.1 cm from the radiometer, two or three using the standard (known) lamp F423 at the correct 50 cm distance, and the final measurements of F442. The irradiance of lamp F442, $\tilde{E}$, was determined using the measured signals from F423, $\hat{S}$, and its irradiance calibration, $\hat{E}$, as well as the measured signals of F442, $\tilde{S}$. The calculation, which is a ratio of the radiometer's response to the two lamps, is simply $\tilde{E} = \tilde{S}\hat{E}/\hat{S}$. The value used for $\hat{S}$ was the average of the results for a given day (optimal position only). A procedural summary for LabIV is given next.

Step 1, Preliminary system alignment:

a) Align the laser to the optical path.
b) Align the lamp to the same path and orient it using the lamp alignment jig.
c) Demonstrate the distance measurement from the lamp to the detector.

Step 2, Operation of the lamp:

a) Turn on the current allowing at least 1 minute to reach 7.8 A.
b) Show the importance of monitoring the current.

Step 3, Effects of baffling:

a) No baffling and the lights on.
b) No baffling and the lights off.
c) Block reflections off the walls.
d) Place a round aperture between the detector and the lamp.
e) Block the mount base.
f) Further limit the FOV of the radiometer with side baffles.
g) Measure the dark signal.

Step 4, Effects of distance:

a) Measure at 50 cm.
b) Change distance to 50.1 cm and measure.
c) Return to 50 cm and measure.
d) Remember to take the background signals.

Step 5, Switching the lamps:

a) Reduce the current to lamp F423 and let it cool for 20 minutes.
b) Check the position of the lamp base using the alignment jig.
c) Insert the unknown lamp (F442), and increase the current to 7.8 A, and let the lamp stabilize for 20 minutes.

Step 6, Radiometer calibration coefficients:

a) As the lamps are cooling, use a spreadsheet to calculate the coefficient values.
b) Compare the values for the various tests.

Step 7, Unknown lamp (F442) measurements:

a) Make several measurements of the lamp.
b) Measure the background signal.

Step 8, Final calculations:

a) Using the derived radiometer calibration coefficient, calculate the irradiance of the unknown lamp.
b) Compare the values of the irradiances of F442 to the NIST values.

5.2 Results

Both lamps (F423 and F442) were calibrated at FASCAL before SIRREX, and F442 was treated as the unknown. For all five days of SIRREX-4, the calculated irradiances for F442 based on the SIRREX-4 measurements of F423 were within 0.4% of each other (Fig. 12), but the derived irradiances for F442 were always 0.4–1.0% below the FASCAL measurement (Fig. 13). This difference is on the order of the standard uncertainty for the irradiance calibrations.

There were several factors critical to a calibration transfer of spectral irradiance that were not investigated due to time limitations, but they ought to be considered under normal circumstances. The radiometer response function is dependent on the actual detector response, the spectral filters with similar wavelength calibration, and the transmittance of the cosine collector. Normally, the response function should be characterized, but because the same detector was used for both lamp measurements and their irradiance spectrums were similar, any detector spectral dependencies factored out in the calculation. The configuration geometry was relevant due to the size of the radiometer's acceptance aperture, which was over two times larger than the 1 cm opening aperture used in a FASCAL calibration. In general, any current sources or shunt resistors used with the lamp should be calibrated, but for this measurement, the same electronics was used for both lamps and did not affect the calibration transfer.

The transferred calibrations for F442 were 0.4–1.0% below the FASCAL values, which suggests a systematic effect. A possible factor that could have contributed to a

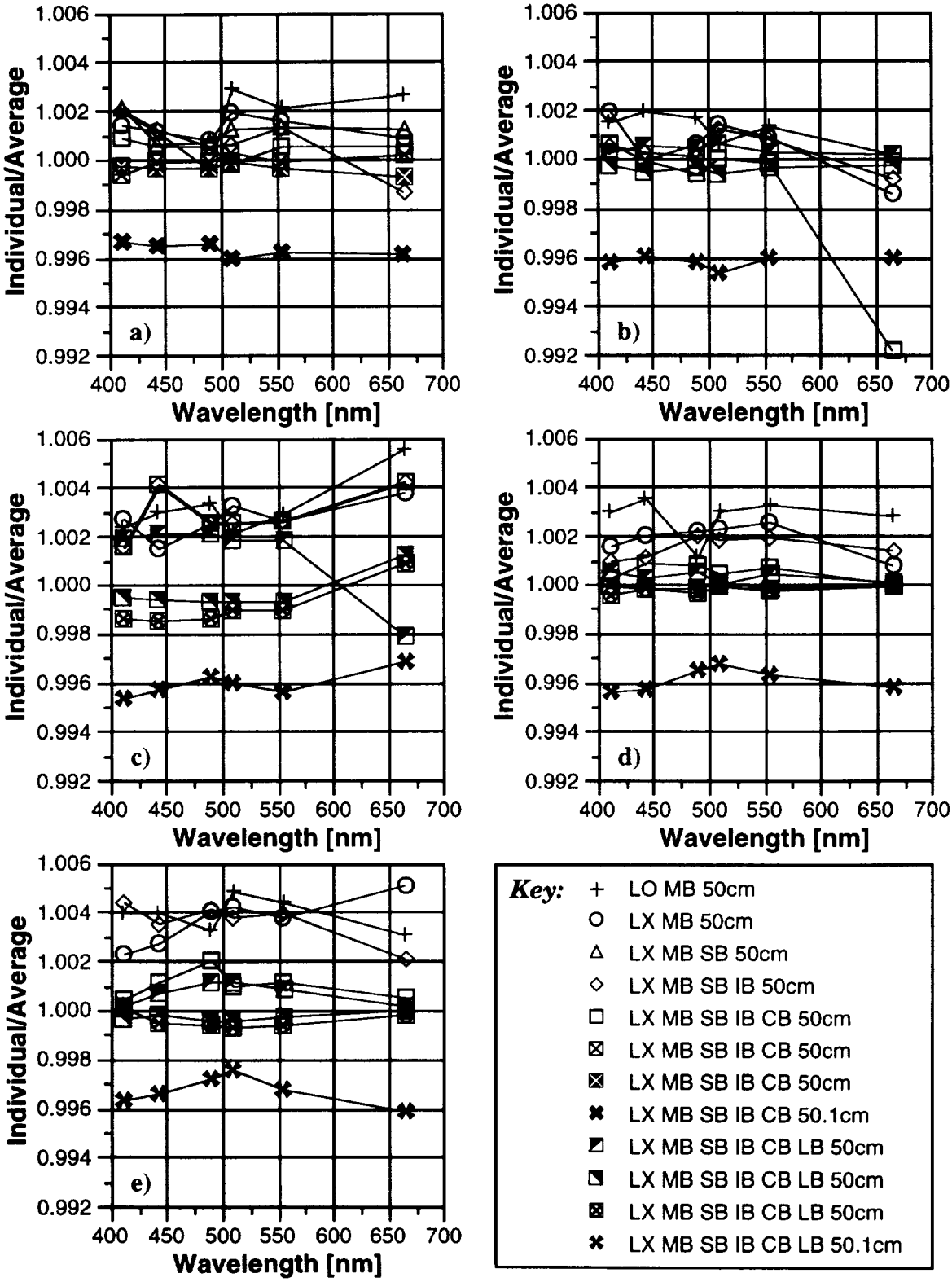

Fig. 11. A summary of the effects of baffling for the five laboratory sessions: **a)** 4 May, **b)** 5 May, **c)** 8 May, **d)** 9 May, and **e)** 10 May. The key codes are as follows: LO means (room) lights on, LX means (room) lights off, MB means (lamp) mount baffled, SB means side baffled, IB means iris baffled, CB means (two) cloth baffles, LB means laser baffled (covered), and the distance refers to the lamp to radiometer distance.

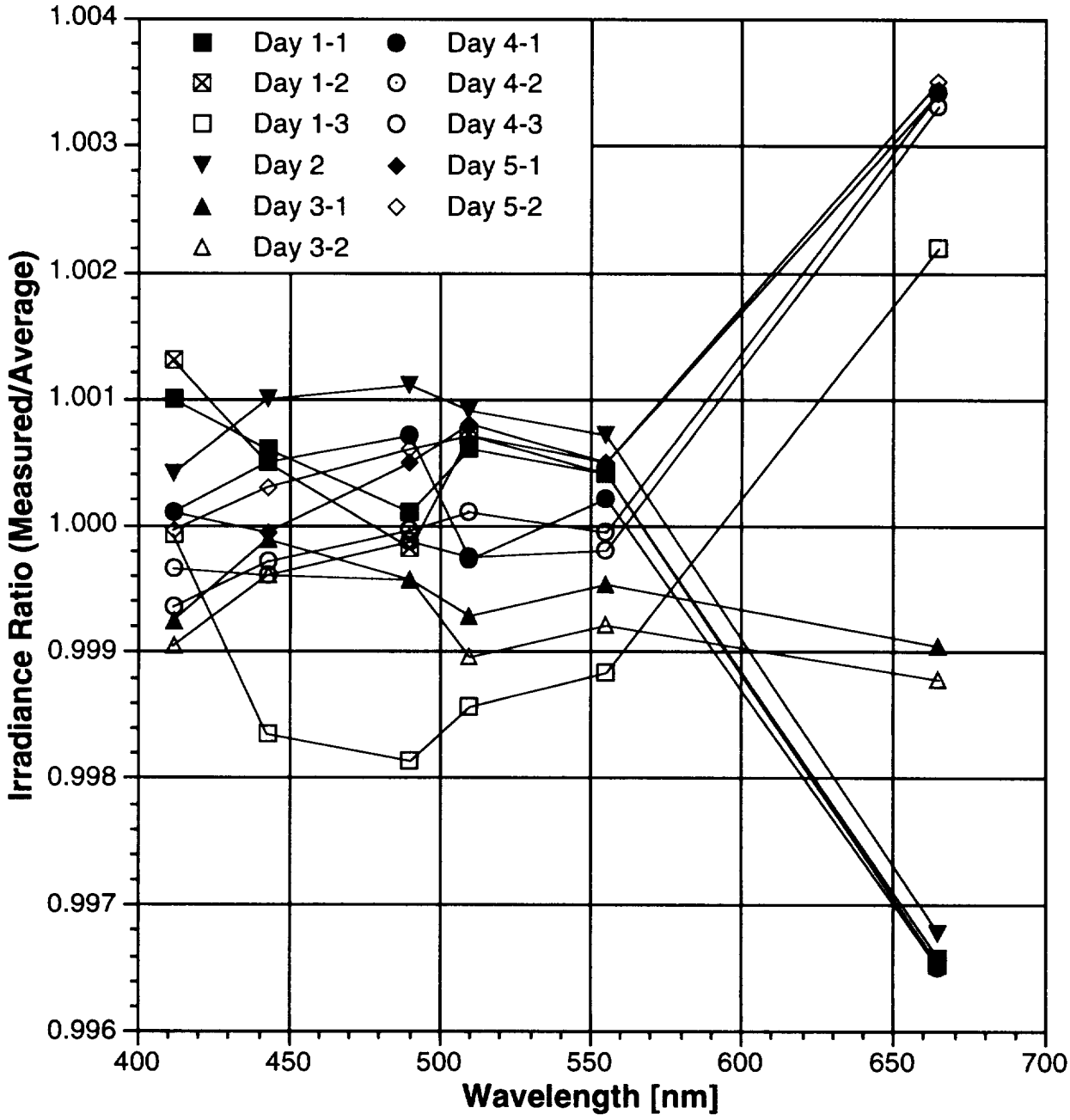

Fig. 12. A summary of F442 irradiance calculations for individual runs with respect to the average of all runs at the final alignment. Day 1, 2, 3, 4, and 5 refers to 4, 5, 8, 9, and 10 May, respectively, while the second numeric code indicates the measurement sequence for the day involved: 4-3 refers to the third measurements taken on 9 May.

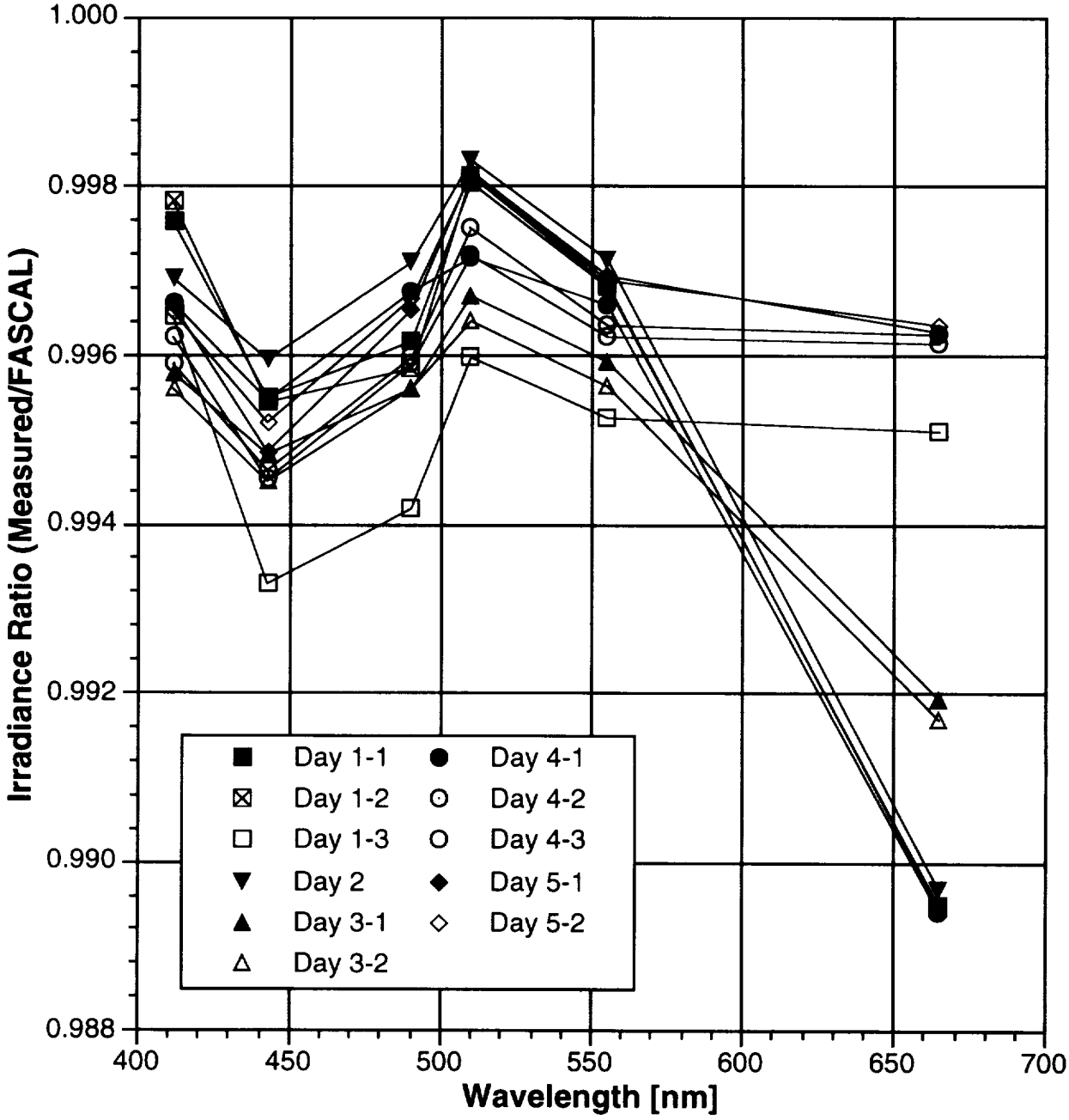

Fig. 13. A summary of F442 irradiance calculations for individual runs with respect to the FASCAL measurement. (The day codes are explained in Fig. 12.)

systematic offset is the goniometric correction in one or both of the lamps. Only one of the lamps used was tested to see if the goniometric dependence was less than 1% per degree, but the effects seen were less than that. In an irradiance calibration transfer intended for use in other experiments, further investigation of the offset would be advised.

5.3 Conclusions

This laboratory focused on the setup and alignment of an irradiance measurement, as well as relevant factors to a calibration transfer of spectral irradiance. The resulting irradiance calibration transfer from F423 to F442 was within the FASCAL stated measurement uncertainties. Participants experienced the difficulties in the most simple of calibration transfers and can utilize the experience in their future work.

6. LAB V: RADIOMETERS

The principal objectives of Lab V were to teach the participants how to measure slit-scattering functions and scattered light (4 May), wavelength calibration and stability (5 May), lamp spectral irradiance (8 May), point-spread response (9 May), and relative spectral response (10 May). The 746/ISIC was used for the first three activities. This radiometer is used by GSFC to transfer the spectral irradiance of standard lamps to other working standards, as well as to determine the spectral radiance of integrating spheres. It is a single grating monochromator with filter order sorting and selectable entrance and exit slit widths. Three diffraction gratings are located on a turret, each of which has a different useful wavelength range. The entrance optic is a 10.2 cm diameter integrating sphere coated with halon whose entrance port has a 2.5 cm diameter. The detector is a silicon photodiode with an optical chopper. The signal from the photodiode is amplified and measured by a lock-in amplifier, which displays the signal in amperes.

Prior to starting the experiments each day, the wavelength and phase angle of the instrument were set. The wavelength display on the monochromator housing was synchronized with the corresponding display on the electronic control by manually adjusting the first display to 400.0 nm and then pressing the PRESET button on the electronic control. With the 1,200 lines/mm (blazed at 500 nm) grating used for all the experiments, the wavelength setting of the monochromator was half that displayed. To set the phase angle of the lock-in amplifier for the maximum signal, the beam from a HeNe laser was directed into the integrating sphere. The wavelength was manually adjusted to approximately 632.8 nm. The signal range was switched to manual and the phase angle was adjusted to obtain a positive signal as close to zero as possible. The phase angle was then increased by 90° and locked. The phase angles on the three days of measurements were 296°, 300°, and 293°. For all succeeding measurements, the monochromator and electronics were controlled by the computer.

All of the measurements consisted of wavelength scans of various sources. The minimum, maximum, and incremental wavelengths were set by the operator, as well as the number of readings at each wavelength, which was set at five for all the scans. These five readings were averaged at each wavelength, unless there was an obvious error in one of the readings, indicated by a spike at one wavelength in a plot of signal versus wavelength. This occurred fairly regularly with an increasing signal, as the gain range on the lock-in amplifier would be read incorrectly by the computer. In these cases, only four readings were averaged.

6.1 Slit-Scattering Function

For wavelength scans of lasers and gas discharge lamps, the quantities of interest were the bandwidth of the slits and the centroid of the laser or emission line. The bandwidth was calculated as the full-width at half-maximum (FWHM). The signals were normalized by the peak signal and linear interpolation was used to find the wavelengths at which the normalized signal was 0.5. The difference between these wavelengths was the bandwidth. For the centroid, a straight line was fit to points with corresponding wavelengths 1.5 times the bandwidth above and below the wavelength of the peak signal. This fit was subtracted from the intervening signals, and the sum of the product of these background-corrected signals and the wavelength was divided by the sum of the corrected signals to obtain the centroid.

Measurements of the slit-scattering function provided information about the bandwidth and wavelength repeatability of the instrument. A series of wavelength scans were performed with beams from either a helium-cadmium (HeCd) laser at 441.565 nm or a HeNe laser at 632.816 nm directed into the integrating sphere. Both of the lasers were warmed up for one hour prior to starting the measurements. For slit-scattering function measurements, wavelength scans were performed at 0.1 nm increments with slit widths of 0.5 and 1.25 mm. The slit-scattering functions for both lasers and slit widths are shown in Fig. 14, where the peak-normalized signal is plotted as a function of wavelength relative to that at the peak signal for a) the HeCd laser, and b) the HeNe laser. The bandwidth at each wavelength and slit width is also indicated in the figure. The average dispersion is $3.8\,\mathrm{nm\,mm^{-1}}$. At both laser wavelengths and slit widths, the slit-scattering function is not symmetric about the zero relative wavelength, indicating a misalignment of the entrance and exit slits.

To check the wavelength reproducibility of the instrument, scans of the HeNe laser beam with the 0.5 mm wide slits were performed after reinserting the slits and after resetting the wavelength at 400.0 nm as described above. The results from these scans are shown in Fig. 15, where

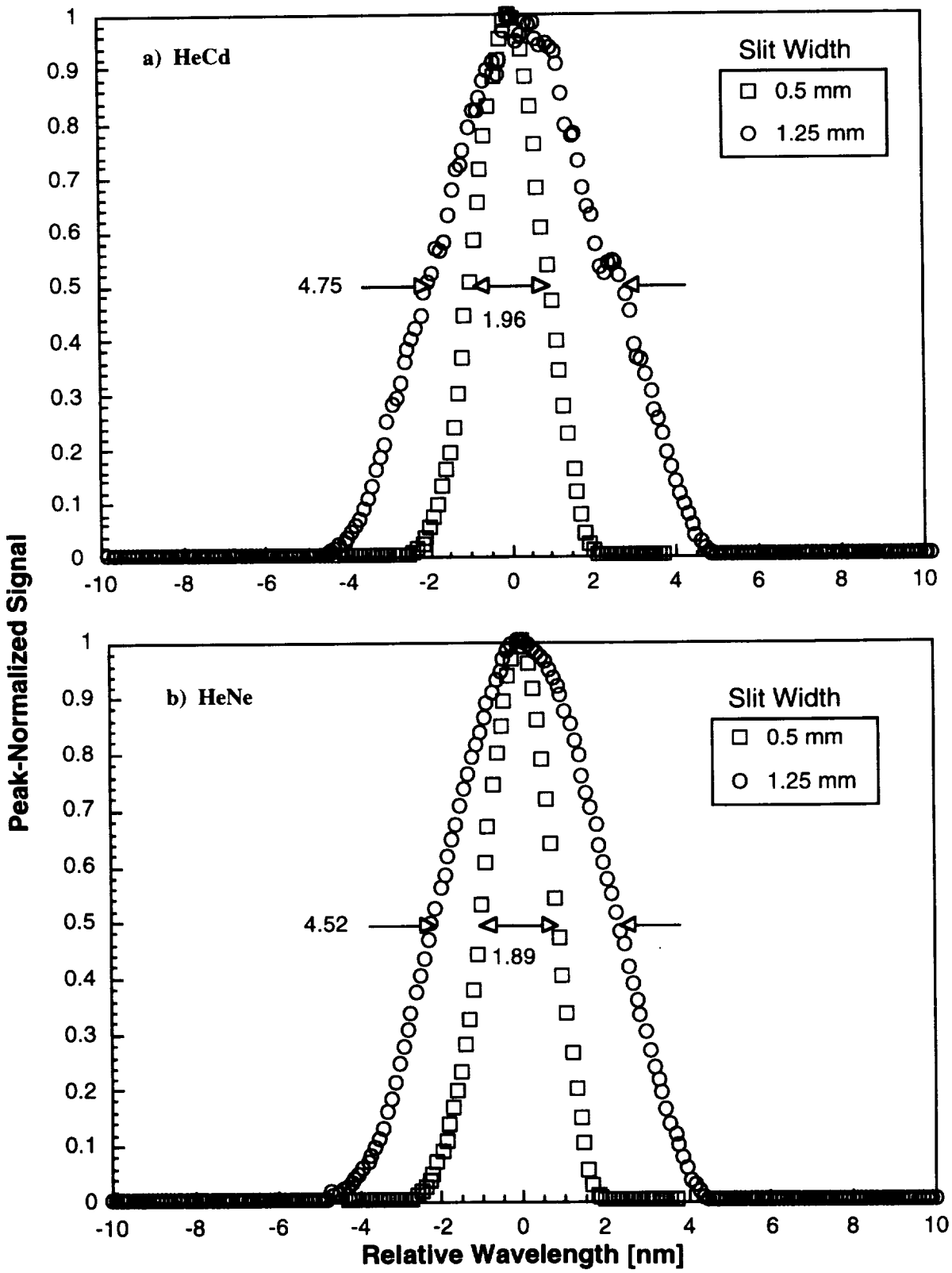

Fig. 14. Peak-normalized signal versus relative wavelength with a) the HeCd laser at 441.565 nm, and b) the HeNe laser at 632.816 nm. The slit widths and bandwidths are indicated in each panel.

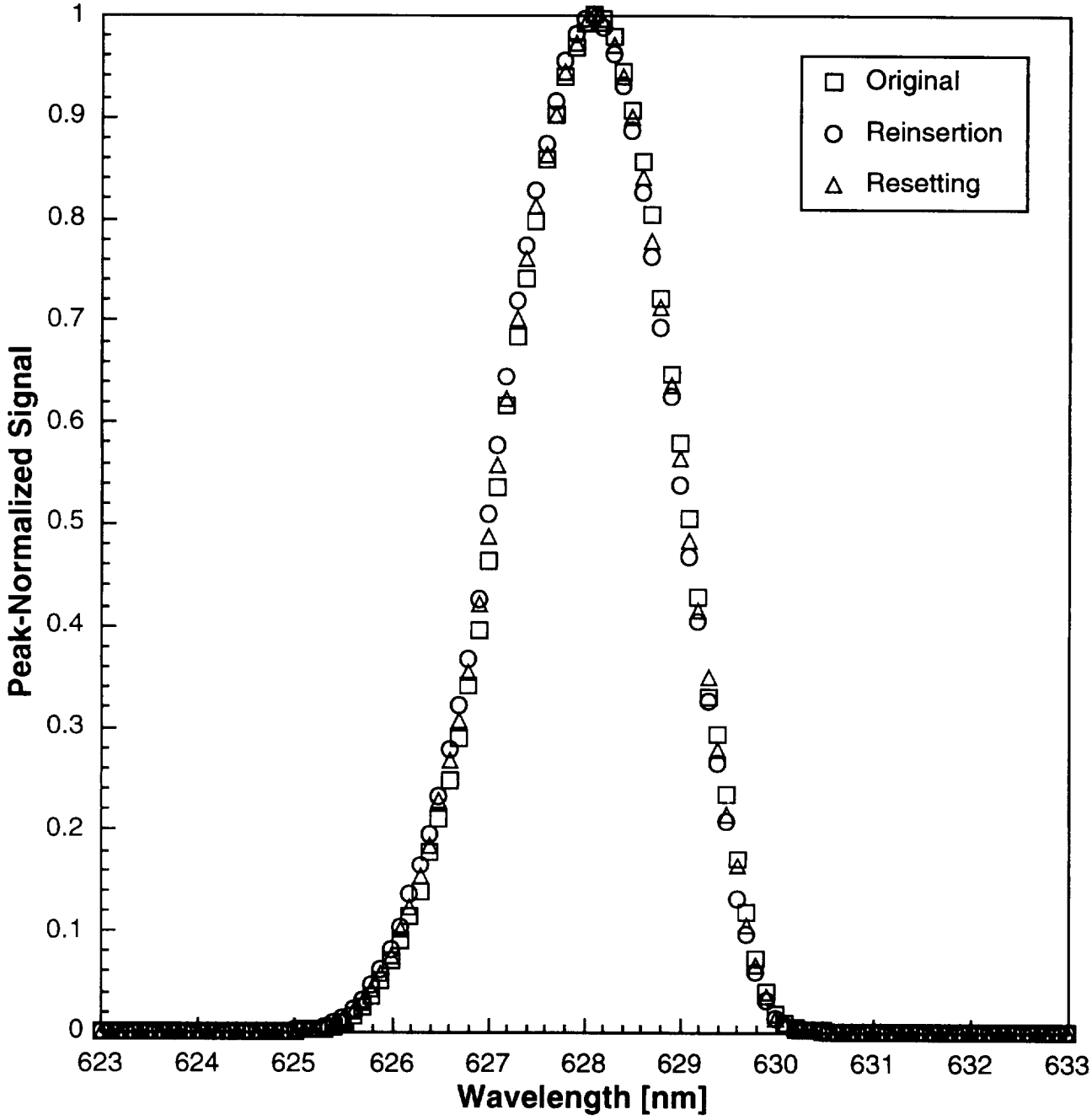

Fig. 15. Peak-normalized signal versus wavelength for three scans with the 0.5 mm wide slits of the HeNe laser: the original scan, a scan after the slits were reinserted, and a scan after the wavelength was reset.

the peak-normalized signal is plotted as a function of wavelength for three scans as indicated in the figure. It is obvious that there is a slight change, with the centroid decreasing relative to that of the original scan by 0.052 nm upon reinserting the slits and by 0.026 nm upon resetting the wavelength. Scans were also performed twice more to check the wavelength repeatability, as shown in Fig. 16, where the peak-normalized signal is plotted as a function of wavelength for three scans. The largest difference between the centroids of any two scans is only 0.015 nm, indicating good repeatability of the monochromator.

From Figs. 15 and 16, it is apparent that the wavelengths at which the peak signals occur are approximately 4.8 nm less than the wavelength of the HeNe laser. The cause for this was traced to incorrect positioning of the grating turret, which was not completely pushed down. Once it was pushed down and positioned properly, another scan was performed, the turret was repositioned again, and a final scan was performed. These scans are shown in Fig. 17, along with a previous scan, where the peak-normalized signal is plotted as a function of wavelength. There is a dramatic improvement in the wavelength accuracy with proper positioning of the turret, and a difference between the centroids of the two repositionings of 0.21 nm, while the shape of the slit-scattering function does not change. Therefore, the wavelength accuracy of the instrument is very sensitive to the positioning of the turret. Each time the turret is rotated and seated, the diffraction grating is at a slightly different angle with respect to the entrance and exit slits, resulting in a change in the wavelength calibration. Thus, the instrument must be calibrated for wavelength each time the turret is moved, and probably should be calibrated after shipping as vibrations could cause the turret to move. A wavelength calibration is described below.

6.2 Stray-Light Rejection

The stray-light rejection of the instrument determines the contribution to the measured signal from flux at wavelengths outside the bandwidth. The uncertainty associated with this is relatively small when comparing two sources with the same spectral shape, such as two FEL lamps, but is larger when comparing two different sources, such as an FEL lamp and an integrating sphere. Wavelength scans from 350–1,100 nm at 5 nm intervals were performed, and the signals were normalized by the peak signals determined from the scans at 0.1 nm intervals used for the bandwidth and centroid calculations. The results are shown in Fig. 18, where the peak-normalized signal is plotted as a function of wavelength for scans of both the HeCd and HeNe laser, the latter with both 0.5 mm wide and 1.25 mm wide slits.

At the longest wavelengths, all of the signals were comparable to the noise of the instrument, determined by performing a scan with both laser beams blocked from entering the integrating sphere. Because the dynamic range of the signal is limited by the peak signal, the apparent stray-light rejection from the scan of the HeNe laser with the 0.5 mm wide slits is worse than that from a scan of the same laser but with the 1.25 mm wide slits. From this latter scan, the stray-light rejection of the instrument is at least 2×10^{-5}. The scan of the HeCd laser line shows an enhanced signal, consistent with fluorescence of some element in the entrance optics, for wavelengths greater than that of the laser. The most likely element is the halon coating of the integrating sphere, since a similar scan without an order sorting filter showed the same enhancement.

6.3 Wavelength Calibration

Given the sensitivity of wavelength on turret positioning detailed above, it is important to calibrate the wavelength of the monochromator to reduce the wavelength uncertainty. This was done by scanning a series of emission lines from mercury (Hg) and Ne gas discharge lamps. Emission lines chosen for these scans had to have measurable signals and be separated from other lines by at least 2 nm, which were the 334.148 and the 1,013.975 nm lines of Hg and the 540.056, 659.895, 692.947, 724.517, 830.033, and 966.542 nm lines of Ne. These were supplemented by a scan of the 441.565 nm line of the HeCd laser. The lamps were mounted so that the lamp envelope was inside the integrating sphere but not in the FOV of the entrance slit. The centroid of each is referred to as the measured wavelength for that line.

The difference between the actual wavelength of each line, λ_a, and the measured wavelength, λ_m, is shown in Fig. 19, where this difference is plotted as a function of measured wavelength. The difference ranges from 0.3–0.8 nm. This difference was fit with a second-order polynomial, also shown in Fig. 19, with the measured wavelength as the independent variable. Therefore, the actual wavelength of the monochromator in terms of the measured wavelength is given by

$$\lambda_a = \lambda_m - 6.8761\times10^{-1} + 3.7110\times10^{-3}\lambda_m - 2.3770\times10^{-6}\lambda_m^2. \quad (11)$$

The residuals between the differences and the fit to the differences are all less than 0.1 nm. Therefore, with this wavelength calibration, the wavelength uncertainty of the instrument is reduced to 0.1 nm.

6.4 Lamp Irradiance

The ability of the instrument to accurately measure the irradiance of an FEL-type lamp is a test not only of the instrument but also of the procedure used to align the lamp and control the current supply to the lamp. Therefore, the spectral irradiance responsivity of the instrument was determined by performing a wavelength scan of a GSFC lamp using the GSFC alignment procedure and current supply.

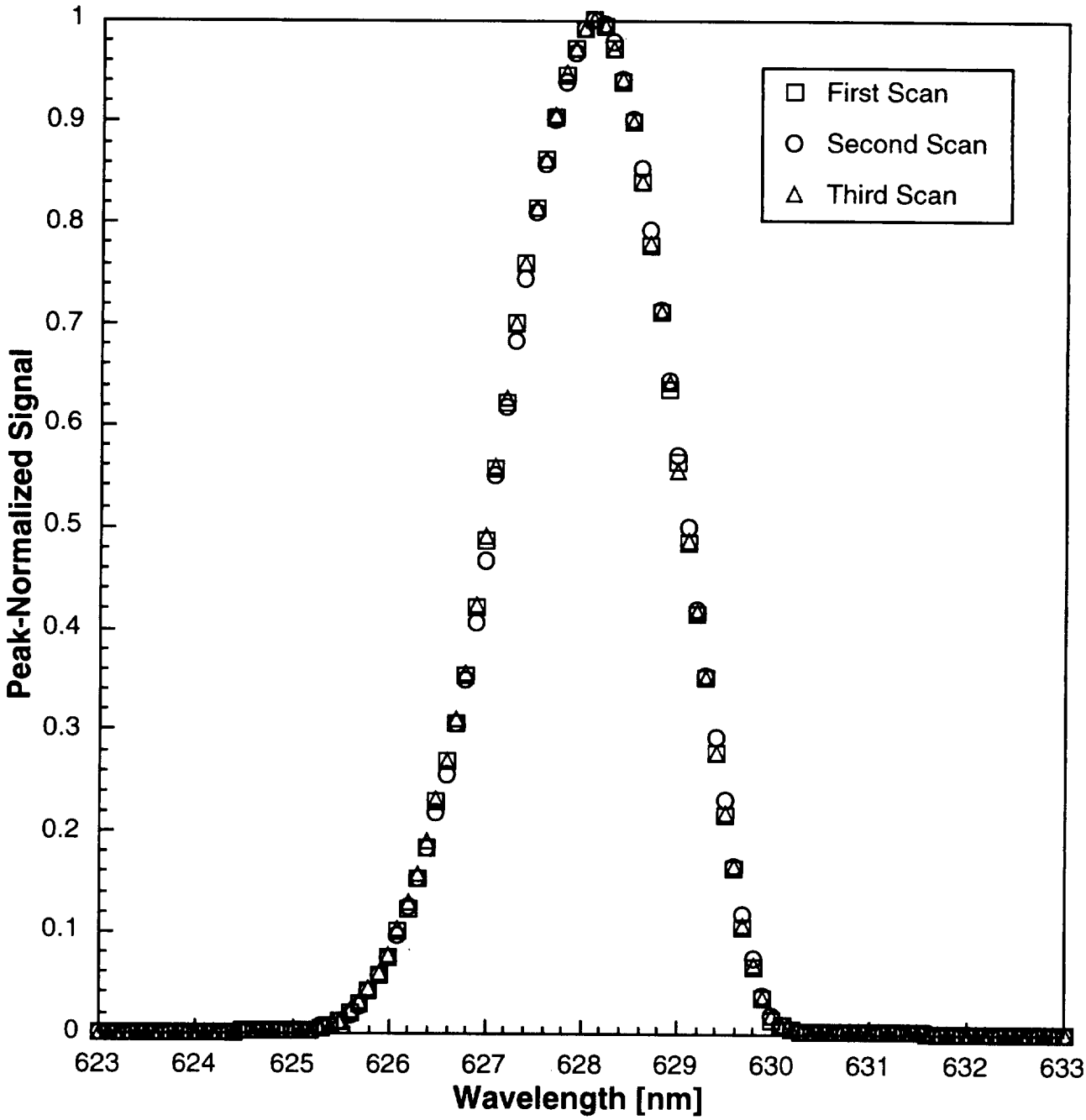

Fig. 16. Peak-normalized signal versus wavelength for three scans, as indicated, with the 0.5 mm wide slits of the HeNe laser.

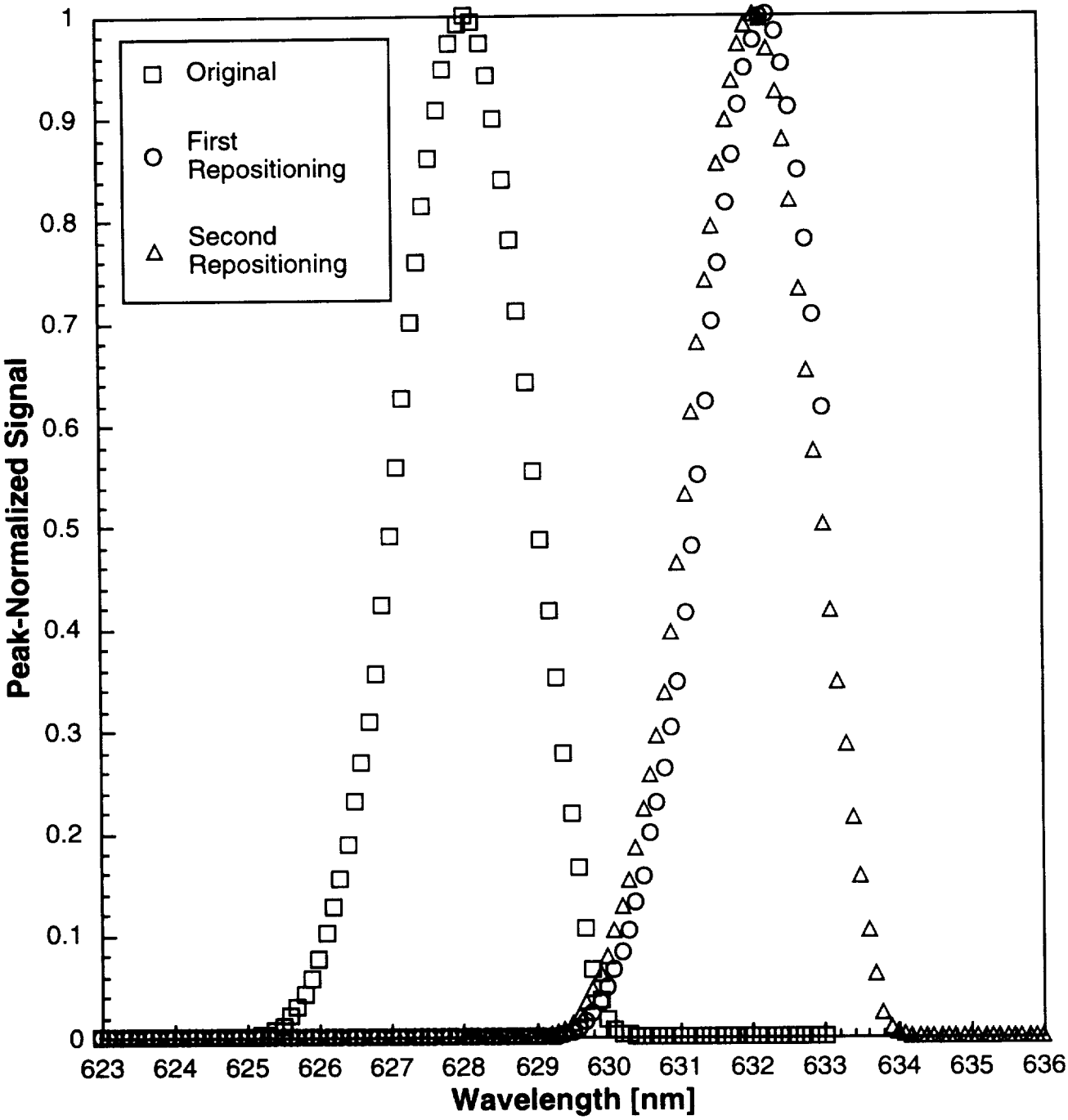

Fig. 17. Peak-normalized signal versus wavelength for three scans with the 0.5 mm wide slits of the HeNe laser: the original scan and two scans after repositioning the diffraction grating turret.

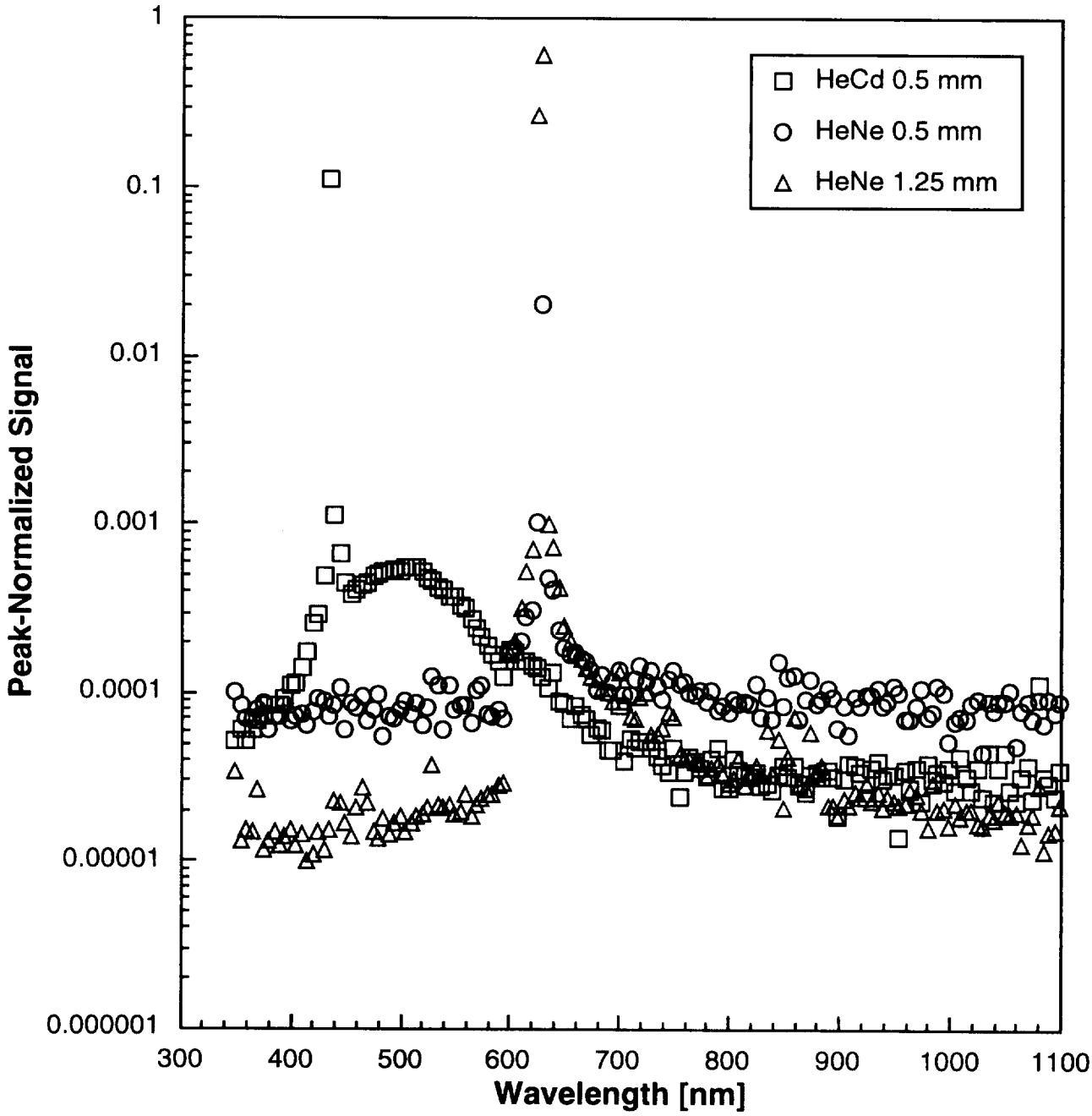

Fig. 18. Peak-normalized signal versus wavelength for scans with the indicated slit widths and lasers.

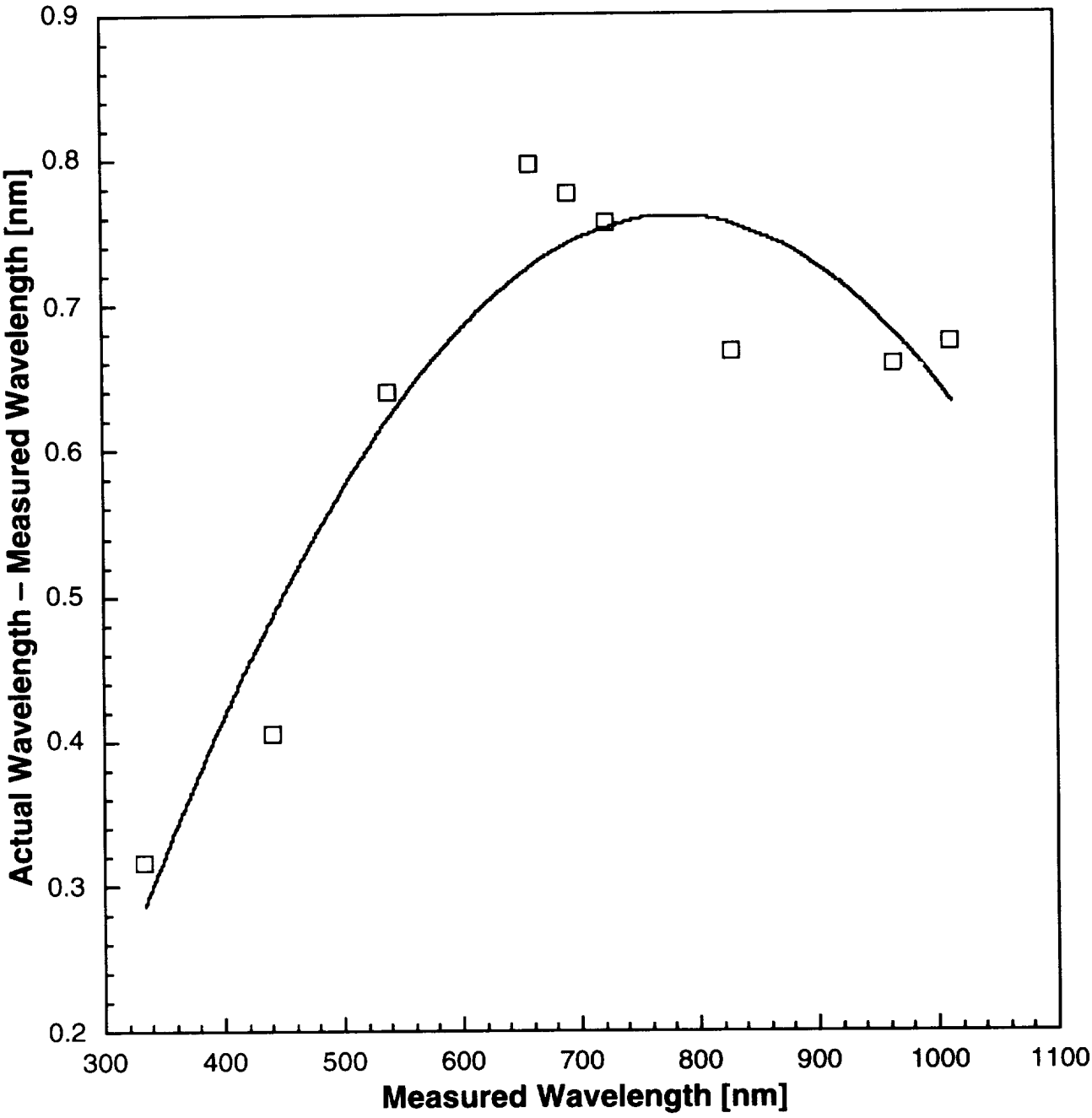

Fig. 19. Actual wavelength minus measured wavelength versus measured wavelength of the centroids of emission lines from Hg and Ne gas discharge lamps and a HeCd laser. The solid line is a second-order polynomial fit to the data.

Wavelength scans of a calibrated NIST lamp were then performed using both the GSFC lamp mount and current supply and with a NIST lamp mount and current supply. Using the responsivity from the first wavelength scan, the spectral irradiance of the NIST lamp was calculated from the other two wavelength scans and compared to its known values.

The wavelength calibration detailed above utilized the 0.5 mm wide slits in order to resolve emission lines. However, since the 1.25 mm wide slits were needed for lamp irradiance measurements, the wavelength calibration had to be adjusted for these wider slits. Wavelength scans were performed on the lines from both the HeCd and HeNe lasers using both slit widths, and the corresponding centroids were calculated. The centroid decreased by 0.7 nm with the wider slits; consequently, the wavelength calibration was adjusted accordingly so that the constant term in (11) was -6.1761×10^{-1}.

Alignment between the entrance port of the integrating sphere and the lamp was first performed using the GSFC procedure. The lamp mount consists of two aluminum blocks with holes for the current leads (metal posts) of the lamp, screws to secure the lamp posts, and screw terminals for the leads from the current supply. The blocks are on a platform on a post attached to a rail slide. Adjustments to the rail and the post height allow translations along three orthogonal axes. Rotations of the post allow a rotation of the lamp about the long axis of the lamp filament. The lamp alignment jig has a glass slide between the posts which is tangent to the front of them with scribe lines to indicate the center of the jig. The optic axis was set by removing the integrating sphere and attaching a HeNe laser with a fitting that sets the distance from the center of the beam exit port to the case of the monochromator to be the same as from the center of the entrance port of the integrating sphere to the case. The laser was leveled horizontally, the lamp alignment jig was placed in the lamp mount, and the jig was translated so that the laser beam passed through the center of the jig and rotated so that the reflection of the laser beam from the glass slide was centered vertically on the line through the center of the laser beam exit port. Because there was not an additional degree of rotational freedom, the reflection did not return along the beam.

The laser was then removed and replaced by the integrating sphere. The rotation of the sphere was set by vertically leveling the plug in the entrance port. The distance between the outer side of the entrance port and the front of the lamp alignment jig was set to 49.95 cm with a brass bar of that length by moving the rail slide. The adjustments with the laser and bar were repeated until the lamp alignment jig was centered on, and perpendicular to, the laser beam and the front was the correct distance from the integrating sphere. This took several iterations. The rail was than clamped to the table and the lamp mount was moved 0.1 cm closer to the integrating sphere to account for the thickness of the wall of the integrating sphere.

The current supply to the lamp consisted of an HP 6030A power supply, a Leeds and Northrup 0.01 Ω shunt, and an HP 34401A DVM. The current leads from the power supply and shunt were attached to the lamp mount with the correct polarity. A 40 cm square baffle with three plates, each with a 3×8 cm^2 rectangular hole in them, was placed between the lamp mount and the integrating sphere, with the center of the holes approximately on the optic axis.

A lamp was placed in the lamp mount, either F268 from GSFC or F331 from NIST. The current from the power supply was increased manually over a few minute interval and adjusted to the correct value by monitoring the voltage across the shunt, either 8.0 A or 7.9 A for lamps F268 and F331, respectively. The direct beam from the lamp to the entrance port of the sphere was blocked by placing a black cloth over the holes of the baffle. A wavelength scan from 350–900 nm with a 5 nm increment was performed, which measured the diffuse signal from light scattered into the sphere. The cloth was then removed and the wavelength scan was repeated, which now measured the total signal. The current to the lamp was then reduced to zero over a 1 minute interval. The total operating time for each lamp using this procedure was 30 minutes.

After the wavelength scans of the two lamps using the GSFC procedure, the NIST lamp was aligned using the typical procedure at NIST for field calibration work. The GSFC rail and baffle were removed and the monochromator was raised by approximately 5 cm. A HeNe laser was mounted, with both translation and rotation stages, 1.5 m from the integrating sphere. The position of the laser was adjusted so that the reflection of the beam off a mirror over the plug of the entrance port returned along the beam and the beam was centered on the plug. This defined the optic axis, and the position of the laser was not changed throughout the remainder of the alignment. The NIST lamp alignment jig was placed in the NIST lamp mount on a platform, approximately 50 cm from the integrating sphere, with translations along three orthogonal directions and rotations about two axes. The translations and rotations of the jig were adjusted so that the laser beam was centered on the jig, the reflection from the jig returned along the beam, and the front of the jig was 50.0 cm from the entrance port as determined by a NIST rod marked with the appropriate distance.

The current supply to the lamp consisted of an HP 6030A power supply operated in the external voltage control mode, a Leeds and Northrup calibrated 0.01 Ω shunt, an HP 3457A DVM, and a 16-bit digital-to-analog (D/A) voltage converter board in a PC computer. The voltage across the shunt was monitored by the DVM, and the computer adjusted the output from the D/A converter to obtain the correct current. Using this technique, the uncertainty in the current is reduced to 0.2 mA. Current

and voltage monitoring leads were attached to the lamp mount. A black aluminum plate was positioned in front of the lamp mount platform to block reflected light from the lamp mount and platform from entering the integrating sphere, and a black cloth was placed in front of the alignment laser. No baffles were used between the lamp and the sphere on the 746/ISIC.

Lamp F331 was placed in the lamp mount and the current was slowly increased to 7.9 A, with 115.2 V across the lamp terminals. The direct beam from the lamp to the entrance port of the sphere was blocked by placing a cloth-covered tube (4 cm across) halfway between the lamp and the integrating sphere. A wavelength scan from 350–900 nm with a 5 nm increment was performed to measure the diffuse signal. The tube was then removed and the wavelength scan was repeated to measure the total signal. The current to the lamp was then slowly reduced to zero. Again, the operating time for the lamp was 30 minutes.

For each wavelength scan, the average signal at each wavelength and the standard deviation of the mean were calculated, ignoring obviously incorrect (spiked) readings. The diffuse signals were subtracted from the total signals to obtain the direct signals and the uncertainties were propagated. The actual wavelength was calculated from the wavelength calibration, and the direct signal was fit with a natural cubic-spline to the wavelength range 355–900 nm at 5 nm intervals. The uncertainty at each fit wavelength was taken to be the uncertainty at the measured wavelength. A natural cubic-spline fit of the irradiance of each lamp was also performed over the same wavelength range and interval.

The spectral irradiance responsivity was calculated by dividing the direct signal from lamp F268 by its irradiance, with propagation of uncertainties. This responsivity is shown in Fig. 20. The effect of changing the order-sorting filter at 600 nm is apparent, as well as the loss of responsivity for wavelengths shorter than 400 nm. The measured irradiance of lamp F331 was calculated by dividing the direct signal by the spectral irradiance responsivity, again propagating uncertainties. This measured irradiance was compared with the actual irradiance by dividing the first by the second. The results from these comparisons are shown in Fig. 21, where the ratio between measured and actual irradiance for lamp F331 is plotted as a function of wavelength for a) the GSFC alignment procedure and current supply, and b) the NIST alignment procedure and current supply. The Type A uncertainties from the noise in the signal measurements are shown as vertical bars at each wavelength.

In both figures, the small responsivity for wavelengths shorter than 400 nm results in a large uncertainty and significant disagreement between measured and actual irradiances. For longer wavelengths, however, the measured irradiance is within 1% of the actual value using the GSFC procedure, as shown in Fig. 21a. The same holds true using the NIST procedure for wavelengths shorter than 700 nm; for longer wavelengths, the ratio increases slightly, as shown in Fig. 21b. This is probably due to increased scattering in the total signal at longer wavelengths since for this measurement there is no baffling using the NIST procedure whereas the GSFC procedure uses a baffle.

6.5 Recommendations

The 746/ISIC has a surprisingly good stray-light rejection, so this should not be a cause of concern when using the instrument. However, the dependence of wavelength on turret position is a potential problem. Because the angle of the diffraction grating changes with positioning of the turret, and probably changes from the vibrations experienced during shipping, the wavelength should be calibrated each time the instrument is moved. Fortunately, the correction to the measured wavelength is smooth over the wavelength range, which reduces the number of emission lines that must be scanned. The wavelength calibration should hold as long as the instrument is not moved based upon the good wavelength repeatability. Determining the spectral irradiance responsivity of the instrument using the GSFC alignment procedure and current supply is adequate. There was insufficient time during the laboratory exercises to thoroughly investigate the change in spectral responsivity with time. The OL 746/ISIC responsivity drifted by as much as 5% during SIRREX-3 (Mueller et al. 1995). Baffling between the instrument and an integrating sphere for radiance determinations should be carefully considered to reduce scattered light.

7. SUPPLEMENTAL STUDIES

As a supplement to SIRREX-4, the experimental setup using a diffuse plaque and a standard irradiance lamp (Section 4) for spectral radiance realizations was used on 6 May with the SXR and the SAS-II instruments. In addition, on 12 May the SAS-II was used to measure the spectral radiance of the GSFC sphere and the SXR was used to remeasure the plaque. The goals of the measurements were to use the SXR and the SAS-II to measure the reflectance factor $R(0°/45°, \lambda)$ of the plaque and to verify the calibration of the SAS-II using the GSFC sphere.

The equipment used was the SXR (Section 3), the SAS-II and the Spectralon plaque (Section 4), and the GSFC sphere (Section 3). For the measurement with the plaque, the standard irradiance lamp F332 was operated at 7.9 A. On 6 May, data were recorded with the SAS-II and the SXR with the optical bench configured as in Lab III. On 12 May, the SXR measurements were repeated using additional baffling compared to what had been used on 6 May in Lab III, and the distance between the lamp and the plaque was increased by 50 cm. Also on 12 May, the SAS-II was used to measure the spectral radiance of the GSFC sphere, which was illuminated with lamps 1–4, the so-called *four-lamp* configuration.

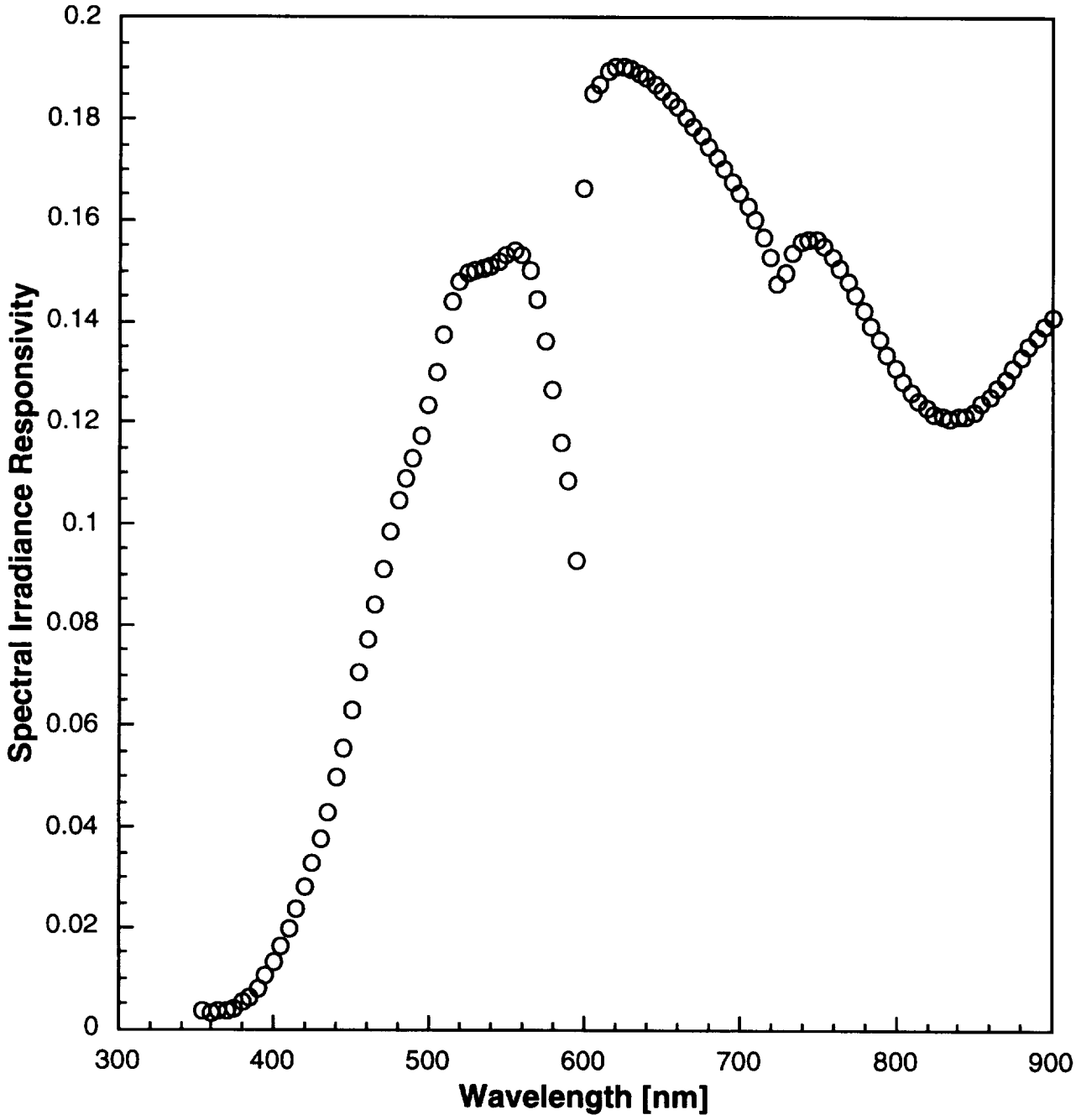

Fig. 20. Spectral irradiance responsivity (units of $\mathrm{nA\,W^{-1}\,cm^{-3}}$) versus wavelength determined from the GSFC alignment procedure and current supply with lamp F268.

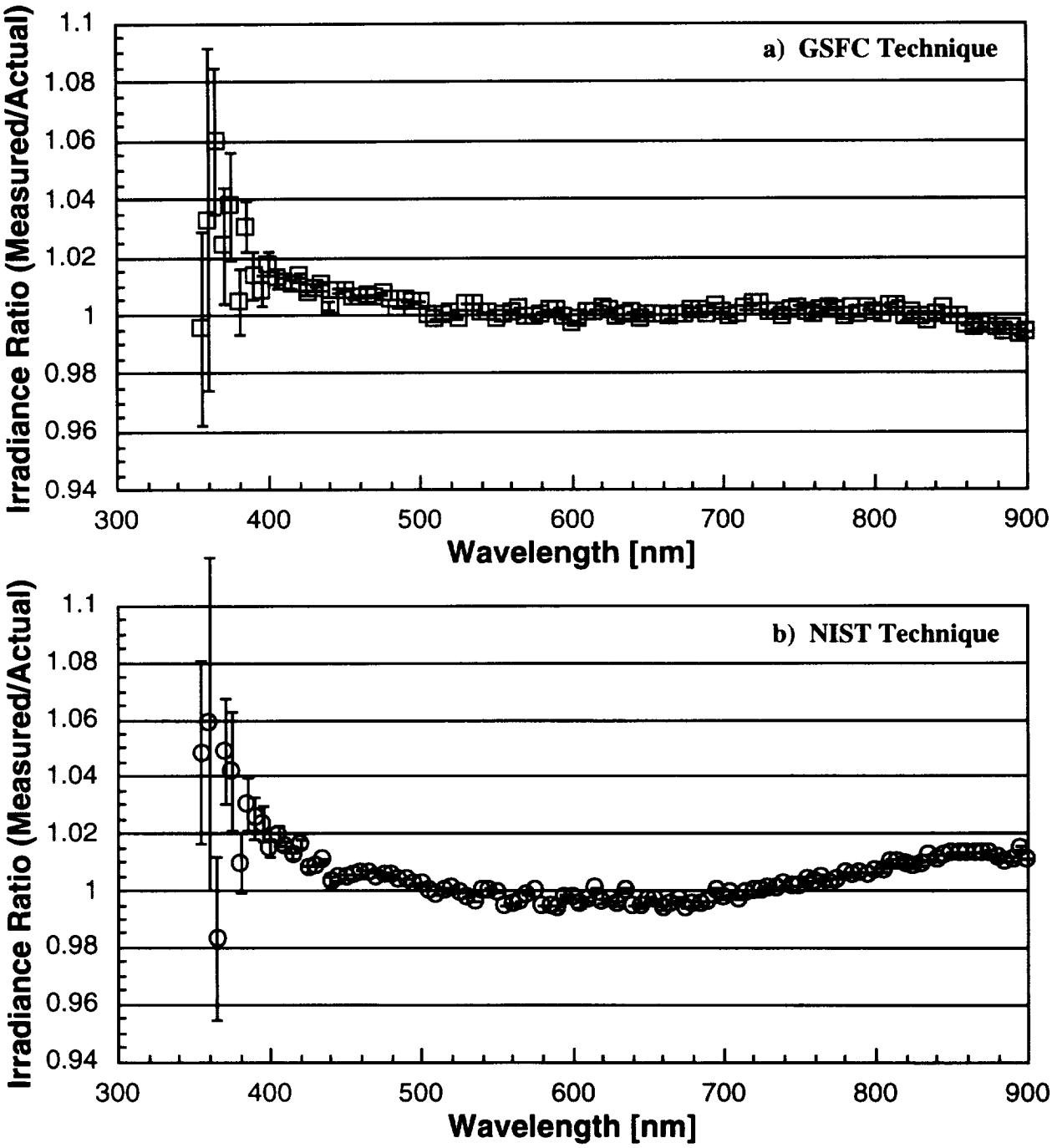

Fig. 21. Ratio of measured to actual irradiance versus wavelength for lamp F331 using a) the GSFC alignment procedure and current supply, and b) the NIST alignment procedure and current supply.

7.1 Plaque Reflectance

On 6 May, lamp F332 was positioned 148.5 cm ±0.2 cm from the plaque and data were recorded with the SAS-II in essentially the same configuration that had been used on the 5 May session of Lab III. The Satlantic instrument was 45.6 cm from the plaque. Then the SXR was aligned to view the plaque at 45°, in place of the SAS-II. The SXR orientation was *north*, as it was for all measurements at SIRREX-4. The ambient temperature was 21.8°C, and the SXR was operated (as normal) at 26°C. The SXR was warmed up for about 30 minutes, which is not the normal procedure (usually several hours are allowed for the temperature of the amplifier board to stabilize), but this was not possible for these studies. The distance to the plaque from the face plate of the SXR was 108 cm and the lens was focused by viewing the alignment lines on the vinyl sheet that Satlantic uses to cover the plaque. SXR data were acquired at gain 1 and 10, and ambient background measurements were taken using the on-axis shutter that cast a shadow over the entire plaque. These ambient background readings were used to calculate the net signals. Readings with the objective lens of the SXR covered with a lens cap, termed *background* were also recorded. For these SXR data, the difference in the net signal, calculated using the ambient background and the background values, was between 5.5% and 8.0%. These values were calculated according to

$$\Delta = 100\,\frac{S_A - S_B}{S_T - S_A} \tag{12}$$

where Δ is the percent difference, S_T is the total signal, S_B is the background signal, and S_A is the ambient background signal.

On 12 May, F332 was positioned 199.9 cm ±0.2 cm from the plaque and data were recorded with the SXR. The distance to the plaque from the face plate of the SXR was 90.5 cm and SXR data were acquired at gain 10 and 100, with ambient background and background measurements taken as before. Measurements were taken as the amount of cloth baffling was increased. It was obvious that the measurements of 6 May were contaminated by interreflections between the white walls of the room and the plaque, since shadows on the plaque were visible once the on-axis shutter was inserted with no other baffling in place. Ambient background and background were recorded as reflective surfaces that were out of the FOV of the SXR but within the FOV of the plaque (walls, ceiling, floor, etc.) were covered with black cloth. The difference in the net signal between the two background configurations was between 0.6–1.7%.

In Lab III, the plaque spectral radiance was calculated assuming r^{-2} scaling for the lamp irradiance, and a nonlambertian diffuser with $R(0°/45°,\lambda) = 1.02R(8°/h,\lambda)$. These values were compared to the spectral radiance measured with the SAS-II with the result that the SAS-II on average underestimated the predicted radiance by about 1% (Fig. 10). In these studies, the spectral irradiance at the intersection of the plaque/lamp optical axis was calculated (as before) assuming r^{-2} scaling, but no assumption was made for the reflectance factor. Instead, the spectral radiance measured with the SXR and the SAS-II was used to determine the reflectance factor according to

$$R(0°/45°,\lambda) = \frac{\pi \tilde{L}(\lambda)}{\left.\hat{E}(\lambda, 50\text{ cm})\right|_{F332}} \left(\frac{\tilde{r}}{50\text{ cm}}\right)^2 \tag{13}$$

where $\tilde{L}(\lambda)$ is the measured spectral radiance (SXR or SAS-II), $\tilde{r}$ is the distance from the lamp posts to the plaque, and $\hat{E}(\lambda, 50\text{ cm})$ is the spectral irradiance of lamp F332 as measured by FASCAL at 50 cm interpolated to the measurement wavelengths using the modified planckian model (9).

The SXR results for 6 May indicate that the target reflectance was between 1.03–1.11 (Fig. 22). Not only are these values larger than those used in Lab III to predict the plaque radiance, $R(0°/45°,\lambda) \approx 1.009$ (Table 4), they increase with increasing wavelength, whereas the reflectance of Spectralon is not very dependent on wavelength for the region studied with these radiometers (Appendix B). When the measurements were repeated on 12 May with the SXR, $1.019 < R(0°/45°,\lambda) < 1.069$ (Fig. 22) was obtained. The SXR measurement at 775 nm appears to be a consistent outlier; the average of the results at the other wavelengths is $R(0°/45°,\lambda) = 1.030$. The SAS-II average results for 6 May are $R(0°/45°,\lambda) = 1.010$.

7.2 Spectral Radiance of the GSFC Sphere

The GSFC sphere was operated with lamps 1–4 on 12 May 1995 and the spectral radiance was measured with the SAS-II. Figure 23 shows the results, normalized to the value expected from the NIST calibration of the GSFC sphere on 25 April 1995. Also included in Fig. 23 are the normalized spectral radiances measured by the SXR on 25 April and on 4 May, during SIRREX-4 (Section 3). A cubic spline was used to interpolate the known radiance to the desired wavelengths. Table 6 gives the numerical results for these measurements.

7.3 Discussion

In Lab III, the average ratio of the SAS-II measured radiance to the radiance predicted from the lamp scale was 0.99 (Fig. 10 and Table 4), so it is possible to infer that either the SAS-II underestimated the spectral radiance or the application of (10) overestimated the plaque radiance. As mentioned in Section 4, using a factor of 1.01, not 1.02, in (10) would bring the SAS-II Lab III results in agreement with the average predicted spectral radiances.

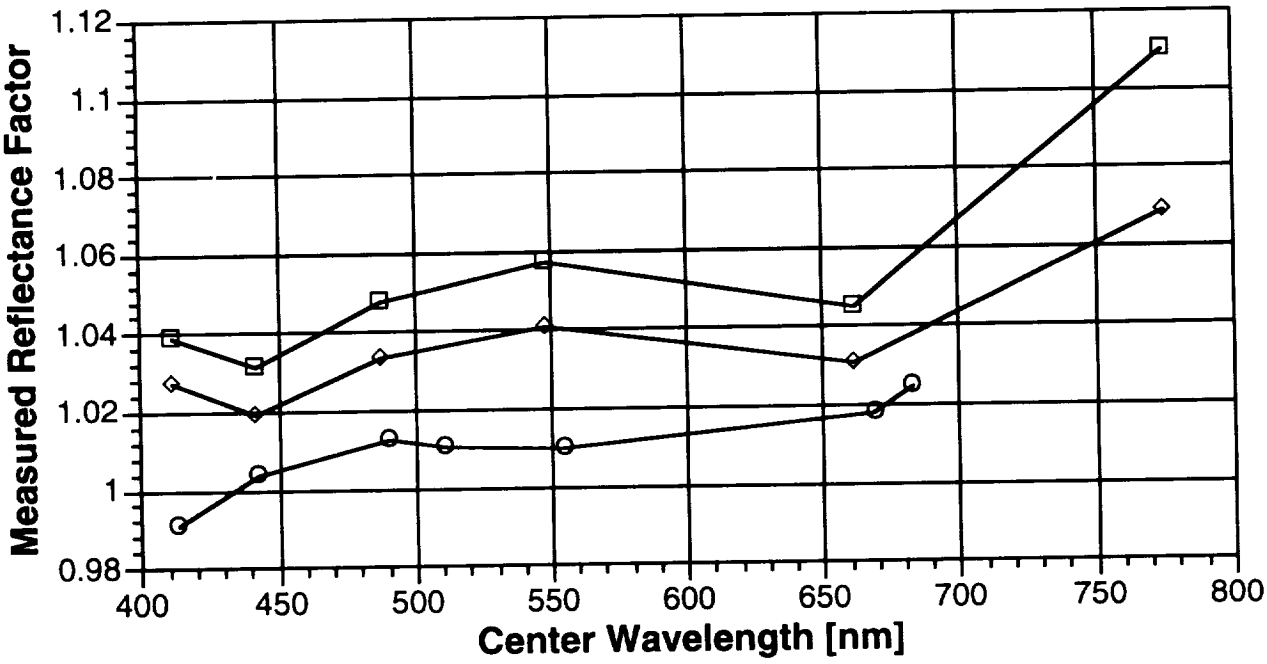

Fig. 22. Measurements of the Satlantic plaque with the SAS-II and the SXR at SIRREX-4. The SAS-II measurements on 6 May are given by the circles and the SXR measurements from 6 and 12 May by the squares and diamonds, respectively.

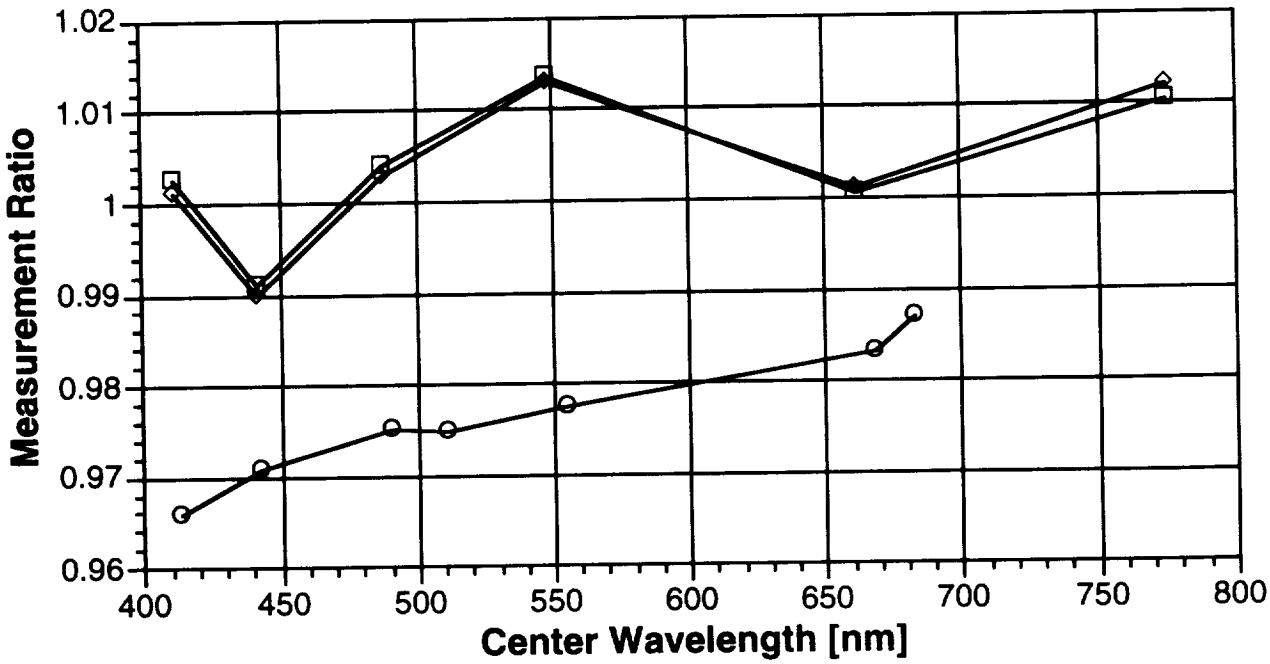

Fig. 23. Comparison of the SAS-II and the SXR using the GSFC sphere. The SAS-II measurements on 12 May are given by the circles and the SXR measurements from 4 and 25 May by the squares and diamonds, respectively.

Table 6. Spectral radiance of the GSFC sphere (four lamps) measured using the SXR (25 April 1995), the SAS-II (12 May 1995), and the standard-lamp-based calibration using the prism-grating monochromator by NIST (25 April 1995). The reported radiance values, $\tilde{L}(\lambda)$ and $\hat{L}(\lambda)$, are in units of $\mu W\,cm^{-2}\,sr^{-1}\,nm^{-1}$

SXR		NIST	SAS-II		NIST
λ [nm]	$\tilde{L}(\lambda)$	$\hat{L}(\lambda)$	λ [nm]	$\tilde{L}(\lambda)$	$\hat{L}(\lambda)$
411.53	0.92299	0.92200	412.83	0.91461	0.94699
441.62	1.5145	1.5298	442.89	1.5135	1.5591
487.10	2.7048	2.6972	490.44	2.7239	2.7937
			510.58	3.3097	3.3947
547.96	4.6374	4.5782	554.42	4.6801	4.7880
661.82	8.0679	8.0593	668.66	8.1036	8.2416
			682.58	8.4772	8.5893
774.78	10.515	10.388			

The measurements of the GSFC sphere in the four-lamp configuration by the SAS-II and the SXR give additional information. As can be seen from Fig. 4c, the GSFC sphere remained fairly stable during SIRREX-4 (as measured by the SXR). In addition, the SXR data from 25 April indicates the GSFC sphere was in calibration during SIRREX-4, again as measured by the SXR (see Fig. 23). It is assumed, therefore, that the GSFC sphere was in calibration on 12 May during the measurements with the SAS-II. Consequently, the results in Table 6 and Fig. 23 indicate the SAS-II values are smaller than the actual sphere radiance by 1.3–3.4% with a mean of 2.4%. There is a distinct trend with wavelength—the largest discrepancies are in the blue. This result is not consistent given the uncertainties assigned to the SAS-II and the sphere calibration (Early and Johnson 1996). This wavelength trend is also seen in the SAS-II plaque results.

If the SAS-II calibration is correct, the results of 6 May with the SAS-II and the plaque 13172 give an average reflectance factor $R(0°/45°, \lambda) = 1.010$. This value is in agreement with the average reflectance factor used in Lab III, $R(0°/45°, \lambda) = 1.02R(8°/h, \lambda)$ (Table 4). In other words, the measurements with the SAS-II on 6 May of plaque 13172 are larger when compared to the predicted radiance than all of the other data (Lab III sessions 1–5), and in fact give consistent results, not the 1% average discrepancy; this is not understood. The measurements with the SAS-II and the GSFC sphere, however, indicate the SAS-II calibration coefficients may be in error in a wavelength-dependent fashion. These measurements with the SAS-II of the GSFC sphere indicate the SAS-II calibration coefficients, F_{SL}, should be increased by about 2.4% (or 2.7% corrected to the average SXR scale).

The measurements with the SXR and the SAS-II of the plaque 13172, although made on two different days, indicate the F_{SL} values should be increased by about 2%; of course, this assumes the SXR measurement of the plaque reflectance on 12 May is accurate (this experiment gave an average $R(0°/45°, \lambda)$ of 1.030). An alternative explanation is that an unexplained effect (spatial nonuniformity of the radiance in the exit aperture of the GSFC sphere, scattered light on the plaque experiment, size-of-source effects in the radiometers, etc.) caused the SAS-II to measure the plaques correctly but the sphere incorrectly, and caused the SXR to measure the plaques incorrectly but the sphere correctly. The trends in wavelength are not understood; they could arise from inaccurate reflectance data, radiant flux that scatters with a strong spectral dependence, changes in the irradiance of the lamp at some wavelengths and not others, size-of-source corrections in the radiometers, and so forth.

The attempt here to measure $R(0°/45°, \lambda)$ is essentially the same experiment that was performed at SIRREX-3 with the SXR, the CXR, and six Spectralon plaques of various sizes. Although there was significant scatter in these data, the results indicated that the target reflectance was greater than unity (Mueller et al. 1995). The reflectance factor measurements using the SXR during SIRREX-4 supports this observation.

A second key result of the supplemental studies is the demonstration of the sensitivity to scattered light in the method of using a 1,000 W standard lamp 1.5–2.0 m from a large (approximately $50 \times 50\,cm^2$) plaque in order to realize spectral radiance. Proper baffling and thorough study of the ambient background was found to be necessary in order to achieve reasonable results with the SXR. For the SXR, the addition of the baffling reduced the effect of the scattered light, and it may be concluded (perhaps optimistically) that scattered light affects the results not in excess of the percent differences (0.6–1.7%) discussed in Section 7.1. Background signals (SAS-II collection optics covered) were only measured for the SAS-II on the first day Lab III (4 May); the difference in the ambient background and the background was between 5.1–6.7%. Scattered light, therefore, could be affecting the SAS-II SIRREX-4 plaque results.

The supplemental studies show $R(0°/45°, \lambda) \approx 1.025$ for plaque 13127. The uncertainty in this result, which is the average of the SAS-II and the SXR result, is difficult to assign, but it is at least 0.020. This uncertainty must

be reduced before progress in understanding this method of realizing spectral radiance can be made.

8. DISCUSSION

This section of the report is composed of two sections. The first deals with an evaluation of the hardware that has been used during this and previous SIRREXs, and the second is a critical evaluation of the SIRREX objectives, which have been and should remain, an evolving set of criteria.

8.1 Hardware Evaluations

The equipment at the various SIRREXs has included a number of integrating sphere sources, plaques, lamps, and radiometers. Internally-illuminated spheres include the GSFC sphere, the CHORS sphere, the BSI sphere, the UA sphere, and the Wallops Flight Facility (WFF) sphere; externally-illuminated spheres include the NOAA 420, the NOAA EG&G source, and the UCSB sphere. Spectralon plaques from 25.4 cm square to 45.7 cm square have been used with FEL-type irradiance lamps to realize a scale of spectral radiance. Filters or single grating monochromators have been used with silicon photodiodes, multiple silicon photodiodes arranged in a light-trapping configuration, or linear silicon photodiode arrays to measure radiant flux, and foreoptics or the double-aperture method have been used to generate a radiance response for the detector system. Various power supplies, shunt resistors, and DVMs have been used and intercompared. Key equipment is selected for critical evaluation here.

8.1.1 GSFC Sphere

The GSFC 107 cm (42 in) diameter sphere source (Section 3) is coated with a paint containing barium sulfate and has a 39.5 cm diameter exit aperture. The sphere is internally illuminated by up to 16 baffled 45 W quartz halogen lamps. Sets of four lamps are connected in series and each set of lamps is controlled by one of four precision current sources at 6.5 A. The source is cooled using a fan that is mounted on a baffled aperture on the top of the sphere; air flows out of the sphere through a baffled aperture at the bottom, after being drawn in through the fan port. Once the source has stabilized at the maximum level (all 16 lamps on), various lower radiance levels are achieved efficiently by turning off lamps associated with a particular power supply, followed by turning off the individual supplies.

8.1.1.1 Summary of Performance

The sphere was recoated by GSFC in April 1994. The measurements by GSFC consist of determinations of the average spectral radiance of the exit aperture using a standard irradiance lamp and a two-aperture method for the irradiance to radiance transfer (Appendix A). The collection optics for the monochromator consist of a small integrating sphere with a known aperture. Once the spectral radiance of the sphere has been established, the source can be used to calibrate radiometers or as a standard for calibrating an unknown sphere source. The resulting uncertainty in the spectral radiance scale on a source such as the GSFC 1.07 m diameter sphere has been estimated to be about 2.5% at 400 nm, 2% at 450 nm, 1.5% at 500 nm, and 1.3% between 500–700 nm (McLean pers. comm.).

Figure 24 compares the spectral radiance of the GSFC sphere (with all 16 lamps on) realized using the GSFC technique at SIRREX-1 (Mueller 1993), SIRREX-2 (Mueller et al. 1993), prior to SIRREX-3 (McLean pers. comm.), SIRREX-3 (Mueller et al. 1995), and on May 10 during SIRREX-4. The measurements made with the OL 746/ ISIC have been normalized using the NIST calibration values that were obtained just prior to SIRREX-4 using a prism-grating monochromator and calibrated tungsten strip lamp (Early and Johnson 1996). According to the OL 746/ISIC measurements, the radiance decreased between SIRREX-1 and SIRREX-2 by about 2.5%, and then increased by as much as 10% after the sphere was recoated in April 1994. As expected, the greatest change was in the blue. The two measurements with lamp F315 just prior to SIRREX-3 agree with the SIRREX-3 data, with a standard deviation of about 0.5%, but between 450–900 nm they are about 1.7% greater than the NIST calibration values from April 1995.

The OL 746/ISIC measurements at SIRREX-4 are anomalous, and without the NIST calibration data, it would be tempting to conclude the reflectivity of the coating on the sphere changed as a function of wavelength between SIRREX-3 and SIRREX-4. As was pointed out earlier (Section 3), it has been concluded that the discrepancy between the OL 746/ISIC measurements on 10 May 1995 and the spectral radiance calibration on 25 April 1995 is due to some aspect of the OL 746/ISIC measurements. Although the NIST calibration values could be in error, they are corroborated by the SXR data and are believed to be correct.

In summary, from 400–900 nm the GSFC technique of realizing spectral radiance for the 16 lamp configuration of the GSFC integrating sphere source has a scatter of about 0.5% for measurements that occurred over a two-month interval in the fall of 1994, but these data disagree in absolute value by about 2.5% from the NIST April 1995 calibration. It is likely that the sphere changed, (see Section 8.1.6), but it is also possible that the irradiance scale on the lamps used to calibrate the OL 746/ISIC was in error, or that there was some other systematic effect.

The SIRREX-4 OL 746/ISIC measurements demonstrate the difficulty in executing this type of measurement, and indicate that the technique may be uncertain by 3–4%. Finally, note in Fig. 24 that some of the OL 746/ISIC normalized data show odd features between 500–700 nm and at about 940 nm. The latter discrepancy is caused by

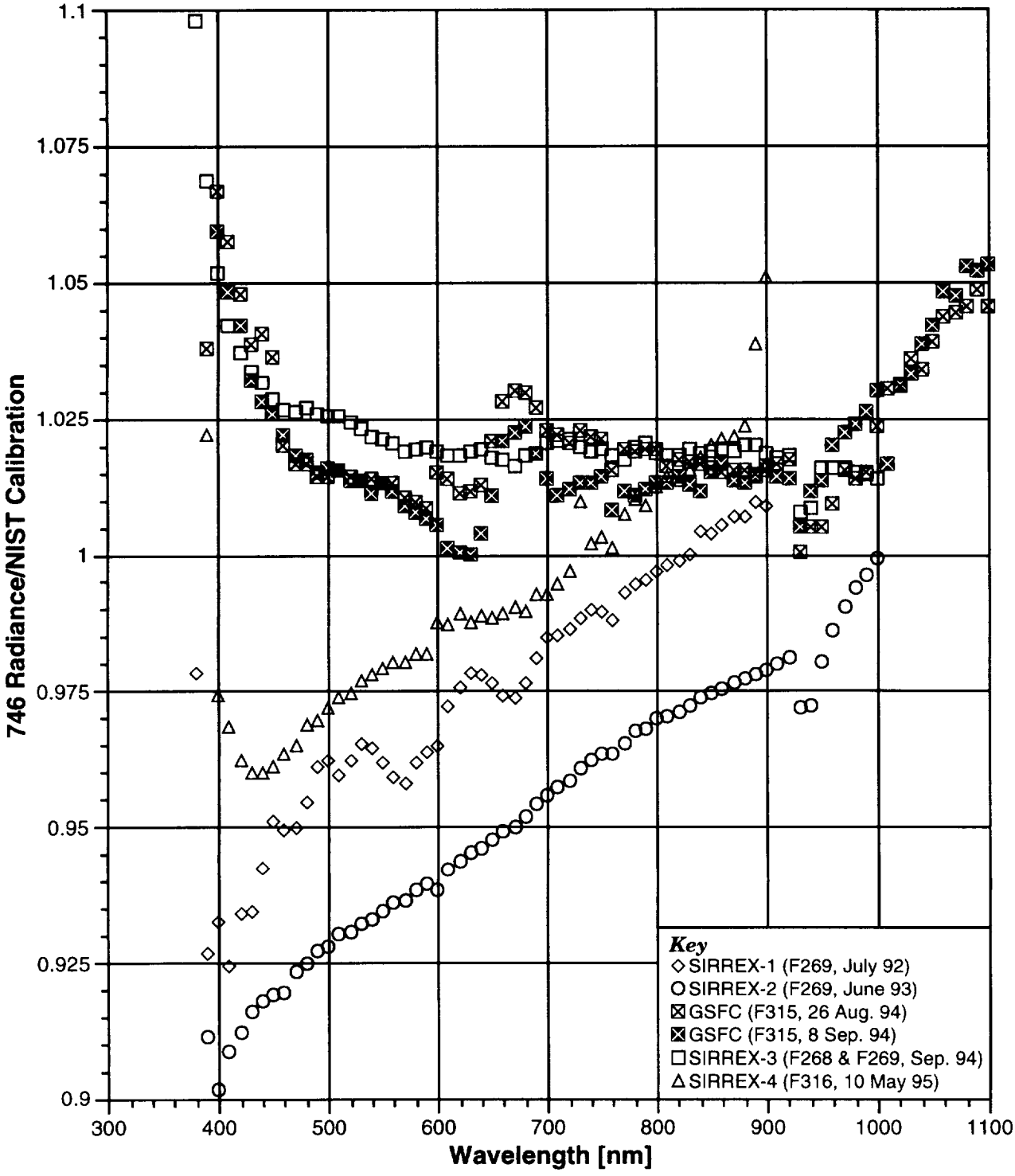

Fig. 24. A comparison of all SIRREX measurements of the spectral radiance of the GSFC sphere source, with 16 lamps operating, using the OL 746/ISIC system and FEL lamps from GSFC. The spectral radiances have been normalized using the NIST calibration values of 25 April 1995.

discontinuities in the spectral responsivity of the prism-grating monochromator that was used as the transfer radiometer and indicates that the spectral radiance calibration values in this region should be adjusted (smoothed). The broad oscillations of about 0.5% at the bluer wavelengths, however, do not correspond to any discontinuities in the spectral response of the prism-grating monochromator at NIST (Early and Johnson 1996) or the OL 746/ISIC system (Fig. 20), so the source of these features is currently unknown.

The SXR and other filter radiometers have been used not only to measure the radiance of the GSFC sphere, but also to characterize the angular and spatial variability of the spectral radiance at the exit aperture of the GSFC sphere. Prior to the recoating of the GSFC sphere, the spatial uniformity for the 16 lamp configuration was about 4% (peak to peak) as measured with a GSFC filter radiometer and the SXR (Mueller et al. 1994). After recoating, this value was about 0.74% (Early and Johnson 1996). At SIRREX-3, the SXR was used to study the dependence of the spectral radiance with observation angle in the horizontal plane in the 16 lamp configuration. At the center of the sphere, the spectral radiance increased by about 1.1% at an observation angle of 15° compared to the value measured at normal incidence (Mueller et al. 1995). The measurements reported here (Section 3) reproduce this result.

For other lamp configurations, fewer data have been acquired. Spectral radiance measurements have been reported in the SIRREX-2 and SIRREX-3 documents for all 16 possible levels (16 lamps to 1 lamp configuration). The variation with observation angle has only been studied for the 16 lamp configuration, but the spatial uniformity was measured for the 16, 8, 4, and 1 lamp configuration (Early and Johnson 1996). These latter two configurations require asymmetric illumination of the sphere and the peak-to-peak variability increased to as much as 2.2%. The relative spectral shape does not change significantly as the lamp configuration is varied, see the results in Section 3 as well as from SIRREX-3 (Mueller et. al 1995) and the NIST characterization of the sphere in April 1995 (Early and Johnson 1996).

8.1.1.2 Recommendations

The GSFC sphere has performed well, but there are issues related to the equipment that are cause for concern.

1. Through a combination of electrical and mechanical design constraints, it is not possible to operate the lamps for symmetric illumination of the sphere for some radiance levels. As pointed out by Early and Johnson (1996), this does not have to be the case. Asymmetric illumination will degrade the uniformity of the radiance in the exit aperture of the sphere.
2. There is no wiring diagram, so it would be difficult to optimize the performance of the source or repair it upon failure.
3. The gauge of the electrical wire used to operate the lamps and the power supplies does not appear to be adequate given the electrical power of the source.
4. The meters for recording lamp hours do not work, so this parameter must be recorded manually. The wiring harness and power supplies should be replaced as soon as possible.
5. There is no monitor photodiode to serve as a reference for the radiance of the source; the addition of a monitor photodiode is desired but not mandatory.

The radiometric techniques employed with this source are lacking in several areas.

1. There is no procedure for accurately recording the key lamp parameters (current, voltage, and total operating time) that are required in order to assess the radiometric performance of the source. It is possible GSFC always calibrates the source using the OL 746/ISIC apparatus prior to its use as a radiometric standard, but even if this is the case, it is imperative to record the lamp parameters so a maintenance schedule can be followed. At a minimum, a notebook should be physically attached to the source so these parameters can be recorded. A preferred and more robust solution would involve adding a computer interface to the power supplies and using computer software to record all of the required parameters into a database.
2. The maintenance schedule for the source is lacking. For example, the procedures and schedules for replacing lamps, recoating the sphere, replacing the filter on the fan, or recalibrating the power supplies do not exist. There is no apparent procedure to ensure that seasoned lamps will always be available if required. Aside from the work at the SIRREXs, there is no apparent plan to monitor the spatial or angular uniformity of the source. In light of the critical role this source has in the SeaWiFS program, a maintenance schedule for all of these factors should be developed and implemented as soon as possible.

8.1.2 Lamps

The 1,000 W quartz-halogen, double-coiled, tungsten lamp designated FEL is the basis for the spectral irradiance and spectral radiance scales in the SeaWiFS Project. As irradiance standards, they are used to assign calibration coefficients to oceanographic radiometers that measure in-water and atmospheric irradiance (see Section 5). Using either the plaque method (Section 4) or the two-aperture method and a monochromator (Section 3), FEL lamps are used by secondary standards laboratories, commercial suppliers, and ocean scientists to realize spectral

radiance scales, which then form the basis of the radiometric calibration of commercial integrating sphere sources or oceanographic radiometers that measure in-water spectral radiance.

8.1.2.1 Summary of Performance

FEL lamps have been issued by NIST and several secondary standards laboratories for many years, with minor modifications to the mechanical design of the coil. The characteristics and performance of FEL lamps has been fully documented by NIST (Walker et al. 1987a). In this document, information is provided on the procedures used by NIST to secure the lamp to the bi-post mount, screen the lamp as a radiometric standard, position and align the lamp using a kinematic base and an alignment jig, assign the values of spectral irradiance and associated uncertainty, estimate errors caused by lamp drift and inaccurate current settings, interpolate in wavelength, and so forth. In a separate publication, information is given on stable lamp operation using computer control (Walker and Thompson 1995b).

With proper care and use, FEL lamps will remain stable for many burning hours, and the uncertainties assigned by NIST or the secondary standards laboratory will be appropriate for incorporation into the uncertainty budget of the particular experiment. The uncertainties assigned by NIST for a typical FEL lamp for wavelengths between 350–1,300 nm are about 0.5% (Gibson pers. comm.), so that with great care, radiometric scales in the SeaWiFS project can be established with combined uncertainties of about 1–2%. Since these calibrated lamps are expensive to acquire and maintain, consideration must be given to their operation and use.

8.1.2.2 Recommendations

It must be recognized that the spectral irradiance scale assigned to an FEL lamp during calibration is valid only when the lamp is operated in the same fashion as when it was calibrated. The most obvious parameter is the current, and it is recommended that a calibrated shunt resistor and DVM be used to determine the current in the lamp. There are many other constraints, however, and these are often neglected.

1. The lamp should be run vertically in air without any housing or baffles close to the lamp.
2. Reflections from the base should be blocked (see Section 5).
3. The calibration is valid only over an area 23 mm in diameter located 50 cm from the front of the mounting posts.
4. The quartz envelope should be pristine and never come into contact with oil or grease (e.g., fingerprints). If it does become contaminated, it should be cleaned with lens tissue or sterile cotton and optical grade ethanol while wearing lint-free cotton gloves.
5. The current should be increased slowly and the lamp should never be moved when it is still warm.
6. NIST recommends recalibration after every 50 burning hours.
7. A complete and thorough plan for maintaining a scale of spectral irradiance with FEL lamps should be written.

In terms of the last item, a simple implementation would be to have one secondary standard and use it to transfer the NIST scale to many other, less expensive, working standards. The working standards can then used for most measurements, with the secondary standard returning for recalibration after a given number of burning hours. Clever use of the working standards will supply information necessary if unexplained results are obtained (e.g., one working standard could be selected to receive zero burning hours after the initial transfer from the secondary standard). The current, voltage, and burning hours must be recorded for each lamp, and this record should be correlated with instrument calibrations.

For oceanographic applications, an FEL lamp is often used at distances greater than 50 cm and for collecting areas greater than 23 mm in diameter. As a special service, NIST can perform measurements that address these issues. Goniometric scans have been done on FEL lamps for angles up to 10° (horizontal) and 6° (vertical). The irradiance can be determined at distances of 0.5, 1.0, and 1.3 m. The expense associated with measurements at NIST, however, may indicate that a suitable approach would be to characterize working standard lamps at the user facility. Finally, it must be noted that FEL lamps have an incorrect spectral shape for oceanographic applications. The uncertainty introduced by this characteristic must be investigated and quantified.

8.1.3 Plaques

Spectralon plaques are well established as reflectance standards for applied radiometry (Jackson et al. 1987, Jackson et al. 1992, Bruegge et al. 1993, and Soffer et al. 1995), and they are used by BSI, Satlantic, CHORS, and other members of the SeaWiFS community to realize a spectral radiance scale using an FEL lamp. With proper care and use, they are adequate radiometric instruments, more consistent than surfaces painted with barium sulphate ($BaSO_4$) and easier to produce in large sizes than pressed PTFE.

8.1.3.1 Summary of Performance

Studies at SIRREX-2 and SIRREX-3 were unable to generate reliable values of spectral radiance and work at

SIRREX-4 indicates this is possible only with more research, analysis, and measurements. The SeaWiFS community has to date applied the lamp/plaque method in a rather simplistic fashion, so a list of some of the factors that should be considered in future work is presented next.

8.1.3.2 Plaque Uncertainty Sources

As discussed in Sections 4 and 7, and Appendix B, the reflectance factors $R(\theta_i/\theta_v, \lambda)$, where θ_i is the incident angle and θ_v is the viewing angle, are usually not provided by the manufacturer, Labsphere. The use of the total directional/hemispherical reflectance, $R(8°/h, \lambda)$, for $R(\theta_i/\theta_v, \lambda)$ may cause an error of several percent (see Table B1). These reflectance data are required for the range of incident and viewing angles, spatial locations on the plaque, and wavelengths that correspond to the measurement geometry and design of the radiometer. The effect of polarization must also be considered, since sources with various polarization properties are used in the process of transferring spectroradiometric scales with Spectralon plaques. Barnes (pers. comm.) found that $R(0°/45°, \lambda)$ for NIST plaque 12127-A differed by about 1% for S- and P-polarized radiation. On the positive side, Spectralon is fairly uniform with respect to spatial location and the wavelengths of interest here, and Jackson et al. (1992) indicates that characteristic equations for $R(\theta_i/\theta_v, \lambda)$ in terms of $R(8°/h, \lambda)$ should be possible.

The reflectance of Spectralon depends on how the material was treated during storage, handling, and use. The greatest change in reflectance occurs for wavelengths between 250–400 nm, but even in the visible spectral region, great care must be taken with these radiometric standards. At SIRREX-3, measurements were made of the CHORS plaque before and after cleaning; the radiance, when illuminated by an FEL lamp at 1.5 m, increased by about 1%. GSFC has developed a set of procedures, which are summarized in Section 8.1.3.3 (Butler pers. comm.).

The spectral irradiance at the surface of the plaque is not well understood with the current practices. First, the FEL lamp is always operated at a distance greater than 50 cm. The 50 cm is measured from the front of the mounting posts, not the radiometric center of the lamp (here we are treating the lamp as a point source). Therefore, if r is defined as in Section 4, then the correct distance scaling factor in (7), (8), or (10) is

$$\xi = \frac{50 + \Delta r}{r + \Delta r} \tag{9}$$

where Δr is likely to be on the order of a few millimeters. If Δr is assumed to be half the diameter of the mounting posts, so that the radiometric center of the FEL lamp is the same as its geometric center, then $\Delta r = 3$ mm and the error at 1.5 m caused by neglecting this effect is 0.8%. Second, the spectral irradiance is not uniform across the plaque. If the FEL lamp is approximated as an ideal point source, the distribution of spectral irradiance across the plane of the plaque follows the $\cos^3$ *law* (O'Shea 1987),

$$E(x, y, \lambda) = E(0, 0, \lambda) \cos^3 \theta \tag{10}$$

where

$$\tan \theta = \frac{\sqrt{x^2 + y^2}}{r} \tag{11}$$

and r is the perpendicular distance from the plaque to the point source, which is located so as to illuminate the center of the plaque ($x = 0, y = 0$). For measurement geometry in Lab III, the spectral irradiance at the edge of the plaque ($\theta = 8.7°$) would be 3.4% smaller than that at the center of the plaque if $r = 150$ cm. The FEL lamps are not point sources, however, and the actual spatial distribution of spectral irradiance is not symmetric with azimuthal angle nor does it follow the $\cos^3 \theta$ law. NIST has measured the change in irradiance at 50 cm caused by rotating an FEL lamp about its vertical and horizontal axes. Variations caused by rotation about the horizontal axis were as large as 8% at 6° and for rotation about the vertical axis as large as 1% at 10°; the combined maximum rotation also resulted in changes of up to 8%. Several lamps were measured and large variabilities (several percent) were observed among the lamps.

Not only is the spectral irradiance spatially nonuniform in an asymmetric fashion, the response of the radiometer also depends on the location of the source (of differential area $dxdy$) with respect to the center location of the instrument's FOV. The ideal radiometer has unity relative response to point sources within its FOV and zero response for all other source locations. The simple, two-aperture design of most commercial oceanographic radiometers results in a vignetted FOV (O'Shea 1987) that has substantial response in the *shadow region*. For example, the SAS-II used in Lab III has a relative response between 100% and 1% for angles between −7° and +10°. The 45° angle between the plaque and the radiometer results in an azimuthally asymmetric situation; the distance from the aperture stop in the radiometer to the source also varies across the FOV.

The high-power FEL lamp, the large plaque, and the large FOV of the radiometer exacerbate problems with scattered light. The use of the on-axis baffle, which is designed to block direct radiation from the lamp, but not to affect the scattered radiation that is present during calibration of the radiometer, may result in misleading results because of the presence of multiple reflections. The reflectivity as a function of wavelength of the surfaces that are used to absorb or scatter the unwanted radiation may be inadequately characterized or understood. For example, anodized aluminum is reflective past about 700 nm.

8.1.3.3 Recommendations

The approach of Jackson et al. (1992) should be investigated, with the goal of developing characteristic equations

to assign reasonable values for $R(\theta_i/\theta_v, \lambda)$ as a function of wavelength, incident and view angles, and polarization in terms of the $R(8°/h, \lambda)$ that is provided by the manufacturer. This will require measurements of the BRDF of several Spectralon plaques as a function of these parameters; the spatial variability of the BRDF must also be characterized. Directional/hemispherical measurements as a function of wavelength must also be performed. This work could be done by several laboratories, e.g., NIST, GSFC, and Labsphere.

Spectralon samples should be stored in either glass or metal containers. In the case of glass, the container should be cleaned and baked out before introducing the sample. In the case of metal, the container should be cleaned with the goal of removing any oil left from the machining process. Spectralon should not be stored in plastic containers due to its ability to adsorb hydrocarbons that may outgas from the plastic. The container should be designed so that the optical surface is not in contact with any material. Spectralon should be stored in darkness. Storage of samples at room temperature and humidities typically experienced in laboratories is permitted for visible and near infrared work.

The samples may be transported in glass or metal containers. These containers may be the same as the ones used for storage, or they may be specially designed for transport. In any case, the same issues apply. The ideal transportation container is rugged, air-tight, and employs a one-way pressure valve. Following closure of the container, the one-way valve blocks the flow of air into the container but allows for its release. At the final destination, and in a clean laboratory, the pressure equalization valve is released so that the container can be opened. Thus, contaminants such as jet fuel vapor, dust, and vehicle exhaust are not deposited on the plaque during air or ground shipment. If this type of container is not available (e.g., due to its high cost), then the storage container can be used, but it should be *double bagged* in clean, nonplastic bags. Anti-static shielding bags or Llumalloy™ † bags may be used and sealed with cleanroom or Kapton® ‡ tape. Cleanroom packaging film or bags may also be used and sealed either with this tape or a heat sealer.

Following removal of the Spectralon sample from either its storage or transportation container, the sample should be used for the amount of time necessary to perform the desired optical tests or calibrations and then returned to its storage container. Spectralon samples are best handled when wearing either latex or lint-free cotton gloves. The optically reflective side of the sample should never be touched with any object. In general, the handling of Spectralon should be minimized. Spectralon is electrostatic and the accumulation of charge on the sample surface should be prevented, especially in dusty environments. In the case of dust accumulation, an aspirator can be used to blow air gently across the surface of the sample to remove the foreign particles. The heavy plastic sheet used by Satlantic to align the plaque to the optical axis caused static charge to accumulate on the surface and probably increased the probability that the surface properties are altered every time the plaque is used, thereby changing the reflectance.

In order to align the plaque on an optical bench, a fiducial, reflective *alignment* plaque such as a polished aluminum plate should be used. The dimensions of the metal or glass alignment plaque should be exactly the same as the Spectralon plaque to be aligned. The use of such a device would aid in determining the distance from the plaque to the front of the lamp mounting posts. Incorporation of Spectralon into field experiments poses special problems. In one case, the extreme temperatures associated with working under sunny conditions compromised the adhesive tape that was used by the manufacturer to adhere the sample to the metal mounting plate, and the sample fell into the water; obviously, for some applications, modifications of the Spectralon plaque is required. Because of the increased possibility of contamination in field work, it is recommended that an additional sample be maintained in the laboratory as a reference standard.

Regarding the measurement equation (7), several recommendations are in order.

1. The distance offset Δr can be investigated by making measurements of the irradiance as a function of the separation between an irradiance detector and the FEL lamp. Care should be exercised in this experiment, as the effects of scattered light may contaminate the results.
2. Using an irradiance detector with a small collection area, the spectral irradiance in the plane represented by the surface of the Spectralon plaque should be measured for spatial uniformity by scanning the detector in x and y. The relative response of the radiometer to point sources across the target plane represented by the plaque should also be measured. Both of these tests must be done for each FEL lamp used to realize spectral radiance and for several radiometers in each class of instruments supplied by the commercial vendors.
3. The proper measurement equation for this experiment is complicated because of the requirement to include the spatial and angular variability of the source and detector, and the correct model must be formulated and adopted by all researchers who use this technique. The approach of the scientists who measure backscattered solar radiation in the ultraviolet is one example (Janz pers. comm.). In this experiment, the spectral radiance response of the Solar Backscatter Ultraviolet Radiometer-2 (SBUV-2) instrument is obtained using diffuse plaques and

† "Llumalloy" is a trademark of Courtaulds Performance Films, Martinsville, Virginia.

‡ "Kapton" is a registered trademark of E.I. DuPont de Nemours & Company, Wilmington, Delaware.

FEL lamps, so it is analogous to the calibration of oceanographic radiometers that measure spectral radiance.

In the meantime, several procedures should be examined by the practitioners of this method to realize spectral radiance. In order to assess the effect of scattered light, the location and size of the baffles should be varied. If measurement channels beyond the visible are important, absorbing surfaces should be made of black felt or painted with flat black paint. To check for systematic errors, the distance between the lamp and the plaque, as well as the radiometer and the plaque, should be varied over as broad a region as possible. The radiometer should never be placed so close to the plaque that it casts a shadow on the plaque.

Measurements should be taken for different orientations (rotation about the mechanical axis) of the radiometer. In the case of radiometers with multiple channels that are physically offset, each channel should be aligned to the center of the plaque; otherwise the FOV of the radiometer is not centered on the irradiance distribution of the lamp. To test that the FOV of the sensor is completely filled by the source, highly reflective and then highly absorptive plates should be mounted next to the sides and in the plane of the plaque, and the measurements recorded for these configurations.

8.1.4 OL 746/ISIC

The 746/ISIC is a far from ideal transfer radiometer for this type of lamp and sphere intercomparison experiments. In the lamp transfers, the SNRs of this instrument are, at best, marginally adequate at wavelengths between 400 and 500 nm, and are too low to be useful below 400 nm. For measurements of the lower radiance level spheres, the OL 746/ISIC SNRs result in uncertainties greater than 5% at wavelengths below 500 nm. Furthermore, at SIRREX-3 the responsivity drift of the OL 746/ISIC approached 1% per hour and it was necessary to recalibrate the instrument by viewing the reference FEL at 2 hour intervals during extended transfer intercomparisons. This requirement both significantly increases the difficulty of transfer experiments, and rapidly accumulates operating hours on the reference lamp.

The measurements at SIRREX-4 of the spectral radiance of the GSFC sphere indicate that there are remaining systematic effects with the OL 746 and/or the measurement procedure. It is possible that the grating shifted during transport from Lab V to Lab II on 6 May 1995. There was no time in Lab II to verify the wavelength scale on the OL 746/ISIC using the HeNe laser, but it is unlikely to have shifted since the grating turret was not manipulated. In any event, estimates using the spectral radiance data measured by NIST on 25 April and the OL 746/ISIC on 10 May indicate that a 3 nm shift in the correct direction could reconcile the OL 746/ISIC data with the NIST measurements. Therefore, it is recommended that all future measurements include one or more scans of the flux from a HeNe laser.

It is also possible that there were problems with scattered light in Lab II. However, the measurement technique was basically the same as was used at SIRREX-3. In order to facilitate measurements of integrating sphere sources with the OL 746/ISIC in the future, it is recommend that a portable baffle tube be designed. The integrating sphere that serves as the collection optic, and the integrating-sphere source both have very large fields of view, making this measurement susceptible to stray radiation. A telescoping baffle tube with adjustable apertures would solve this problem. Careful design could also address alignment issues. The proper design of the baffle tube is shown in Fig. 25 (Vukobratovich pers. comm.).

8.1.5 SXR

The SXR is a multichannel imaging radiometer that utilizes interference filters for spectral selection and whose primary purpose is to verify the spectral radiance of calibration sources (Johnson et al. 1996). The radiometer is portable, stable, and provides a detector-based verification of the spectral radiance of integrating sphere sources and illuminated diffuse plaques at six wavelengths from 412–775 nm. Custom electronic circuits are used to provide a DC voltage that is related to the spectral radiance of the source, remote control of the measurement wavelength, and gain.

The SXR is used to compare the predicted voltage for a given source of spectral radiance, which can be calculated from the known spectral radiance of the source and the spectral radiance responsivity of the SXR, to that measured by the SXR. Since the spectral radiance of the source is determined from independent measurements (that may be traceable to NIST), this type of comparison should agree to within the combined uncertainties assigned to the SXR and the source.

8.1.5.1 Summary of Performance

The SXR has been proven to be a reliable transfer radiometer, with a Type A uncertainty in spectral radiance repeatability of less than 0.1% and an estimated uncertainty of approximately 1.5% in radiance responsivity at all measurement wavelengths. The nonideal point-spread response, consisting of weak side lobes in the channels corresponding to measurement wavelengths at 662 and 775 nm, results in size-of-source corrections on the order of 0.5–1.6% (depending on the size of the source being measured). These corrections, which have not been applied to any of the SIRREX-4 measurements, introduce additional uncertainties on the order of 0.3–0.5%.

In Fig. 26, the spectral radiance of the GSFC sphere is compared, with all 16 lamps on, measured with the SXR at SIRREX-2 (Mueller et al. 1993), before SIRREX-3

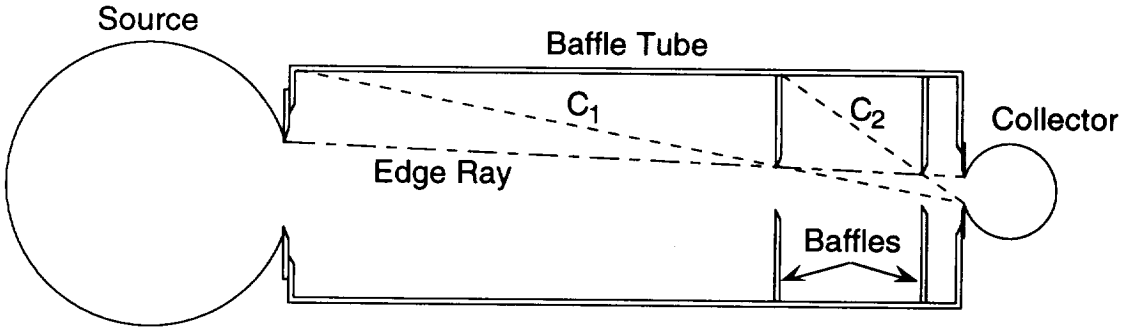

Fig. 25. An illustration of the proper design principles for a baffle system. The edge ray connects the edges of the source and collection aperture as shown (broken dashed line). The first corner ray connects the corner of the baffle housing in the plane of the source and the opposite edge of the collection aperture (dashed line). The first baffle is located at the intersection of the edge ray and the first corner ray. This geometric construction is repeated for as many baffles (with the corner rays connecting the corners of the associated baffles) that can be accommodated in the baffle tube. The inside diameter of the baffle tube is arbitrary as long as these design steps are followed. The inside of the baffle tube should be painted with a spectrally flat, highly absorbing paint. Geometric considerations would indicate that the paint should be specular, but in fact good performance is realized with diffuse paints because the emissivity is very large (with diffuse paint it is usually easier to achieve a uniform result). The orientation of the bevels on all of the baffles is of secondary importance; the critical design feature is to make them as sharp as is possible, after Vukobratovich (pers. comm.).

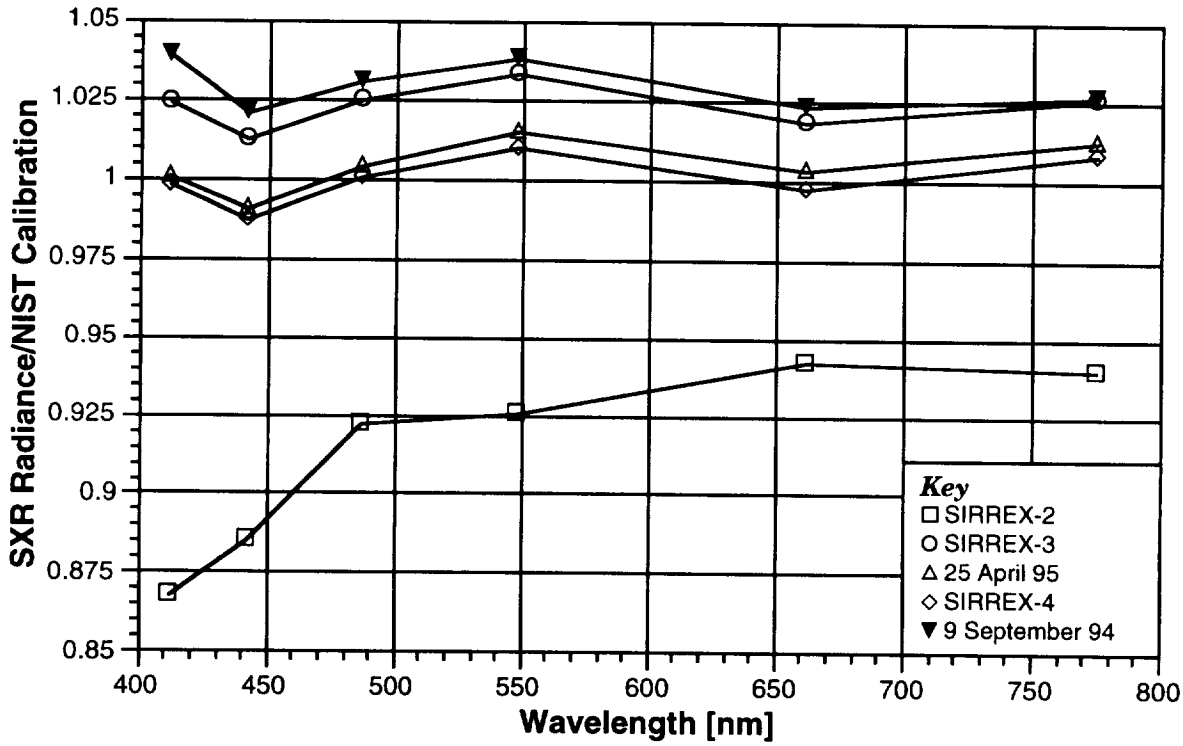

Fig. 26. A comparison of all SIRREX measurements of the spectral radiance of the GSFC sphere source with 16 lamps on using the SXR. The spectral radiances have been normalized using the NIST calibration values of 25 April 1995.

and SIRREX-3 (Mueller et al. 1995), and SIRREX-4 (Section 3). The measurements with the SXR have been normalized using the NIST 25 April 1995 calibration values as was done for the OL 746/ISIC data in Fig. 24. The SXR data also indicate that the radiance increased when the sphere was recoated in April 1994, and that at the time of SIRREX-3, the sphere was about 2.6% brighter than the 25 April NIST calibration values. The SXR data at SIRREX-4 are in good agreement with the NIST calibration. Figures 24 and 26 taken together indicate that the SXR and the OL 746/ISIC data are in general agreement, and that the GSFC sphere increased in radiance by as much as 10% when it was recoated, but that between SIRREX-3 and SIRREX-4, the radiance has decreased by about 2%.

8.1.5.2 Recommendations

Sufficient experience has been acquired with the SXR so that modifications to the data acquisition software can be implemented in a useful manner. It is recommended that an automated data analysis program be developed that will operate in conjunction with the data acquisition software. The radiometric response of the SXR should be checked at NIST before and after each field exercise and the results documented. Finally, the characterization and calibration data should be incorporated into the SeaWiFS database. The characteristic shape of the discrepancy between the SXR measurements and independent radiometric scales, with the SXR appearing to underestimate the spectral radiance at 442 nm and overestimating it at 548 and 775 nm, although within the uncertainties, indicates that the calibration coefficients of the SXR should be studied in further detail.

8.2 SIRREX Objectives

After executing four SIRREXs the authors are in a position to critically evaluate the various experimental procedures employed so far in terms of the hardware performance and experimental techniques as well as a reassessment of the SIRREX objectives outlined in Section 1.1.

Irradiance Lamps: Because of the decision to incorporate the training and lecture format, the intercalibration of a set of working standard irradiance lamps was not done at SIRREX-4. Lab V (Section 6), however, demonstrated that when the proper measurement procedures are used, the irradiance of a test lamp could be measured with sufficient accuracy (an uncertainty of 1% or less) for the SeaWiFS calibration and validation program from about 500–900 nm (Fig. 21a) using the OL 746/ISIC. Two problems remain with the original SIRREX objective: the reliability of the irradiance values assigned to the GSFC lamp and the requirement to make accurate transfers below 450 nm. It is also a very time consuming activity to measure many lamps. Consequently, it was decided to curtail this objective in the future in favor of intercomparisons of actual field instruments, using a setup similar to Lab IV (Section 5). The lamp irradiance should be maintained by the user via periodic recalibration at NIST or a secondary standards laboratory.

Radiance of Spheres: Intercalibration of a set of integrating sphere sources was not done at SIRREX-4 because of the decision to incorporate the training and lecture format. Lab I (Section 2), however, demonstrated that when the proper measurement procedures are used, the radiance of a test sphere could be realized with sufficient accuracy (an uncertainty of 1% or less) for the SeaWiFS Calibration and Validation Program from 400–900 nm using a single grating monochromator with foreoptics (Fig. 3). The problem with the original SIRREX objective is in acquiring sphere sources that have adequate stability and in the techniques used to realize and transfer spectral radiance. Consequently, it was decided for the future to reevaluate this objective and incorporate intercomparisons of actual field instruments, using a setup similar to the SXR and photometer exercises in Lab II (Section 3). Ideally, sphere radiances should be assessed by the user via periodic recalibration at NIST or a secondary standards laboratory.

Radiance Scales on Plaques: Previous SIRREXs established diffuse plaques could be used in a straightforward fashion, but that the value of the spectral radiance was not determined easily. SIRREX-4 identified several areas of concern and these are described in Section 8.1.3. The study of diffuse plaques as a method to realize spectral radiance from an irradiance lamp will continue to be a key SIRREX objective.

Intercompare Radiometers and Ancillary Equipment: This objective will be expanded in future SIRREXs to include comparison of the irradiance and radiance calibration of field instruments using NIST-traceable standards. In-water intercomparisons will also form a significant component of future work.

Protocols and Measurement Techniques: The execution of SIRREX-1, SIRREX-2, and SIRREX-3 indicated the need for training. A variety of measurement practices were observed among the participants, some of which are known to be poor choices for the methods and techniques in radiometry that consistently result in the best possible measurements. In addition, the lack of emphasis on experimental radiometry in US academic institutions results in a constant flow of fresh talent in need of practical training. Therefore training, with participation by NIST personnel, will be a key SIRREX objective, with the goal of implementing uniform and excellent measurement practices by all oceanographic and atmospheric researchers relevant to the SeaWiFS mission.

ACKNOWLEDGMENTS

Several individuals at NIST distinguished themselves during SIRREX-4 in either technical planning (Robert Saunders and Chris Cromer), logistical support (Jaqueline Hardware and Ruth Lenhart), or conference facilities (Patrice Boulanger and Diane Harrison). Charles Gibson provided calibrated lamps and supplies for several of the laboratory experiments. The authors thank all of these individuals for contributing selflessly to the success of this challenging activity. In addition, Chris Cromer participated in several useful discussions during the initial preparation of the manuscript, and Scott McLean provided Satlantic instrumentation and plaque discussion material. Yvonne Barnes at NIST measured a Spectralon plaque and contributed the results of that effort. Jim Butler at NASA provided data from his facility at GSFC and is thanked for useful discussions.

APPENDICES

A. The Two-Aperture Method

B. Reflectance Factors for Spectralon

C. Spectral Shape of Radiometric Sources

D. Attendees to SIRREX-4

Appendix A

The Two-Aperture Method

The illuminance E_v ($\mathrm{lm\,m^{-2}}$) incident on a photometer is given by

$$E_v = 683.002\,F \int E_e(\lambda)V(\lambda)d\lambda \qquad (A1)$$

where $E_e(\lambda)$ is the spectral irradiance, $V(\lambda)$ is the normalized photopic response function, and F is the spectral correction factor given by

$$F = \frac{\int \phi_e(\lambda)V(\lambda)d\lambda}{\int \phi_e(\lambda)R_n(\lambda)d\lambda} \qquad (A2)$$

for source spectral flux $\phi_e(\lambda)$ and photometer normalized spectral responsivity $R_n(\lambda)$.

In this exercise, the photometer normalized spectral responsivity was measured at the NIST Spectral Comparator Facility (see Fig. 6) and the spectral radiance of the sphere measured at NIST was used for $\phi_e(\lambda)$, since the relative spectral shapes are the same. The F factors at the four different lamp settings were calculated by fitting a 1 nm interval cubic spline to the normalized spectral responsivity values and using the accepted values for $V(\lambda)$, giving values between 1.00569 and 1.00577. In addition to F and $V(\lambda)$, the spectral irradiance $E_e(\lambda)$ at the photometer must be calculated from known sphere spectral radiance $L(\lambda)$ and the measurement geometry, using the two-aperture method.

For the circular sphere source aperture of radius r_1 and circular photometer detector aperture with radius r_2 and separated by distance d (Fig. A1), if the two apertures are parallel and coaxial the spectral irradiance reduces to

$$E(\lambda) = \frac{\pi r_1^2 L(\lambda)}{d^2 + r_1^2 + r_2^2}[1 + \delta + 2\delta^2 + \ldots] \qquad (A3)$$

where $\delta = r_1^2 r_2^2 (d^2 + r_1^2 + r_2^2)^{-2}$. Here $L(\lambda)$ is the average spectral radiance in the aperture source.

Appendix B

Reflectance Factors for Spectralon

To calculate the spectral radiance of a diffuse plaque in terms of the incident irradiance, the BRDF, $R(\theta_i/\theta_v, \lambda)$, must be known. The value for $R(\theta_i/\theta_v, \lambda)$ is simply π times the BRDF. The calibration procedure of the Spectralon manufacturer, Labsphere, provides the total directional/hemispherical reflectance, $R(8°/h, \lambda)$ (by special request $R(0°/45°, \lambda)$ can be provided). The specular component in the $R(8°/h, \lambda)$ component, if any, is included in this measurement. This directional/hemispherical reflectance factor indicates the amount of absorption by the diffuser; it is know that for pressed PTFE samples, this parameter varies with angle of incidence and wavelength (Weidner and Hsia 1981). For PTFE, a good approximation for $\theta_i < 10°$ is that $R(\theta_i/h, \lambda)$ is constant with θ_i. This is relevant because slightly different angles of incidence are used at various laboratories in the directional/hemispherical measurements, and in addition the value $R(0°/h, \lambda)$ is sometimes required.

The directional/directional reflectance factor, $R(\theta_i/\theta_v, \lambda)$, is a measure of the scattering distribution function of the material. The sense of the angles is interchangeable due to the Helmholtz reciprocity principle assuming isotropic behavior for the azimuthal angles. For lambertian diffuse surfaces, the scattered radiance is constant with the viewing angle and the reflectance factor $R(\theta_i/\theta_v, \lambda)$ equals $R(\theta_i/h, \lambda)$. In fact, this is never true; for PTFE at 550 nm, $R(0°/45°)/R(0°/h, \lambda)$ is equal to 1.015, not 1.000 (Hsia and Weidner 1981). Recent directional/directional measurements of PTFE (Barnes and Hsia 1995) and the directional/hemispherical data published by Weidner and Hsia (1981) can be used to calculate this ratio for pressed PTFE for wavelengths from 380–770 nm.

The failure of materials to perform as lambertian diffusers at near-grazing angles of incidence is probably caused by absorption and multiple scattering, since more multiple scattering events occur at larger angles of incidence, with the result that the directional/directional reflectance factor is smaller than the directional/hemispherical reflectance factor. For angles near normal incidence, the deviation from lambertian is largely due to the fact that Spectralon (and other samples) have a significant specular component (on the order of 6–8%).

Detailed studies of the relationship between these two quantities for Spectralon are not known to have been done. However, there have been several studies of $R(\theta_i/\theta_v, \lambda)$ (simply *reflectance factor* in what follows). Using a pressed PTFE sample for a reference standard, the sun as a source, and a field radiometer, Jackson et al. (1992) measured the reflectance factors of 11 Spectralon and 16 $BaSO_4$ plaques using a field goniometer. The angle of incidence was 0° and the angle of viewing was variable. They found that the Spectralon plaques could be modeled in terms of a characteristic equation involving $R(0°/h)$, representing the absorption, and polynomials in θ_v for the different wavelength intervals; that is, Spectralon is not a perfect (lossless) lambertian diffuser, but all plaques were the same type of nonlambertian diffuser.

Seven spectral regions were studied, from 450–2,300 nm. For the $BaSO_4$ plaques, no such characteristic equation could be used to describe the reflectance factors. Soffer et al. (1995) measured reflectance factors for four Spectralon plaques in support of the Boreal Ecosystem-Atmosphere Study (BOREAS) field program using goinometric measurements in the laboratory. Their results show that the reflectance factors of Spectralon vary by 20% as the view angle varies from 15–80°, in

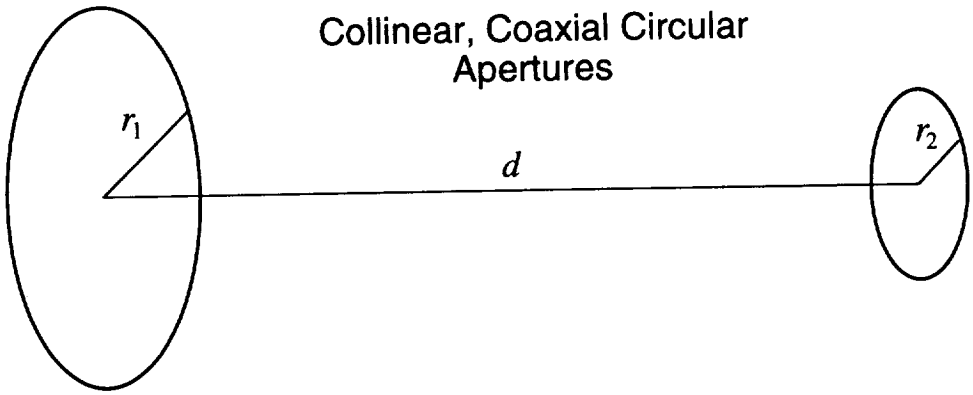

Fig. A1. Schematic of the two-aperture method.

agreement with the results of Jackson et al. (1992). Soffer et al. (1995) observed very little dependence with wavelength for the measured region from 450–860 nm, and they confirmed the characteristic equations proposed by Jackson et al. (1992).

Butler (pers. comm.) has measured reflectance factors using a facility at GSFC that incorporates lasers and a xenon arc source with a monochromator to select the wavelength (Schiff et al. 1993); the results at 400 and 632.8 nm are shown in Fig. B1. The angle of incident was 0° and a single 50.8 mm diameter Spectralon plaque was studied (S/N 8933). Four measurements at 400 nm were made between October 1993 and May 1995 and two measurements at 632.8 nm were made in June and July 1994. The averages are shown along with a third-order polynomial fit to the data. These results are in general agreement with the previous work.

Barnes (pers. comm.) has measured reflectance factors using a new monochromator-based facility, Spectral Tri-function Automated Reference Reflectometer (STARR), in the Radiometric Physics Division at NIST (Proctor and Barnes 1996). The results at 400 and 632.8 nm are show in Fig. B2. The angle of incident was 0° and the NIST Spectralon plaque that was used in SIRREX-3 (25.4×25.4 cm^2, SRT-99-100, S/N 12127-A) was measured for viewing angles from −38° to 40°. In Fig. B2, reflection symmetry with the viewing angle are assumed and the results are shown in terms of $|\theta|$. The solid lines are a fit to the data using a second-order polynomial; the single point at 40° and 632.8 nm was excluded from the fit. The ratio of the reflectance factors for the NIST measurements of plaque 12127-A to the reflectance factors measured at NASA for plaque 8933 are shown in Fig. B1. To calculate the ratio, the model describing the NIST measurements was evaluated at the NASA measurement angles and divided by the NASA measurements (the viewing angles were not exactly the same). The results for the two different Spectralon plaques using the two different experimental configurations agree to about ±0.5%, including the extrapolation of the NIST data to 45° using the second-order polynomial.

The NIST plaque 12127-A was calibrated for $R(8°/h, \lambda)$ by Labsphere and the values in the wavelength range of interest are given in Table B1. In the second column, the quadratic fit to the NIST reflectance measurements at 400 and 632.8 nm was extrapolated to predict reflectance factors for a 45° viewing angle. The resulting ratio of the directional/directional to the directional/hemispherical reflectance is given; the mean value is 1.028 and this can be used to estimate the reflectance factors for a Spectralon plaque for which only the 8°/hemispherical reflectance is known.

Table B1. The relationship between 0°/45° reflectance factors and directional hemispherical reflectance for the NIST Spectralon 12127-A plaque.

λ [nm]	Labsphere $R(8°/h), \lambda$	STARR $R(0°/45°, \lambda)$	$R(0°/45°), \lambda/$ $R(0°/h, \lambda)$
350.0	0.986		
400.0	0.988	1.017	1.029
450.0	0.987		
600.0	0.989		
632.8		1.015	1.026
650.0	0.988		

Appendix C

Spectral Shape of Radiometric Sources

The measurement equation for a single channel of a filter radiometer is

$$S = \int L(\lambda) D(\lambda) d\lambda \qquad (C1)$$

where S is the net counts or signal, $L(\lambda)$ is the spectral radiance of the source, and $D(\lambda)$ is the absolute spectral response of the radiometer for the channel of interest. In the method of realizing spectral radiance using a diffuse plaque with a standard lamp for which the irradiance is known (which is one approach taken to calibrate filter radiometers), a simple expression for the spectral radiance in terms of the spectral irradiance is

$$\begin{aligned} L(\lambda) &= \frac{R(0°/45°, \lambda)}{\pi} \left(\frac{50}{r}\right)^2 E(\lambda, 50 \text{ cm}) \\ &= \alpha(R, r, \lambda) E(\lambda, 50 \text{ cm}) \\ &\approx \alpha E(\lambda, 50 \text{ cm}) \end{aligned} \qquad (C2)$$

where $R(0°/45°, \lambda)$ is the directional/directional reflectance factor for the typical measurement configuration (illumination at normal incidence, viewing at 45°), r is the distance from the lamp to the plaque in cm, and $E(\lambda, 50 \text{ cm})$ is the spectral irradiance of the standard lamp at 50 cm. Since the reflectance factors for Spectralon do not depend strongly on wavelength for the spectral region where $D(\lambda)$ is a maximum, it is assumed here that to a good approximation the spectral radiance is proportional to the spectral irradiance by the factor α, which is evaluated according to the particular measurement conditions independent of the integral in (C1).

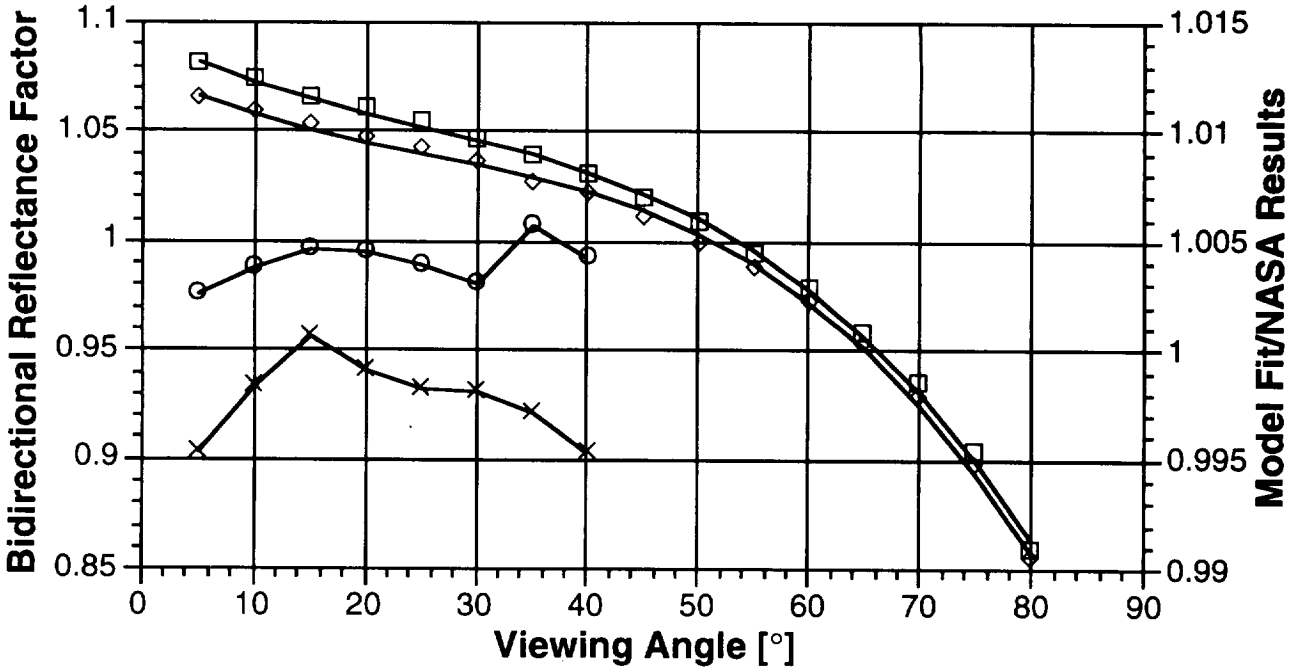

Fig. B1. Spectralon reflectance factors for normal incidence illumination using the NASA/GSFC facility for 400 nm (diamonds) and 632.8 nm (squares). The model results for each wavelength are shown as solid lines. The measurements were taken over the October 1993 to May 1995 time period. Also shown are the model fits to the NIST results ratioed to the NASA results for 400 nm (circles) and 632.8 nm (crosses). This comparison is for different Spectralon samples.

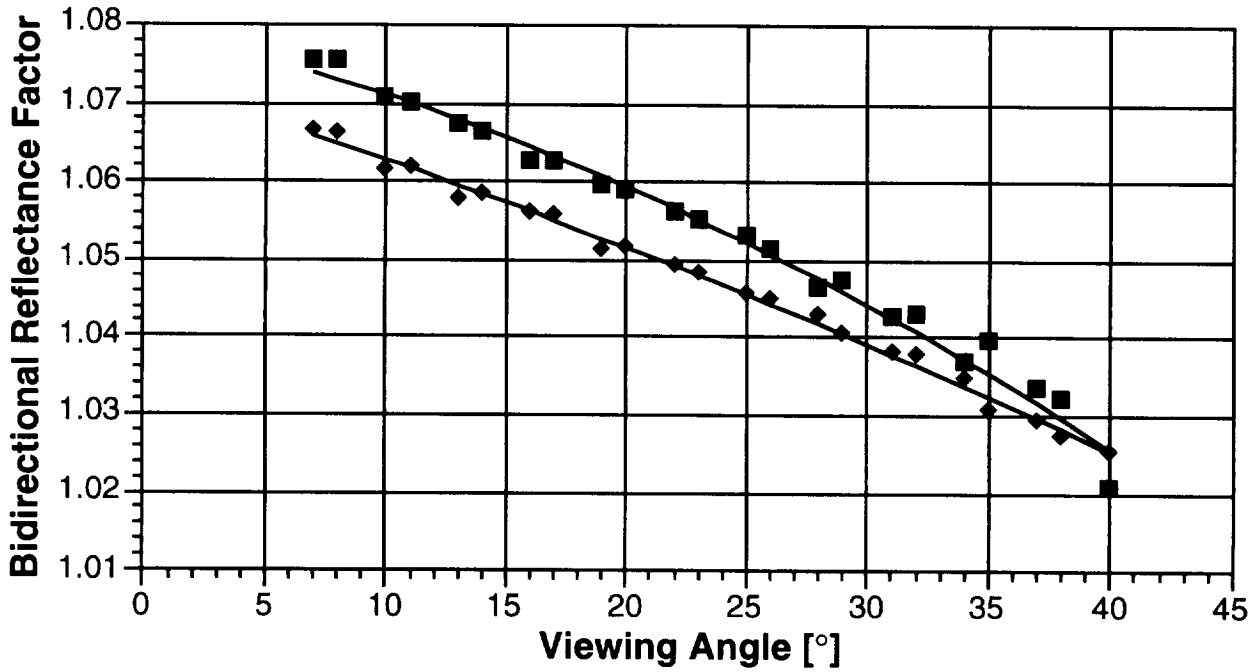

Fig. B2. Spectralon reflectance factors for normal incidence illumination measured with the NIST apparatus in July 1995 for 400 nm (diamonds) and 632.8 nm (squares). The model results are shown as solid lines.

Associated with (C1) is the spectral radiance to be determined, $L(\lambda_0)$:

$$L(\lambda_0) = \Gamma \int L(\lambda)\delta(\lambda - \lambda_0)d\lambda, \qquad (C3)$$

where Γ is a normalized bandwidth in units of $d\lambda$, λ_0 is the measurement wavelength (see below) and the Dirac δ function has been chosen to describe the relationship between the distribution of spectral radiance and $L(\lambda_0)$. Some other functional form or fiducial data instead of $\delta(\lambda - \lambda_0)$ could have been chosen.

To calibrate the radiometer, the signal (S) is measured using a source of known spectral radiance, $\hat{L}(\lambda)$. Then, for a source of unknown spectral radiance $\tilde{L}(\lambda_0)$,

$$\begin{aligned}\tilde{L}(\lambda_0) &= \frac{\tilde{S}}{\hat{S}}\alpha\hat{E}(\lambda_0)\frac{\int \hat{L}(\lambda)D(\lambda)d\lambda}{\int \hat{L}(\lambda)\delta(\lambda-\lambda_0)d\lambda}\times \\ &\quad \frac{\int \tilde{L}(\lambda)\delta(\lambda-\lambda_0)d\lambda}{\int \tilde{L}(\lambda)D(\lambda)d\lambda} \qquad (C4)\\ &= \frac{\tilde{S}}{\hat{S}}\alpha\hat{E}(\lambda_0)\kappa(\lambda_0).\end{aligned}$$

Note that the choice for λ_0 is in principle arbitrary, although it makes sense to choose λ_0 somewhere in the region where $D(\lambda)$ is a maximum. Note also that (C4) requires a priori knowledge of the source that is being measured, which means measurement with the filter radiometer is nothing more than a verification of the spectral radiance scale that has been assigned to that particular source, and (C4) can never be applied directly. Consequently, the choice of the measurement wavelength is important, and some algorithm for solving (C4) must be adopted.

First, common methods to select the measurement wavelength will be discussed. For the SAS-II instrument used during SIRREX-4, the CWLs of the filter radiometer were used for λ_0, as recommended in the SeaWiFS protocols (Mueller and Austin 1995). The CWL, λ_c, is defined as the mean of the wavelengths where the relative spectral responsivity is 50% of the maximum value. For the SXR instrument at SIRREX-4, a moment analysis was used for λ_0:

$$\begin{aligned}\lambda_0 &= \lambda_{MT} \\ &= \frac{\int \lambda\hat{L}(\lambda)D(\lambda)d\lambda}{\int \hat{L}(\lambda)D(\lambda)d\lambda} \qquad (C5)\end{aligned}$$

Cromer (pers. comm.) suggests an expansion in wavelength for $\hat{L}(\lambda)$ and $\tilde{L}(\lambda)$: $\hat{L}(\lambda) = a_0 + a_1\lambda$ and $\tilde{L}(\lambda) = b_0 + b_1\lambda$. Substitution into (C4) and taking $\kappa(\lambda_0) = 1$ results in

$$\begin{aligned}\lambda_0 &= \lambda_{TS} \\ &= \frac{\int \lambda D(\lambda)d\lambda}{\int D(\lambda)d\lambda} \qquad (C6)\end{aligned}$$

which has the attractive feature of being independent of $\hat{L}(\lambda)$ and $\tilde{L}(\lambda)$.

With some idea for what are reasonable choices for λ_0, algorithms for solving (C4) in a self-consistent manner will now be discussed. First, which was the approach taken at SIRREX-4, simply ignore $\kappa(\lambda_0)$. This was a good assumption since the bandwidths in the SAS-II instrument are narrow and in both cases the source was a 1,000 W quartz halogen coiled-coiled tungsten lamp with an apparent blackbody temperature between 3,000–3,200 K. The spectral irradiance data for F360 (used to calibrate the SAS-II), which was calibrated by OL on 26 August 1994, were fit to the modified planckian model (Section 4), as were the NIST calibration data for the four lamps used in SIRREX-4 (F332, F331, F423, and F442).

The model parameters for the spectral irradiance and the relative spectral response data provided by Satlantic for the SAS-II were used to calculate $\kappa(\lambda_c, \hat{l}, \tilde{l})$, where $\hat{l}$ is the calibration lamp and $\tilde{l}$ is the measured lamp. These correction factors for the four SIRREX-4 lamps using F360 as the calibration reference agree to within approximately 100 ppm except for the channel at 412.83 nm, where the discrepancy is larger, but still less than 0.03% (Table C1). When the measurement consists of determining in-water radiances, the correction factors will not agree for the calibration and measurement experiment since the in-water spectral radiance has a different spectral shape than that of a standard irradiance lamp.

In a second approach, ancillary spectroradiometric data on the relative shape of the spectral radiance of the unknown source are used to estimate $\kappa(\lambda_c, \hat{l}, \tilde{l})$. These data may be available, e.g., in the case of simultaneous measurements with a oceanographic filter radiometer and a spectrometer such as the MOBY system, or from a physical model of the source, but more likely an iterative approach based on the results obtained when the correction factors are ignored would be used. For example, the spectral radiance measured for seven wavelengths from 400–900 nm could be fit to a simple model such as a low-order polynomial multiplied by Planck's function, and the model could be used to calculate $\tilde{L}(\lambda)$ and obtain an estimate for $\kappa(\lambda_c, \hat{l}, \tilde{l})$. The expression for λ_0 given in (C6) would seem to be reasonable. The feasibility and robustness of this approach must be tested with simulated oceanographic data, but results at SIRREX-3 indicate filter radiometers can be used to model integrating sphere sources (Mueller et al. 1995). If the types of sources likely to be encountered can be standardized in terms of the relative spectral distribution, then correction factors can be developed much in the same way as in the field of photometry and colorimetry (Ohno and Sauter 1995). In photometry, the correction factors include the departure of the relative spectral response of the sensors from the standard color-matching functions, which serve the same purpose as $\delta(\lambda - \lambda_0)$ in this discussion.

A third approach, based on the field of radiation thermometry (pyrometry), arises from the requirement to measure spectral radiance ratios of two blackbody sources—one with a known radiance temperature and the other for which the temperature is to be determined from the radiance ratio. This is the same measurement equation as discussed in this work, except that the spectral radiance of a blackbody with unity emissivity can be characterized in terms of a single parameter, temperature (T): $L(\lambda) = P(\lambda, T)$, where $P(\lambda, T)$ is Planck's law. Since the relative spectral shape of a continuum source for a particular wavelength interval can often be described in terms of an apparent blackbody temperature, this approach is just a way to formalize the notion of estimating $\kappa(\lambda_0, \hat{l}, \tilde{l})$; information on the relative spectral shape of the unknown source is still required. However, this approach results in a self-consistent expression for the measurement wavelength.

Nutter (1988) shows that for the case where the spectral radiance can be approximated as a planckian,

$$\frac{\int \hat{L}(\lambda)D(\lambda)d(\lambda)}{\int \tilde{L}(\lambda)D(\lambda)d(\lambda)} = \frac{\hat{L}(\overline{\lambda}_c)}{\tilde{L}(\overline{\lambda}_c)} \qquad (C7)$$

Table C1. Correction Factors expressed as $1 - k(\lambda_c, \mathrm{F360}, l')$ using the SAS-II CWLs. Units are ppm and T_{fit} is from the modified planckian model.

Lamp ID	T_{fit} [K]	λ_c [nm]						
		412.83	442.89	490.44	510.58	554.42	668.66	682.58
F360	3,028.0							
F332	3,083.4	180	98	−14	14	−91	−89	−38
F331	3,105.1	250	140	−19	21	−130	−140	−59
F423	3,083.6	210	120	−11	22	−110	−120	−55
F442	3,070.8	160	95	−8	18	−88	−100	−46

Table C2. The difference between the SAS-II CWL and EWL, $\lambda_c - \lambda_{\mathrm{EWL}}$, as a function of particular FEL lamp used as the source. All shifts are in nanometers.

Lamp ID	T_{fit} [K]	λ_c [nm]						
		412.83	442.89	490.44	510.58	554.42	668.66	682.58
F360	3,028.0	−0.400	−0.259	0.044	−0.053	0.431	0.697	0.326
F332	3,083.4	−0.385	−0.246	0.055	−0.044	0.439	0.702	0.328
F331	3,105.1	−0.378	−0.240	0.060	−0.039	0.443	0.705	0.328
F423	3,083.6	−0.383	−0.244	0.057	−0.042	0.441	0.704	0.328
F442	3,070.8	−0.386	−0.247	0.054	−0.044	0.439	0.703	0.328

where the mean effective wavelength (EWL), $\overline{\lambda}_c$, is the same as the measurement wavelength:

$$\frac{1}{\lambda_0} = \frac{1}{\overline{\lambda}_c} = \frac{1}{2}\left(\frac{1}{\hat{\lambda}} + \frac{1}{\tilde{\lambda}}\right). \quad (C8)$$

Here, $\hat{\lambda}$ and $\tilde{\lambda}$ are the EWLs corresponding to the calibration and measurement source, respectively. The analytical expression for the EWL in terms of the spectral radiance (or irradiance) of the source is

$$\frac{1}{\lambda_{\mathrm{EWL}}} = \frac{\int \lambda^{-1} L(\lambda) D(\lambda) d(\lambda)}{\int L(\lambda) D(\lambda) d(\lambda)}. \quad (C9)$$

Therefore, as above, a priori knowledge of the relative spectral distribution of the unknown source is required in order to determine λ_0, and this measurement wavelength will be different for each unknown source. For a fixed calibration source, however, the problem can now be cast in terms of the mean EWL as a function of the spectral shape (black body temperature) of the unknown source, which is often a more convenient way to characterize the problem. If the measurement wavelength is determined from (C8) and (C9), then (C4) becomes

$$\tilde{L}(\lambda_0) = \frac{\tilde{S}}{\hat{S}} \alpha \hat{E}(\lambda_0). \quad (C10)$$

The shifts between the EWL and the CWL for the five lamps are given in Table C2. The spread in the shifts is 0.022 nm at 413 nm and decreases monotonically to essentially zero at 683 nm. In other words, the EWL for a single channel in the SAS-II is nearly the same for all the lamps; this is just another way to say that the correction factors are nearly unity (Table C1).

In conclusion, it can be seen that a number of approaches are possible, and that simulations with in-water and atmospheric spectral radiance and irradiance data would be beneficial. Two correct analytical expressions for the measurement wavelength, each which have certain limitations, have been indicated here, and the iterative nature of achieving solutions for the measurement equation have been stressed. Finally, it is pointed out that it would be possible to adopt a fiducial set of relative spectral response data (e.g., the SeaWiFS sensor, see Barnes et al. 1994) instead of $\delta(\lambda - \lambda_0)$ for facilitating the comparison of field data with satellite data.

Appendix D

Attendees to SIRREX-4

The attendees to SIRREX-4 are presented alphabetically. Lecturers are identified by the general subject of their presentation and laboratory instructors are noted, as well as those individuals who participated in the laboratory sessions as active participants or observers.

Peter Abel
NASA/GSFC/Code 925
Greenbelt, MD 20771
Voice: 301-286-6829
Fax: 301-286-1757
Net: abel@highwire.gsfc.nasa.gov

Katsuaki Akaike *Laboratory*
Remote Sensing Tech. Ctr. of Japan
Ohashi Numanoue 1401
Hiki-gun Hatoyama-machi
Saitama-ken 350-03, Japan
Voice: 81-49-298-1360
Net: *Not Provided*

Tom Arnold
Applied Research Corp.
8282 Imperial Drive
Laurel, MD 20708
Voice: 301-286-4805
Fax: 301-725-2450
Net: arnold@climate.gsfc.nasa.gov

Clara Asmail — *NIST Lecturer*
NIST/Bldg. 220, Room A305
Gaithersburg, MD 20899
Voice: 301-975-2339
Fax: 301-840-8551
Net: asmail@onyx.nist.gov

Robert Barnes — *SeaWiFS Lecturer*
Mantech/Bldg. F160
Wallops Island, VA 23337
Voice: 301-286-0501
Fax: 301-286-1775
Net: rbarnes@calval.gsfc.nasa.gov

Bill Barnes — *MODIS Lecturer*
NASA/GSFC/Code 970
Greenbelt, MD 20771
Voice: 301-286-8670
Fax: 301-286-1761
Net: wbarnes@neptune.gsfc.nasa.gov

Dick Berry — *Laboratory*
NASA/AOL/Bldg. N159
Wallops Island, VA 23337
Voice: 804-824-1745
Fax: 804-824-1036
Net: yungel@osb1.wff.nasa.gov

Sally Bruce — *Instructor*
NIST/Bldg. 220, Room A305
Gaithersburg, MD 20899
Voice: 301-869-2322
Fax: 301-869-5700
301-840-8551
Net: bruce@garnet.nist.gov

James Butler — *EOS Lecturer*
NASA/GSFC/Code 925
Bldg. 22, Room 390D
Greenbelt, MD 20771
Voice: 301-286-4606
Fax: 301-286-1616
Net: butler@highwire.gsfc.nasa.gov

Rene Castaneda — *Laboratory*
NASA/ARC/MS 240-6
Moffett Field, CA 94035
Voice: 415-604-3006
Fax: 415-604-4987
Net: rcastaneda@msmail.arc.nasa.gov

Feng-I (Robert) Chen — *Laboratory*
USF/Dept. of Marine Science
140 Seventh Avenue, South
St. Petersburg, FL 33701
Voice: 813-893-9590
Fax: 813-893-9189
Net: chen@monty.marine.usf.edu

John Cooper — *Laboratory*
NASA/GSFC/Code 925
Greenbelt, MD 20771
Voice: 301-286-1210
Fax: 301-286-1616
Net: cooper@highwire.gsfc.nasa.gov

Christopher Cromer — *NIST Lecturer*
NIST/Bldg. 220, Room A305
Gaithersburg, MD 20899
Voice: 301-975-3216
Fax: 301-840-8551
Net: cromer@micf.nist.gov

Curtiss Davis — *NRL Lecturer*
NRL/Code 7212
4555 Overlook Ave., SW
Washington, DC 20375
Voice: 202-767-9296
Fax: 202-404-7453
Net: davis@rira.nrl.navy.mil

Ted Early — *NIST Lecturer*
NIST/Bldg. 220, Room A305 — *Instructor*
Gaithersburg, MD 20899
Voice: 301-975-2343
Fax: 301-840-8551
Net: early@enh.nist.gov

James Ehramjian — *BSI Lecturer*
Biospherical Instruments, Inc. — *Laboratory*
5340 Riley Street
San Diego, CA 92110
Voice: 619-686-1888
Fax: 619-686-1887
Net: jime@biospherical.com

Mike Feinholz — *Laboratory*
Moss Landing Marine Laboratory
PO Box 450
Moss Landing, CA 95039
Voice: 408-755-8675
Fax: 408-753-2826
Net: feinholz@mlml.calstate.edu

Yuntao Ge — *Laboratory*
NOAA/WWB/Room 104
5200 Auth Road
Camp Springs, MD 20746
Voice: 301-763-8102
Fax: 301-763-8020
Net: ge@oramab3.wwb.noaa.gov

Charles Gibson — *NIST Lecturer*
NIST/Bldg. 220, Room B208
Gaithersburg, MD 20899
Voice: 301-975-2329
Fax: 301-840-8551
Net: gibson@enh.nist.gov

William Graver — *Laboratory*
NRL/Code 7120
4555 Overlook Ave., SW
Washington, DC 20017
Voice: 703-790-7492
Fax: 703-821-1647
Net: *Not Provided*

Pavel Hajek — *Laboratory*
AMES Research Labs/MS 15A
290 E River Road
Rochester, NY 14623
Voice: 716-424-5157
Fax: 716-249-4936
Net: hajek@optics.rochester.edu

Edward Hildum — *Laboratory*
Sverdrup Technology/NASA/MS 213-15
Moffett Field, CA 94035
Voice: 415-604-1606
Fax: 415-604-4987
Net: ehildum@msmail.arc.nasa.gov

Stanford Hooker — *SIRREX Lecturer, Observer*
NASA/GSFC/Code 970.2
Bldg. 28, Room W121
Greenbelt, MD 20771
Voice: 301-286-9503
Fax: 301-286-1775
Net: stan@ardbeg.gsfc.nasa.gov

Jeanne Houston — *Instructor*
NIST/Bldg. 220, Room A305
Gaithersburg, MD 20899
Voice: 301-975-2327
Fax: 301-840-8551
Net: houston@garnet.nist.gov

Samantha Hudson — *PACE Lecturer, Laboratory*
IMS/Univ. of Plymouth
Drake Circus
Plymouth PL4 8AA
United Kingdom
Voice: 44-1-752-232-457
Fax: 44-1-752-232-406
Net: shudson@plymouth.ac.uk

B. Carol Johnson — *NIST Lecturer, Observer*
NIST/Bldg. 221, Room B208
Gaithersburg, MD 20899
Voice: 301-975-2322
Fax: 301-869-5700
Net: cjohnson@enh.nist.gov

Samuel Kramer — *NIST Speaker*
NIST/Admin., Room A1123
Gaithersburg, MD 20899
Voice: 301-975-2303
Net: kramer@micf.nist.gov

Thomas Larason — *NIST Lecturer*
NIST/Bldg. 221, Room B208
Gaithersburg, MD 20899
Voice: 301-975-2344
Fax: 301-869-5700
Net: larason@garnet.nist.gov

Li-Shing Lee — *ROCSAT Lecturer, Laboratory*
NSPO
8th Floor, No. 9 Prosperity Rd. I
Science Based Industrial Park
Hsin Chu, Taiwan
Republic of China
Voice: 886-35-770-134
Net: *Not Provided*

Mark Levenson — *NIST Lecturer*
NIST/Bldg. 101, Room A337
Gaithersburg, MD 20899
Voice: 301-975-2848
Net: mlev@cam.nist.gov

Tang-Huang Lin — *Laboratory*
Ctr. for Space & Remote Sensing Res.
National Central University
Chung-Li, Taiwan
Republic of China
Voice: *Not Provided*
Voice: 886-03-425-4908
Net: t602544@twncu865.ncu.edu.tw

Gin-Rong Liu — *Laboratory*
Ctr. for Space & Remote Sensing Res.
National Central University
Chung-Li, Taiwan
Republic of China
Voice: *Not Provided*
Voice: 886-03-425-4908
Net: t602544@twncu865.ncu.edu.tw

Jim McLean — *GSFC Lecturer, Laboratory*
NASA/GSFC/Code 925
Bldg. 22, Room 380A
Greenbelt, MD 20771
Voice: 301-286-8134
Fax: 301-926-1757
Net: mclean@highwire.gsfc.nasa.gov

Scott McLean — *Satlantic Lecturer, Laboratory*
Satlantic, Inc.
Richmond Terminal Pier 9
3295 Barrington Street
Halifax, Nova Scotia B3K 5X8
Canada
Voice: 902-492-4780
Fax: 902-492-4781
Net: scott@predator.ocean.dal.ca

Dave Menzies — *Laboratory*
ICESS/UCSB
Santa Barbara, CA 93106
Voice: 805-893-8496
Fax : 805-893-2578
Net: davem@icess.ucsb.edu

Gerald Moore — *SEI Lecturer*
Plymouth Marine Laboratory
Prospect Place
Plymouth, Devon PL1 3DH
United Kingdom
Voice: 44-1-752-222-772
Fax: 44-1-752-670-637
Net: g.moore@pml.ac.uk

John Morrow
Biospherical Instruments, Inc.
5340 Riley Street
San Diego, CA 92110
Voice: 619-686-1888
Fax: 619-686-1887
Net: morrow@biospherical.com

James Mueller — *SIRREX Lecturer, Observer*
SDSU/CHORS/Suite 206
6505 Alvarado Road
San Diego, CA 92120-5005
Voice: 619-594-2230
Fax: 619-594-4570
Net: jmueller@chors.sdsu.edu

Thomas O'Brian — *Instructor*
NIST/Bldg. 245, Room B119
Gaithersburg, MD 20899
Voice: 301-975-2395
Fax: 301-869-5700
Net: obrian@bruce.nist.gov

Heiko Rinck — *MERIS Lecturer, Laboratory*
GKSS Forschungszentrum
Measurement and Info. Techniques
Max Planck Strasse
D-21502, Geesthacht
Germany
Voice: *Not Provided*
Net: heiko.rinck@gkss.de

Bob Saunders — *NIST Lecturer*
NIST/Bldg. 221, Room B208
Gaithersburg, MD 20899
Voice: 301-975-2355
Net: rds@enh.nist.gov

Karl-Heinz Sümnich — *MOS Lecturer, Laboratory*
German Aerospace Research Est.
Inst. for Space Sensor Tech.
Rudower Chaussee
D-12489, Berlin
Germany
Voice: 49-30-69545-570
Fax: 49-30-69545-572
Net: karl-heinz.suemnich@dlr.de

Ambler Thompson — *NIST Lecturer, Instructor*
NIST/Bldg. 220, Room A305
Gaithersburg, MD 20899
Voice: 301-975-2333
Net: ambler@enh.nist.gov

Clay Titus — *Laboratory*
SDSU/CHORS/Suite 206
6505 Alvarado Road
San Diego, CA 92120-5005
Voice: 619-594-2244
Fax: 619-594-4570
Net: clay@chors.sdsu.edu

Naoya Tomii — *Laboratory*
Remote Sensing Tech. Ctr. of Japan
Ohashi Numanoue 1401
Hiki-gun Hatoyama-machi
Saitama-ken 350-03
Japan
Voice: 81-492-98-1360
Fax: 81-492-98-1399
Net: *Not Provided*

Giuseppe Zibordi — *PICASSO Lecturer, Laboratory*
JRC/IRSA-ME/TP 272
21020 Ispra (VA)
Italy
Voice: 39-332-785-902
Fax: 39-332-789-034
Net: giuseppe.zibordi@cen.jrc.it

GLOSSARY

AOL Airborne Oceanographic Lidar
ARC Ames Research Center
ASCII American Standard Code for Information Interchange
ASTER Advanced Spaceborne Thermal Emission and Reflection Radiometer

BOREAS Boreal Ecosystem-Atmosphere Study
BRDF Bidirectional Reflectance Distribution Function
BSI Biospherical Instruments, Incorporated

CHORS Center for Hydro-Optics and Remote Sensing
CoASTS Coastal Atmosphere and Sea Time Series
CWL Center Wavelength
CZCS Coastal Zone Color Scanner

D/A Digital-to-Analog
DC Direct Current
DVM Digital Voltmeter

EG&G Not an acronym, but the former name of Gamma Scientific.
EWL Effective Wavelength

FASCAL Facility for Automated Spectroradiometric Calibrations
FEL Not an acronym, but a lamp designator.
FOV Field of View
FWHM Full-Width at Half-Maximum

GKSS Originally, *Gesellschaft für Kernenergie Verwertung in Schiffbau und Schiffahrt* (Germany), but more recently not associated with a specific meaning.
GSFC Goddard Space Flight Center

HACR High Accuracy Cryogenic Radiometer
Hg Not an acronym, but the chemical symbol for mercury.
HP Hewlett Packard

ICESS Institute for Computational Earth System Science (UCSB)
IEEE Institute of Electrical and Electronic Engineers
IMS Institute for Marine Studies (Univ. of Plymouth)
IRS Indian Research Satellite
IRSA-ME Institute for Remote Sensing Applications-Marine Environment
ISIC Integrating Sphere Irradiance Collector
ISO International Organization for Standardization

JRC Joint Research Centre

LLR Low Level Radiance
LPC Lamp Position Correction

MER Marine Environmental Radiometer
MERIS Medium Resolution Imaging Spectrometer
MLML Moss Landing Marine Laboratory
MOBY Marine Optical Buoy
MODIS Moderate Resolution Imaging Spectroradiometer
MOS Marine Optical Spectroradiometer

NASA National Aeronautics and Space Administration
NEC Nippon Electric Company
NIST National Institute of Standards and Technology
NOAA National Oceanic and Atmospheric Administration
NRL Naval Research Laboratory
NSPO National Space Program Office (Taiwan)

OCI Ocean Color Imager
OCTS Ocean Color Temperature Sensor (Japan)
OL Optronic Laboratories, Inc.
OSC Orbital Sciences Corporation

PACE Plymouth Atmospheric Correction Experiment
PTFE Polytetrafluoroethylene
PICASSO Pan-European Investigations into Calibration of Atmosphere and Sea Surface Optics
PRIME Plankton Reactivity in the Marine Environment
PML Plymouth Marine Laboratory
Priroda Not an acronym, but the name for a Russian scientific program of Earth environmental observation.

ROCSAT Republic of China Satellite (Taiwan)

S/N Serial Number
SAS SeaWiFS Aircraft Simulator
SBRC (Hughes) Santa Barbara Research Center
SDSU San Diego State University
SEI SeaWiFS Exploitation Initiative
SeaWiFS Sea-viewing Wide Field-of-view Sensor
SIRREX SeaWiFS Intercalibration Round-Robin Experiment
SIRREX-1 The First SIRREX (July 1992)
SIRREX-2 The Second SIRREX (June 1993)
SIRREX-3 The Third SIRREX (September 1994)
SIRREX-4 The Fourth SIRREX (May 1995)
SIRREX-5 The Fifth SIRREX (tentatively July 1996)
SNR Signal-to-Noise Ratio
SOS Size of Source
STARR Spectral Trifunction Automated Reference Reflectometer
SBUV-2 Solar Backscatter Ultraviolet Radiometer-2
SXR SeaWiFS Transfer Radiometer

TEC Thermoelectric Cooler

UA University of Arizona
UCSB University of California at Santa Barbara
UM University of Miami
USF University of South Florida
UV Ultraviolet

WFF Wallops Flight Facility (NASA)

Symbols

d Separation distance.
$D(\lambda)$ The spectral radiance responsivity.
$\overline{D}$ Average responsivity (calibration coefficient).
$E(\lambda)$ Spectral irradiance.
$\hat{E}(\lambda)$ Calibrated (known) spectral irradiance.
$\tilde{E}(\lambda)$ Measured (unknown) spectral irradiance.
$\check{E}(\lambda_c, 50\text{ cm})$ The spectral irradiance of the standard lamp at 50 cm interpolated onto λ_c.
$E_e(\lambda)$ Integrated irradiance (versus spectral irradiance); used most often when trying to distinguish illuminance from irradiance.
E_v Illuminance.
$\hat{E}(\lambda_c, 50\text{ cm})_{\text{F332}}$ The spectral irradiance measured with FEL F332.
F Spectral correction factor.
F_{SL} The inverse calibration coefficient.
k Coverage factor.
$\hat{l}$ Calibration lamp designator.
$\tilde{l}$ Measured lamp designator.
$L(\lambda)$ Spectral radiance.
$L(\lambda_0)$ Spectral radiance when a filter radiometer is used to determine the measurement wave length.
$\hat{L}(\lambda)$ Spectral radiance of the calibrated (known) source.
$\tilde{L}(\lambda)$ Spectral radiance of the measured (unknown) source.
$\check{L}(\lambda)$ Predicted radiance.
$P(\lambda, T)$ Planck's law.
$\tilde{r}$ The measured distance from the lamp to the plaque.
r_1 The circular sphere source aperture radius.
r_2 The circular photometer detector aperture radius.
$R(\lambda)$ Spectral responsivity.
$R(0°/45°, \lambda_c)$ The directional/directional reflectance factor (see Appendix B).
$R_n(\lambda)$ Normalized spectral responsivity.
S Measured net signal.
$\hat{S}$ The signal from a calibrated (known) source.
$\tilde{S}$ The signal from a measured (unknown) source.
S_A The ambient background signal.
S_B The background signal.
S_T The total signal.
T Temperature.
$V(\lambda)$ The human spectral photopic efficiency function.
x, y, z The Cartesian coordinate system.
α The ratio of spectral radiance to spectral irradiance; a proportionality factor.
Γ The normalized bandwidth.
δ The geometric configuration factor correction term.
Δr The distance offset.
θ_i Incident angle.
θ_v Viewing angle.
$\kappa(\lambda)$ Radiance normalization factor.
λ Wavelength.
$\hat{\lambda}$ EWL corresponding to the calibration source.
$\tilde{\lambda}$ EWL corresponding to the measurement source.
λ_0 The true measurement wavelength.
λ_a The actual measurement wavelength.
λ_c Measurement wavelength for a filter radiometer determined from the 50% response levels.
$\overline{\lambda}_c$ The mean EWL.
λ_i Indicated wavelength.
λ_m Measured wavelength.

λ_{MT} The measurement wavelength for a filter radiometer determined from the *moment equation*.

λ_{TS} The measurement wavelength for a filter radiometer determined from the *Taylor Series* approach.

$\phi_e(\lambda)$ Source spectral flux.

REFERENCES

Barnes, P.Y., and J.J. Hsia, 1995: 45°/0° reflectance factors of pressed PTFE resins. *NIST Tech. Note 1413,* U.S. Dept. of Commerce, National Institute of Standards and Technology, Washington, D.C., 13 pp. plus appendix.

Barnes, R.A., W.L. Barnes, W.E. Esaias, and C.L. McClain, 1994a: Prelaunch Acceptance Report for the SeaWiFS Radiometer. *NASA Tech. Memo. 104566, Vol. 22,* S.B. Hooker, E.R. Firestone, and J.G. Acker, Eds., NASA Goddard Space Flight Center, Greenbelt, Maryland, 32 pp.

Bruegge, C.J., A.E. Stiegman, R.A. Rainen, and A.W. Springsteen, 1993: Use of Spectralon as a diffuse reflectance standard for in-flight calibration of Earth-orbiting sensors. *Opt. Eng.,* **32,** 805–814.

Cromer, C.L., G. Eppeldauer, J.E. Hardis, T.C. Larason, and A.C. Parr, 1993: National Institute of Standards and Technology detector-based photometric scale. *Appl. Opt.,* **32,** 2,936–2,948.

Early, E.A., and B.C. Johnson, 1996: Calibration and Characterization of the Goddard Space Flight Center Sphere. *NASA Tech. Memo. 104566,* S.B. Hooker and E.R. Firestone, Eds., NASA Goddard Space Flight Center, Greenbelt, Maryland, (accepted).

Hooker, S.B., C.R. McClain, and A. Holmes, 1993: Ocean color imaging: CZCS to SeaWiFS. *Mar. Tech. Soc. J.,* **27,** 3–15.

——, C.R. McClain, J.K. Firestone, T.L. Westphal, E-n. Yeh, and Y. Ge, 1994: The SeaWiFS Bio-Optical Archive and Storage System (SeaBASS), Part 1. *NASA Tech. Memo. 104566, Vol. 20,* S.B. Hooker and E.R. Firestone, Eds., NASA Goddard Space Flight Center, Greenbelt, Maryland, 40 pp.

Hovis, W.A., and J.S. Knoll, 1983: Characteristics of an internally-illuminated calibration sphere. *Appl. Opt.,* **22,** 4,004–4,007.

Hsia, J.J., and V.R. Weidner, 1981: NBS 45°/normal reflectometer for absolute reflectance factors. *Metrologia,* **17,** 97–102.

Jackson, R.D., M.S. Moran, P.N. Slater, and S.F. Biggar, 1987: Field calibration of reference reflectance panels. *Remote Sens. Environ.,* **22,** 145–158.

——, T.R. Clarke, and M.S. Moran, 1992: Bidirectional calibration results for 11 Spectralon and 16 barium sulfate reference reflectance panels. *Remote Sens. Environ.,* **40,** 231–239.

Johnson, B.C., C.L. Cromer, and J.B. Fowler, 1996: The SeaWiFS Transfer Radiometer (SXR). *NASA Tech. Memo. 104566,* S.B. Hooker and E.R. Firestone, Eds., NASA Goddard Space Flight Center, Greenbelt, Maryland, (accepted).

McClain, C.R., W.E. Esaias, W. Barnes, B. Guenther, D. Endres, S.B. Hooker, G. Mitchell, and R. Barnes, 1992: Calibration and Validation Plan for SeaWiFS. *NASA Tech. Memo. 104566, Vol. 3,* S.B. Hooker and E.R. Firestone, Eds., NASA Goddard Space Flight Center, Greenbelt, Maryland, 41 pp.

Mueller, J.L., 1993: The First SeaWiFS Intercalibration Round-Robin Experiment, SIRREX-1, July 1992. *NASA Tech. Memo. 104566, Vol. 14,* S.B. Hooker and E.R. Firestone, Eds., NASA Goddard Space Flight Center, Greenbelt, Maryland, 60 pp.

——, and R.W. Austin, 1992: Ocean Optics Protocols for SeaWiFS Validation. *NASA Tech. Memo. 104566, Vol. 5,* S.B. Hooker and E.R. Firestone, Eds., NASA Goddard Space Flight Center, Greenbelt, Maryland, 45 pp.

——, B.C. Johnson, C.L. Cromer, J.W. Cooper, J.T. McLean, S.B. Hooker, and T.L. Westphal, 1994: The Second SeaWiFS Intercalibration Round-Robin Experiment (SIRREX-2), June 1993. *NASA Tech. Memo. 104566, Vol. 16,* S.B. Hooker and E.R. Firestone, Eds., NASA Goddard Space Flight Center, Greenbelt, Maryland, 121 pp.

——, and R.W. Austin, 1995: Ocean Optics Protocols for SeaWiFS Validation, Revision 1. *NASA Tech. Memo. 104566, Vol. 25,* S.B. Hooker, E.R. Firestone, and J.G. Acker, Eds., NASA Goddard Space Flight Center, Greenbelt, Maryland, 67 pp.

——, B.C. Johnson, S.B. Hooker, J.T. McLean, and S. Biggar, 1995: The Third SeaWiFS Intercalibration Round-Robin Experiment (SIRREX-3), 19–30 September 1994. *NASA Tech. Memo. 104566, Vol. 34,* S.B. Hooker, E.R. Firestone, and J.G. Acker, Eds., NASA Goddard Space Flight Center, Greenbelt, Maryland, 78 pp.

Nutter, G.D., 1988: Radiation Thermometers: Design Principles and Operating Characteristics. In: *Radiation Thermometry.* D.P. DeWitt and G.D. Nutter, Eds., John Wiley and Sons, 231–337.

Ohno, Y., and G. Sauter, 1995: 1993 Intercomparison of Photometric Units Maintained at NIST (USA) and PTB (Germany). *J. Res. Natl. Inst. Stand. Technol.,* **100,** 227–239.

O'Shea, D.C., 1987: Chapter 3, Radiometry, In: *Elements of Modern Optical Design.* John Wiley and Sons, 402 pp.

Proctor, J., and Y.P. Barnes, 1996: NIST High Accuracy Reference Reflectometer-spectrophotometer. *J. Res. Natl. Inst. Stand. Technol.,* **101,** (accepted).

Saunders, R.D., and J.B. Shumaker, 1977: Optical Radiation Measurements: The 1973 NBS Scale of Spectral Irradiance. *NBS Tech. Note 594-13,* National Bureau of Standards, Gaithersburg, Maryland, 28 pp.

Schiff, T.F., M.W. Knighton, D.J. Wilson, F.M. Cady, J.C. Stover, and J.J. Butler, 1993: Design review of a high accuracy UV to near IR scatterometer, *Proceedings of the SPIE,* **1995,** 121–130.

Soffer, R.J., J.W. Harron, and J.R. Miller, 1995: Characterization of Kodak grey cards as reflectance reference panels in support of BOREAS field activities. *Proc. Canadian Remote Sens. Symp.,* (submitted).

Stiegman, A.E., C.J. Bruegge, and A.W. Springsteen, 1993: UV stability and contamination analysis of Spectralon diffuse reflectance material. *Opt. Eng.,* **32,** 799–804.

Taylor, B.N., and C.E. Kuyatt, 1994: Guidelines for Evaluating and Expressing the Uncertainty of NIST Measurement Results. *NIST Technical Note 1297, 1994 Edition,* National Institute of Standards and Technology, Gaithersburg, Maryland, 20 pp.

Tsai, B., B.C. Johnson, R.S. Saunders, and C.L. Cromer, 1995: Comparison of Filter Radiometer Spectral Responsivity with the NIST Spectral Irradiance and Illuminance Scales. *Metrologia,* (accepted).

Walker, J.H., R.D. Saunders, J.K. Jackson, and D.A. McSparron, 1987a: Spectral Irradiance Calibrations. *NBS Special Publication 250-20,* U.S. Dept. of Commerce, National Bureau of Standards, Washington, D.C., 37 pp. plus appendices.

——, ——, and A.T. Hattenburg, 1987b: Spectral Radiance Calibrations. *NBS Special Publication 250-1,* U.S. Dept. of Commerce, National Bureau of Standards, Washington, D.C., 26 pp. plus appendices.

——, C.L. Cromer, and J.T. McLean, 1991: A Technique for Improving the Calibration of Large-Area Sphere Sources. *Proc. of the SPIE,* **1493,** 224–230.

——, and A. Thompson, 1995a: Spectral Radiance of Large-Area Integrating Sphere Sources. *J. Res. Natl. Inst. Stand. Technol.,* **100,** 37–41.

——and ——, 1995b: Improved Automated Current Control for Standard Lamps. *J. Res. Natl. Inst. Stand. Technol.,* **100,** 255–261.

Weidner, V.R., and J.J. Hsia, 1981: Reflection properties of pressed PTFE powder. *J. Opt. Soc. Am.,* **71,** 856–861.

——, and ——, 1987: Spectral reflectance. *NBS Special Publication 250-8,* U.S. Dept. of Commerce, National Bureau of Standards, Washington, D.C., 31 pp. plus appendices.

The SeaWiFS Technical Report Series

Vol. 1

Hooker, S.B., W.E. Esaias, G.C. Feldman, W.W. Gregg, and C.R. McClain, 1992: An Overview of SeaWiFS and Ocean Color. *NASA Tech. Memo. 104566, Vol. 1,* S.B. Hooker and E.R. Firestone, Eds., NASA Goddard Space Flight Center, Greenbelt, Maryland, 24 pp., plus color plates.

Vol. 2

Gregg, W.W., 1992: Analysis of Orbit Selection for SeaWiFS: Ascending vs. Descending Node. *NASA Tech. Memo. 104566, Vol. 2,* S.B. Hooker and E.R. Firestone, Eds., NASA Goddard Space Flight Center, Greenbelt, Maryland, 16 pp.

Vol. 3

McClain, C.R., W.E. Esaias, W. Barnes, B. Guenther, D. Endres, S.B. Hooker, G. Mitchell, and R. Barnes, 1992: Calibration and Validation Plan for SeaWiFS. *NASA Tech. Memo. 104566, Vol. 3,* S.B. Hooker and E.R. Firestone, Eds., NASA Goddard Space Flight Center, Greenbelt, Maryland, 41 pp.

Vol. 4

McClain, C.R., E. Yeh, and G. Fu, 1992: An Analysis of GAC Sampling Algorithms: A Case Study. *NASA Tech. Memo. 104566, Vol. 4,* S.B. Hooker and E.R. Firestone, Eds., NASA Goddard Space Flight Center, Greenbelt, Maryland, 22 pp., plus color plates.

Vol. 5

Mueller, J.L., and R.W. Austin, 1992: Ocean Optics Protocols for SeaWiFS Validation. *NASA Tech. Memo. 104566, Vol. 5,* S.B. Hooker and E.R. Firestone, Eds., NASA Goddard Space Flight Center, Greenbelt, Maryland, 43 pp.

Vol. 6

Firestone, E.R., and S.B. Hooker, 1992: SeaWiFS Technical Report Series Summary Index: Volumes 1–5. *NASA Tech. Memo. 104566, Vol. 6,* S.B. Hooker and E.R. Firestone, Eds., NASA Goddard Space Flight Center, Greenbelt, Maryland, 9 pp.

Vol. 7

Darzi, M., 1992: Cloud Screening for Polar Orbiting Visible and IR Satellite Sensors. *NASA Tech. Memo. 104566, Vol. 7,* S.B. Hooker and E.R. Firestone, Eds., NASA Goddard Space Flight Center, Greenbelt, Maryland, 7 pp.

Vol. 8

Hooker, S.B., W.E. Esaias, and L.A. Rexrode, 1993: Proceedings of the First SeaWiFS Science Team Meeting. *NASA Tech. Memo. 104566, Vol. 8,* S.B. Hooker and E.R. Firestone, Eds., NASA Goddard Space Flight Center, Greenbelt, Maryland, 61 pp.

Vol. 9

Gregg, W.W., F.C. Chen, A.L. Mezaache, J.D. Chen, J.A. Whiting, 1993: The Simulated SeaWiFS Data Set, Version 1. *NASA Tech. Memo. 104566, Vol. 9,* S.B. Hooker, E.R. Firestone, and A.W. Indest, Eds., NASA Goddard Space Flight Center, Greenbelt, Maryland, 17 pp.

Vol. 10

Woodward, R.H., R.A. Barnes, C.R. McClain, W.E. Esaias, W.L. Barnes, and A.T. Mecherikunnel, 1993: Modeling of the SeaWiFS Solar and Lunar Observations. *NASA Tech. Memo. 104566, Vol. 10,* S.B. Hooker and E.R. Firestone, Eds., NASA Goddard Space Flight Center, Greenbelt, Maryland, 26 pp.

Vol. 11

Patt, F.S., C.M. Hoisington, W.W. Gregg, and P.L. Coronado, 1993: Analysis of Selected Orbit Propagation Models for the SeaWiFS Mission. *NASA Tech. Memo. 104566, Vol. 11,* S.B. Hooker, E.R. Firestone, and A.W. Indest, Eds., NASA Goddard Space Flight Center, Greenbelt, Maryland, 16 pp.

Vol. 12

Firestone, E.R., and S.B. Hooker, 1993: SeaWiFS Technical Report Series Summary Index: Volumes 1–11. *NASA Tech. Memo. 104566, Vol. 12,* S.B. Hooker and E.R. Firestone, Eds., NASA Goddard Space Flight Center, Greenbelt, Maryland, 28 pp.

Vol. 13

McClain, C.R., K.R. Arrigo, J. Comiso, R. Fraser, M. Darzi, J.K. Firestone, B. Schieber, E-n. Yeh, and C.W. Sullivan, 1994: Case Studies for SeaWiFS Calibration and Validation, Part 1. *NASA Tech. Memo. 104566, Vol. 13,* S.B. Hooker and E.R. Firestone, Eds., NASA Goddard Space Flight Center, Greenbelt, Maryland, 52 pp., plus color plates.

Vol. 14

Mueller, J.L., 1993: The First SeaWiFS Intercalibration Round-Robin Experiment, SIRREX-1, July 1992. *NASA Tech. Memo. 104566, Vol. 14,* S.B. Hooker and E.R. Firestone, Eds., NASA Goddard Space Flight Center, Greenbelt, Maryland, 60 pp.

Vol. 15

Gregg, W.W., F.S. Patt, and R.H. Woodward, 1994: The Simulated SeaWiFS Data Set, Version 2. *NASA Tech. Memo. 104566, Vol. 15,* S.B. Hooker and E.R. Firestone, Eds., NASA Goddard Space Flight Center, Greenbelt, Maryland, 42 pp., plus color plates.

Vol. 16

Mueller, J.L., B.C. Johnson, C.L. Cromer, J.W. Cooper, J.T. McLean, S.B. Hooker, and T.L. Westphal, 1994: The Second SeaWiFS Intercalibration Round-Robin Experiment, SIRREX-2, June 1993. *NASA Tech. Memo. 104566, Vol. 16,* S.B. Hooker and E.R. Firestone, Eds., NASA Goddard Space Flight Center, Greenbelt, Maryland, 121 pp.

Vol. 17

Abbott, M.R., O.B. Brown, H.R. Gordon, K.L. Carder, R.E. Evans, F.E. Muller-Karger, and W.E. Esaias, 1994: Ocean Color in the 21st Century: A Strategy for a 20-Year Time Series. *NASA Tech. Memo. 104566, Vol. 17,* S.B. Hooker and E.R. Firestone, Eds., NASA Goddard Space Flight Center, Greenbelt, Maryland, 20 pp.

Vol. 18

Firestone, E.R., and S.B. Hooker, 1995: SeaWiFS Technical Report Series Summary Index: Volumes 1–17. *NASA Tech. Memo. 104566, Vol. 18,* S.B. Hooker and E.R. Firestone, Eds., NASA Goddard Space Flight Center, Greenbelt, Maryland, 47 pp.

Vol. 19

McClain, C.R., R.S. Fraser, J.T. McLean, M. Darzi, J.K. Firestone, F.S. Patt, B.D. Schieber, R.H. Woodward, E-n. Yeh, S. Mattoo, S.F. Biggar, P.N. Slater, K.J. Thome, A.W. Holmes, R.A. Barnes, and K.J. Voss, 1994: Case Studies for SeaWiFS Calibration and Validation, Part 2. *NASA Tech. Memo. 104566, Vol. 19,* S.B. Hooker, E.R. Firestone, and J.G. Acker, Eds., NASA Goddard Space Flight Center, Greenbelt, Maryland, 73 pp.

Vol. 20

Hooker, S.B., C.R. McClain, J.K. Firestone, T.L. Westphal, E-n. Yeh, and Y. Ge, 1994: The SeaWiFS Bio-Optical Archive and Storage System (SeaBASS), Part 1. *NASA Tech. Memo. 104566, Vol. 20,* S.B. Hooker and E.R. Firestone, Eds., NASA Goddard Space Flight Center, Greenbelt, Maryland, 40 pp.

Vol. 21

Acker, J.G., 1994: The Heritage of SeaWiFS: A Retrospective on the CZCS NIMBUS Experiment Team (NET) Program. *NASA Tech. Memo. 104566, Vol. 21,* S.B. Hooker and E.R. Firestone, Eds., NASA Goddard Space Flight Center, Greenbelt, Maryland, 43 pp.

Vol. 22

Barnes, R.A., W.L. Barnes, W.E. Esaias, and C.R. McClain, 1994: Prelaunch Acceptance Report for the SeaWiFS Radiometer. *NASA Tech. Memo. 104566, Vol. 22,* S.B. Hooker, E.R. Firestone, and J.G. Acker, Eds., NASA Goddard Space Flight Center, Greenbelt, Maryland, 32 pp.

Vol. 23

Barnes, R.A., A.W. Holmes, W.L. Barnes, W.E. Esaias, C.R. McClain, and T. Svitek, 1994: SeaWiFS Prelaunch Radiometric Calibration and Spectral Characterization. *NASA Tech. Memo. 104566, Vol. 23,* S.B. Hooker, E.R. Firestone, and J.G. Acker, Eds., NASA Goddard Space Flight Center, Greenbelt, Maryland, 55 pp.

Vol. 24

Firestone, E.R., and S.B. Hooker, 1995: SeaWiFS Technical Report Series Summary Index: Volumes 1–23. *NASA Tech. Memo. 104566, Vol. 24,* S.B. Hooker and E.R. Firestone, Eds., NASA Goddard Space Flight Center, Greenbelt, Maryland, 36 pp.

Vol. 25

Mueller, J.L., and R.W. Austin, 1995: Ocean Optics Protocols for SeaWiFS Validation, Revision 1. *NASA Tech. Memo. 104566, Vol. 25,* S.B. Hooker and E.R. Firestone, Eds., NASA Goddard Space Flight Center, Greenbelt, Maryland, 66 pp.

Vol. 26

Siegel, D.A., M.C. O'Brien, J.C. Sorensen, D.A. Konnoff, E.A. Brody, J.L. Mueller, C.O. Davis, W.J. Rhea, and S.B. Hooker, 1995: Results of the SeaWiFS Data Analysis Round-Robin (DARR-94), July 1994. *NASA Tech. Memo. 104566, Vol. 26,* S.B. Hooker and E.R. Firestone, Eds., NASA Goddard Space Flight Center, Greenbelt, Maryland, 58 pp.

Vol. 27

Mueller, J.L., R.S. Fraser, S.F. Biggar, K.J. Thome, P.N. Slater, A.W. Holmes, R.A. Barnes, C.T. Weir, D.A. Siegel, D.W. Menzies, A.F. Michaels, and G. Podesta, 1995: Case Studies for SeaWiFS Calibration and Validation, Part 3. *NASA Tech. Memo. 104566, Vol. 27,* S.B. Hooker, E.R. Firestone, and J.G. Acker, Eds., NASA Goddard Space Flight Center, Greenbelt, Maryland, 46 pp.

Vol. 28

McClain, C.R., K.R. Arrigo, W.E. Esaias, M. Darzi, F.S. Patt, R.H. Evans, J.W. Brown, C.W. Brown, R.A. Barnes, and L. Kumar, 1995: SeaWiFS Algorithms, Part 1. *NASA Tech. Memo. 104566, Vol. 28,* S.B. Hooker, E.R. Firestone, and J.G. Acker, Eds., NASA Goddard Space Flight Center, Greenbelt, Maryland, 38 pp., plus color plates.

Vol. 29

Aiken, J., G.F. Moore, C.C. Trees, S.B. Hooker, and D.K. Clark, 1995: The SeaWiFS CZCS-Type Pigment Algorithm. *NASA Tech. Memo. 104566, Vol. 29,* S.B. Hooker and E.R. Firestone, Eds., NASA Goddard Space Flight Center, Greenbelt, Maryland, 34 pp.

Vol. 30

Firestone, E.R., and S.B. Hooker, 1996: SeaWiFS Technical Report Series Summary Index: Volumes 1–29. *NASA Tech. Memo. 104566, Vol. 30,* S.B. Hooker and E.R. Firestone, Eds., NASA Goddard Space Flight Center, Greenbelt, Maryland, 43 pp.

Vol. 31

Barnes, R.A., A.W. Holmes, and W.E. Esaias, 1995: Stray Light in the SeaWiFS Radiometer. *NASA Tech. Memo. 104566, Vol. 31,* S.B. Hooker, E.R. Firestone, and J.G. Acker, Eds., NASA Goddard Space Flight Center, Greenbelt, Maryland, 76 pp.

Vol. 32

Campbell, J.W., J.M. Blaisdell, and M. Darzi, 1995: Level-3 SeaWiFS Data Products: Spatial and Temporal Binning Algorithms. *NASA Tech. Memo. 104566, Vol. 32,* S.B. Hooker, E.R. Firestone, and J.G. Acker, Eds., NASA Goddard Space Flight Center, Greenbelt, Maryland, 73 pp., plus color plates.

Vol. 33

Moore, G.F., and S.B. Hooker, 1996: Proceedings of the First SeaWiFS Exploitation Initiative (SEI) Team Meeting. *NASA Tech. Memo. 104566, Vol. 33,* S.B. Hooker and E.R. Firestone, Eds., NASA Goddard Space Flight Center, Greenbelt, Maryland, 53 pp.

Vol. 34

Mueller, J.L., B.C. Johnson, C.L. Cromer, S.B. Hooker, J.T. McLean, and S.F. Biggar, 1996: The Third SeaWiFS Intercalibration Round-Robin Experiment (SIRREX-3), 19–30 September 1994. *NASA Tech. Memo. 104566, Vol. 34,* S.B. Hooker, E.R. Firestone, and J.G. Acker, Eds., NASA Goddard Space Flight Center, Greenbelt, Maryland, 78 pp.

Vol. 35

Robins, D.B., A.J. Bale, G.F. Moore, N.W. Rees, S.B. Hooker, C.P. Gallienne, A.G. Westbrook, E. Marañón, W.H. Spooner, and S.R. Laney, 1996: AMT-1 Cruise Report and Preliminary Results. *NASA Tech. Memo. 104566, Vol. 35,* S.B. Hooker and E.R. Firestone, Eds., NASA Goddard Space Flight Center, Greenbelt, Maryland, 87 pp.

Vol. 36

Firestone, E.R., and S.B. Hooker, 1996: SeaWiFS Technical Report Series Summary Index: Volumes 1–35. *NASA Tech. Memo. 104566, Vol. 36,* S.B. Hooker and E.R. Firestone, Eds., NASA Goddard Space Flight Center, Greenbelt, Maryland, (in production).

Vol. 37

B.C. Johnson, S.S. Bruce, E.A. Early, J.M. Houston, T.R. O'Brian, A. Thompson, S.B. Hooker, and J.L. Mueller, 1996: The Fourth SeaWiFS Intercalibration Round-Robin Experiment (SIRREX-4), May 1995. *NASA Tech. Memo. 104566, Vol. 37,* S.B. Hooker and E.R. Firestone, Eds., NASA Goddard Space Flight Center, Greenbelt, Maryland, 65 pp.

REPORT DOCUMENTATION PAGE

Form Approved
OMB No. 0704-0188

1. AGENCY USE ONLY *(Leave blank)*	2. REPORT DATE	3. REPORT TYPE AND DATES COVERED
	May 1996	Technical Memorandum

4. TITLE AND SUBTITLE
SeaWiFS Technical Report Series
Volume 37–The Fourth SeaWiFS Intercalibration Round-Robin Experiment (SIRREX-4), May 1995

5. FUNDING NUMBERS
Code 970.2

6. AUTHOR(S)
B. Carol Johnson, Sally S. Bruce, Edward A. Early, Jeanne M. Houston
Thomas R. O'Brian, Ambler Thompson, Stanford B. Hooker, and
James L. Mueller
Series Editors: Stanford B. Hooker and Elaine R. Firestone

7. PERFORMING ORGANIZATION NAME(S) AND ADDRESS(ES)
Laboratory for Hydrospheric Processes
Goddard Space Flight Center
Greenbelt, Maryland 20771

8. PERFORMING ORGANIZATION REPORT NUMBER
96B00088

9. SPONSORING/MONITORING AGENCY NAME(S) AND ADDRESS(ES)
National Aeronautics and Space Administration
Washington, D.C. 20546–0001

10. SPONSORING/MONITORING AGENCY REPORT NUMBER
TM–104566, Vol. 37

11. SUPPLEMENTARY NOTES Elaine R. Firestone: General Sciences Corporation, Laurel, Maryland; B. Carol Johnson, Sally S. Bruce, Edward A. Early, Jeanne M. Houston, Thomas R. O'Brian, and Ambler Thompson: National Institute of Standards and Technology, Gaithersburg, Maryland; and James L. Mueller: CHORS/San Diego State University, San Diego, California

12a. DISTRIBUTION/AVAILABILITY STATEMENT
Unclassified–Unlimited
Subject Category 48
Report is available from the Center for AeroSpace Information (CASI), 800 Elkridge Landing Road, Linthicum Heights, MD 21090; (301)621-0390

12b. DISTRIBUTION CODE

13. ABSTRACT *(Maximum 200 words)*

This report documents the fourth Sea-viewing Wide Field-of-view Sensor (SeaWiFS) Intercalibration Round-Robin Experiment (SIRREX-4), which was held at the National Institute of Standards and Technology (NIST) on 3–10 May 1995. The agenda for SIRREX-4 was established by a consensus reached at the conclusion of SIRREX-3: there should be an emphasis on training and work to foster and encourage uniform use of accepted protocols for calibrating radiometric instruments in the laboratory. The goal was to host the activity in a setting where proper techniques could be discussed and demonstrated. It seemed appealing to split the day between morning lectures and afternoon laboratory exercises or *practicals*. The former gave the user community a chance to present what was important to them and discuss it with acknowledged experts in radiometry, while the latter presented a unique opportunity for training and evaluation in the presence of these same experts. The five laboratory sessions were concerned with 1) determining the responsivity of a spectroradiometer and the spectral radiance of an unknown integrating sphere source, 2) demonstrating spectral field calibration procedures for an integrating sphere using three different instruments, 3) measuring spectral radiance using the plaque method, 4) setting up and aligning lamp calibration transfer standards using the NIST specifications for irradiance measurements, and 5) characterizing radiometric instruments. In addition to documenting some supplemental studies performed outside the laboratory sessions, this report includes an evaluation of the hardware that has been used during the SIRREX activities plus a critical evaluation of SIRREX objectives.

14. SUBJECT TERMS
SeaWiFS, Oceanography, SIRREX-4, Monochromators, Spheres, Plaques, Lamps, Radiometers

15. NUMBER OF PAGES
65

16. PRICE CODE

17. SECURITY CLASSIFICATION OF REPORT	18. SECURITY CLASSIFICATION OF THIS PAGE	19. SECURITY CLASSIFICATION OF ABSTRACT	20. LIMITATION OF ABSTRACT
Unclassified	Unclassified	Unclassified	Unlimited

National Aeronautics and
Space Administration

Goddard Space Flight Center
Greenbelt, Maryland 20771

SPECIAL FOURTH-CLASS RATE
POSTAGE & FEES PAID
NASA
PERMIT No. G27